[American Journal of Science, Vol. 316, September, 2016, P. 614–668, DOI 10.2475/07.2016.02]

ASSESSING THE MAGMATIC AFFINITY AND PETROGENESIS OF GRANITOIDS AT THE GIANT AKTOGAI PORPHYRY Cu DEPOSIT, CENTRAL KAZAKHSTAN

MING-JIAN CAO*,†, GUANG-MING LI*,†, KE-ZHANG QIN*, NOREEN J. EVANS**, and ELEONORA YUSUPOVHA SEITMURATOVA***

ABSTRACT. Most mineralized porphyries associated with large to giant oxidized porphyry Cu deposits show an affinity with high Sr/Y rocks, while barren or weakly mineralized granitoids show typical low Sr/Y features. The Aktogai giant porphyry Cu deposit occurs in the Koldar pluton and provides a good natural laboratory in which to investigate this relationship, while determining the petrogenesis of the pluton and its mineralization. Zircon U-Pb dating, mineral chemistry, whole rock geochemistry and Sr-Nd-Pb and zircon Hf-O isotopic analyses were carried out on the pre-ore granodiorite (the major component of the Koldar pluton) and on the mineralized granodiorite porphyry. Zircon U-Pb ages indicate that the pre-ore granodiorite and mineralized granodiorite porphyries were emplaced at 345 and 328 to 331 Ma, respectively. Distinctly higher apatite SO_3 contents in the granodiorite porphyry relative to the granodiorite suggest an increase in fO_2 during the petrogenesis of the mineralized porphyries (>NNO+1). Although all rocks share similar geochemical characteristics (calc-alkaline, strong depletion in Nb, Ta and Ti, and enrichment in LREE and LILE), the pre-ore Koldar pluton has normal arc related magmatic features [low Sr/Y and $(La/Yb)_N$, high Y and Yb_N], while the granodiorite porphyries and diorite (trace component of Koldar pluton) exhibit high Sr/Y and $(La/Yb)_N$, low Y and Yb_N features. All samples show similar Sr-Nd-Pb-Hf-O isotopic compositions [$(^{87}Sr/^{86}Sr)_i = 0.70369$ to 0.70413, ε_{Nd} (t) = + 3.6 to + 5.6, $(^{206}Pb/^{204}Pb)_i = 18.16$ to 19.32, zircon ε_{Hf} (t) = + 11.8 to + 15.9, and $\delta^{18}O$ = + 3.8 to + 5.9 ‰], and very young whole rock T_2DM (Nd) (640 – 680 Ma) and zircon $T_{DM}{}^{C}$ (Hf) (320 – 590 Ma) values, suggesting that they were probably derived from partial melting of juvenile lower crust. Geochemical patterns and partial melt modeling indicate that the high Sr/Y rocks were probably formed by partial melting of eclogitized, thickened lower crust, while the Koldar pluton formed by partial melting of normal thick lower crust. We propose that pre-ore low Sr/Y rocks were probably generated earlier via subduction of Junggar-Balkhash oceanic crust, and that the high Sr/Y rocks were formed later by partial melting of sulfide-enriched, thickened juvenile lower crust. High oxygen fugacity and the high melting temperature of the high Sr/Y rocks ensured that all sulfide was dissolved in the magma, which intruded the previously emplaced low Sr/Y pluton and resulted in significant mineralization.

Keywords: normal arc magmatism, high Sr/Y rocks, thickened lower crust, Aktogai porphyry Cu deposit, Central Kazakhstan

INTRODUCTION

With a few notable exceptions (reduced porphyry Cu deposit; Rowins, 2000; Smith and others, 2012; Cao and others, 2014a), almost all large to giant porphyry Cu deposits emplaced in subduction zones or in post-subduction orogenic belts are

* Key Laboratory of Mineral Resources, Institute of Geology and Geophysics, Chinese Academy of Sciences, P.O. Box 9825, Beijing 100029, China

** John de Laeter Center, TIGeR, Department of Applied Geology, Curtin University, Perth Western Australia, Australia 6945

*** Laboratory of Geological Formations, K. Satpaev Institute of Geological Sciences, Almaty 050010, Kazakhstan

† Corresponding authors: Key Laboratory of Mineral Resources, Institute of Geology and Geophysics, Chinese Academy of Sciences, P.O. Box 9825, Beijing 100029, China; Phone: +86-10-82998190; Fax: +86-10-62010846; E-mail: caomingjian@mail.iggcas.ac.cn (Ming-Jian Cao), lgm@mail.iggcas.ac.cn (Guang-Ming Li)

spatially and genetically related to oxidized magmatic systems (Hedenquist and Lowenstern, 1994; Qin and Ishihara, 1998; Audétat and others, 2004; Li and others, 2007; Sillitoe, 2010; Xiao and others, 2012; Qin and others, 2014), with oxygen fugacities (f_{O2}) varying between the hematite-magnetite (HM) and nickel-nickel oxide (NNO) oxygen buffers (mostly > NNO+1; Mungall, 2002; Richards, 2003). In addition, many oxidized magmatic rocks in large porphyry Cu deposit systems have a geochemical affinity with high Sr/Y rocks (Baldwin and Pearce, 1982; Thieblemont and others, 1997; Sajona and Maury, 1998; Oyarzun and others, 2001; Reich and others, 2003; Zhang and others, 2004; Wang and others, 2006; Li and others, 2011). For example, Thieblemont and others (1997) determined that 38 out of 43 epithermal and porphyry deposit systems from different regions show high Sr/Y characteristics. Oyarzun and others (2001) reported on the contrast between the small and giant porphyry copper deposit magmatic systems in northern Chile, with the former showing normal calc-alkaline (low Sr/Y) affinity and the latter, high Sr/Y features.

Central Kazakhstan (66°N–84°N, 43°E–54°E) is a famous metallogenic province, known worldwide for the abundance of granite-related ore deposits (fig. 1). Central Kazakhstan hosts many large (Bozshakol, Samarsk, Borly and Koksai) to giant (defined as > 2 Mt Cu, after Singer, 1995) Aktogai and Kounrad porphyry Cu deposits (fig. 1). The Aktogai ore field (in the Koldar pluton; Bespaev and Miroshnichenko, 2004) is characterized by the widespread occurrence of veinlet anhydrite (Li and others, 2008), suggesting an oxidized magmatic source for the mineralized rocks. A broad range of ages for granitoids have been obtained by previous workers (366–312 Ma; Syromyatnikova and others, 1990; Singer and others, 2005); however, more recent U-Pb dating (Chen and others, 2014) determined Koldar pluton quartz diorite and mineralized granodiorite porphyry ages of 335.7 ± 1.3 Ma and 327.5 ± 1.9 Ma, respectively. Although some whole rock geochemical data have already been published (Heinhorst and others, 2000; Liu and others, 2012; Shen and others, 2015), there are still a lot of unresolved issues surrounding the petrogenesis of the Aktogai mineralized porphyries.

Mineral chemistry is widely used to constrain the crystallization processes and physicochemical conditions (Ruprecht, P. and Wörner, 2007; Cao and others, 2013, 2015), which are very important tracers of rock petrogenesis. Fluctuating An and FeO content in plagioclase profile can be used to identify magmatic processes; for example magma mixing or replenishment (Tepley and others, 2000; Ruprecht, P. and Wörner, 2007; Cao and others, 2014c). The contents of SO_3 in primary apatite and the assemblage of Fe-Ti oxide could be used to estimate the oxygen fugacity of the magma (Peng and others, 1997; Parat and Holtz, 2005; Smith and others, 2012; Cao and others, 2014b, 2016).

In this study, we apply a broad range of geochronological [secondary ion mass spectrometry (SIMS) zircon U-Pb] and geochemical (mineral chemistry, whole rock geochemistry and Sr-Nd-Pb isotopes, and zircon O-Hf isotopes) methods to the pre-ore granodiorite and diorite, and mineralized granodiorite porphyry. These data, along with previously published work (Heinhorst and others, 2000; Liu and others, 2012; Shen and others, 2015) are used to determine: (1) whether the pre-ore Koldar pluton and mineralized porphyries show an affinity with typical low Sr/Y or high Sr/Y magmatism, respectively; (2) the petrogenesis of the Koldar pluton and mineralized system, and (3) the geodynamic processes responsible for generation of the Koldar pluton and mineralized system.

GEOLOGICAL BACKGROUND

The Central Asian Orogenic Belt (CAOB), also known as the Altaid Tectonic Collage (Sengör and others, 1993; Windley and others, 2007), extends from the Urals in the west, through Kazakhstan, northern China, Mongolia, and southern Siberia to the Okhotsk Sea along the eastern Russian coast (fig. 1A; Windley and others, 2007). It

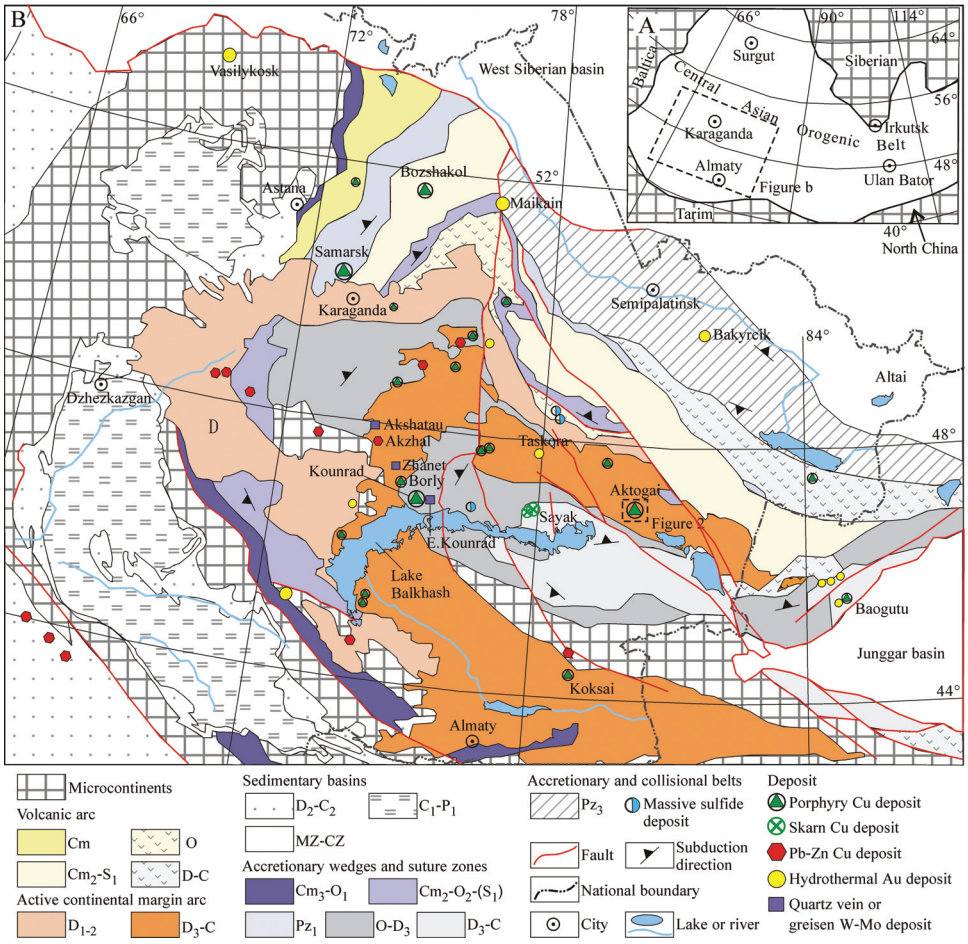

Fig. 1. (A) Location of the study area in the Central Asian Orogenic Belt (modified after Windley and others, 2007). (B) Simplified geological map of Central Kazakhstan showing major ore deposits (modified after Abdulin and others, 1996; Windley and others, 2007 and Li and others, 2008).

is located between the Siberian Craton to the north and the North China and Tarim Cratons to the south (fig. 1A). Central Kazakhstan, located in the midwest of the CAOB, displays a large oroclinal bend of Paleozoic fold belts, which show Early to Middle Devonian ages in the outer portion and Late Devonian to Carboniferous ages in the central region (fig. 1B). Precambrian microcontinental fragments consist of Paleoproterozoic basement and Neoproterozoic to Early Paleozoic cover, and mainly occur in the west and south of Central Kazakhstan. A number of island arcs occur within the Early Paleozoic accretionary collage of the Kazakhstan microcontinent and show age variations from Cambrian to Early Silurian. Microcontinents and island arcs are separated by suture zones within which fragmented Paleozoic oceanic crust was emplaced.

Windley and others (2007) indicated that the amalgamation of microcontinents and major island arcs was completed by the Late Silurian. Andean-type magmatic arcs (the 'Devonian' belt; $D_{1\text{-}2}$ in fig. 1B) then formed as a result of subduction under the Kazakhstan continental margin commencing in the Early Devonian. Continued

accretion led to oceanward rollback of the subduction zone and magmatic arc, forming the Devonian to Carboniferous magmatic arc (D_3-C Balkhash-Yili) within which many magmatic-hydrothermal deposits are developed (Aktogai, Kounrad, Koksai and Borly porphyry Cu deposits, the Sayak skarn Cu deposit, and the East Kounrad, Zhanet and Akshatau W-Mo deposits; fig. 1B). Orocline bending was a result of the oblique collision between the Siberian and Tarim continents and probably occurred in the Permian (Filippova and others, 2001; Levashova and others, 2003), giving rise to the curved shape of the Balkhash-Yili belt and also to large-scale post-collisional strike slip displacements.

The giant Aktogai ore field is located 22 km east of the Aktogai railway station, northeast of Lake Balkhash (fig. 1), and includes two large porphyry copper deposits (Aktogai and Aidarly) and one small deposit (Kyzylkiya). Aktogai contains a combined resource of more than 3.25 Gt of ore with 12.5 Mt Cu @ 0.4 percent (Sokolov, 1998). The Aktogai ore field occurs in the Koldar granitoid pluton, which intrudes into the Early Carboniferous Keregetasskaya volcanic suite. The latter is composed primarily of andesite with minor rhyolite, sandstone and siltstone and is overlain by Late Carboniferous to Early Permian volcano-sedimentary rocks of the Koldarskaya suite. The 75 km^2 Koldar pluton is a complex intrusion primarily comprising granodiorite and granite but with minor to trace components of gabbro, gabbro diorite, diorite and quartz diorite. It was intruded by an elongate stock of ore-forming granodiorite porphyry (fig. 2A).

The ore-bearing stockwork of the Aktogai deposit is elliptical and partially open to the west, with a maximum diameter of 2500 m and a width of 50 to 830 m (Bespaev and Miroshnichenko, 2004; fig. 2B). A stock of granodiorite porphyry occurs in the center of the mineralized stockwork. Four types of hydrothermal alteration have been recognized, including I-alkaline (silica, K-feldspar, biotite), II-acid (silica, sericite, chlorite and carbonate), III-boron- aluminosilicate (tourmaline) and IV-late propylitic (carbonate, chlorite, zeolite, prehnite) (Bespaev and Miroshnichenko, 2004).

The main mineralization of the deposit took place in the alkali alteration zones that consist of an inner zone of potassic alteration and silicification, and an outer zone of biotite and albite alteration (fig. 2C). The Aktogai deposit is dominated by disseminated Cu mineralization with moderate amounts of vein-type mineralization. The occurrence and width of quartz-K-feldspar veins increases from the outer zone to the inner zone with sulfide mineralization concentrated in the transitional zones. Bornite only occurs in the inner zone, while magnetite and pyrite are widely developed in the outer biotite zone. At the Aidarly deposit (fig. 2A), the inner silicification core is surrounded by anhydrite veinlets and disseminated anhydrite that increases in abundance (up to 25 vol.%) from the outer zone to the inner zone (Li and others, 2008).

The acidic stage of alteration is manifest by lenticular bodies in a NW-oriented, discontinuous belt along the periphery of the alkali alteration zone (fig. 2C). The central part of the acidic alteration zone is characterized by quartz-sericite rocks, surrounded by sericitized and chloritized rocks, with chloritized and carbonatized rocks on the periphery (fig. 2C). The quartz-sericite alteration zone consists of disseminated pyrite with rare molybdenite and locally, sphalerite and galena. Cu-bearing minerals are rare in the completely sericitized rocks, but are abundant in the alkali alteration zone partially overprinted by sericite alteration, which is characterized by the richest Cu mineralization in the area.

Boron-aluminosilicate assemblages formed the tourmaline cement of alkaline and acid altered breccias. The copper grade of the breccias is related to the abundance of these mineralized fragments. The late propylitic alteration produced epidote-chlorite-prehnite assemblages with veins of carbonate and zeolite, which crosscut the previous alkaline and acid altered rocks.

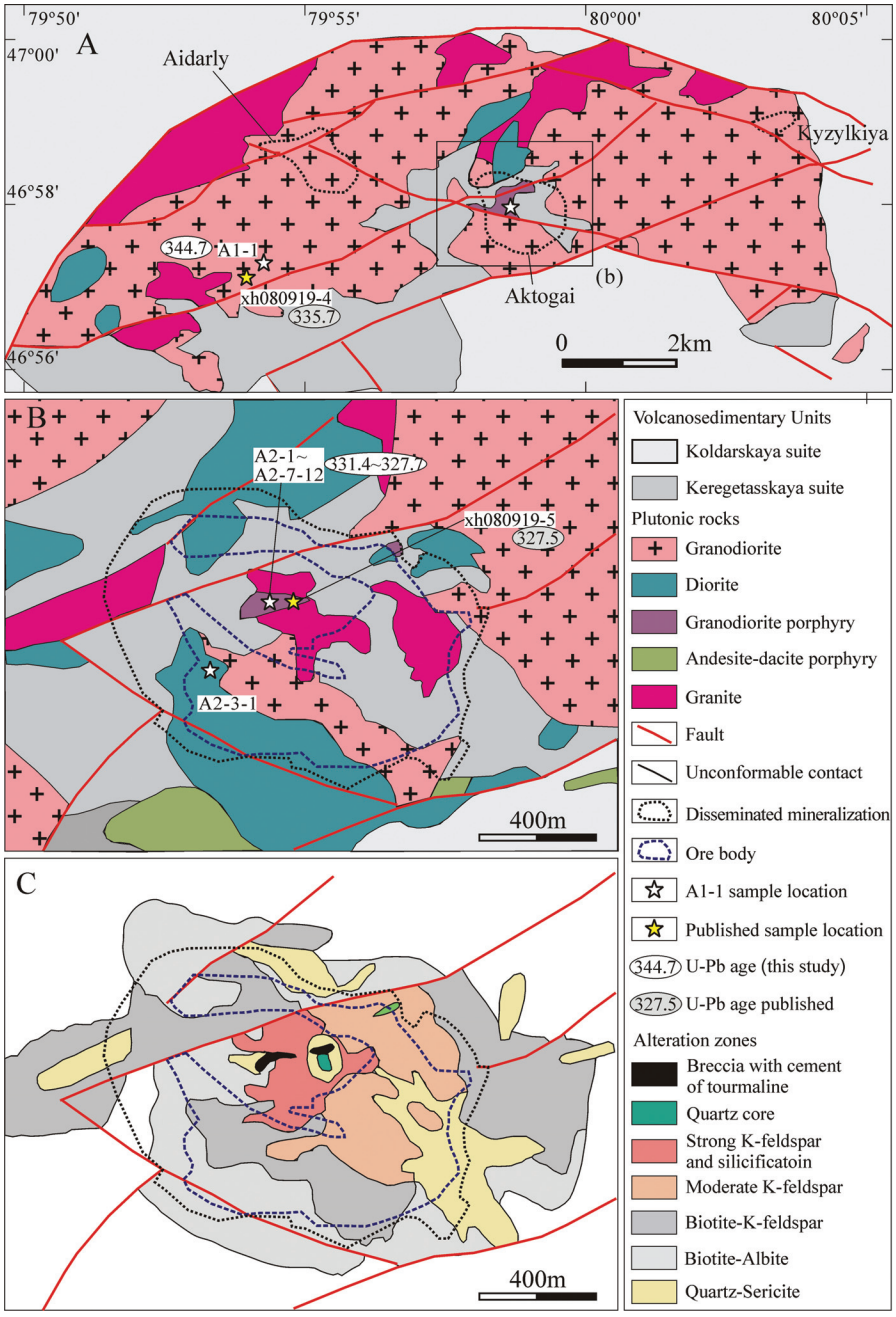

Fig. 2. Geological map of the Aktogai porphyry Cu deposit area showing the Aktogai, Aidarly and Kyzylkiya Cu deposits (after Zhukov and others, 1997), and sample localities with U-Pb ages. The published data are from Chen and others (2014). The samples A2-1, A2-3-2, A2-3-3, A2-6, A2-7-1, A2-7-5, A2-7-9 and A2-7-12 were collected from the similar location. For simplicity and clarity, we just show one star in figure 2B representing these samples.

Previous work to determine the age of the granitoids yielded a variety of results. Syromyatnikova and others (1990) gave whole rock Rb-Sr isochron ages of 366 ± 10 Ma to 346 ± 20 Ma, and mineral Rb-Sr isochron ages of 332-319 ± 15 Ma for the granitoids from the Koldar pluton. Singer and others (2005) suggested mineralization ages of 354 to 312 Ma for the Aktogai. Recently, Chen and others (2014) obtained SHRIMP zircon U-Pb ages of quartz diorite (335.7 ± 1.3 Ma) and granodiorite porphyry (327.5 ± 1.9 Ma). Heinhorst and others (2000) analyzed the whole rock geochemistry and Sr-Nd isotopes of five granitoid rocks and illustrated their primitive characteristic ($\varepsilon Nd(300) = +2.9$ to $+5.9$). Liu and others (2012) and Shen and others (2015) both analyzed the whole rock geochemistry of three granitoids and proposed that their magmatic arc affinity suggested that the Aktogai deposit developed in a subduction zone.

PETROGRAPHY

The pre-ore granodiorite (A1-1), major component of the Koldar pluton (fig. 2A), was collected from the western part of Aktogai deposit (fig. 2A). The A1-1 sample is fine-grained, gray to light gray in color, massive with a subhedral to euhedral granular texture, and is composed of plagioclase (50 vol%, 0.3–1 mm), K-feldspar (20 vol%, 0.1–1 mm), quartz (20 vol%, 0.1–1 mm), biotite (3 vol%, 0.1–0.6 mm) and hornblende (5 vol%, 0.2–0.6 mm) (figs. 3A and 3E). The pre-ore diorite (A2-3-1), a trace component of the Koldar pluton (fig. 2A), was collected from the western part of Aktogai ore-body. The diorite shows fine-grained, grayish in color, massive with a subhedral granular texture, and is composed of plagioclase (65 vol%, 0.2~1 mm), K-feldspar (12 vol%, 0.2~1 mm), quartz (4 vol%, 0.1~0.7 mm), biotite (10 vol%, 0.1~1 mm) and hornblende (8 vol%, 0.1~2 mm). Accessory minerals are magnetite, titanite, apatite and zircon in diorite and granodiorite. In these rocks, subhedral to euhedral magnetite and apatite are usually contained in, or grew together with, euhedral hornblende (fig. 3F) and biotite, suggesting magnetite and apatite were crystallizing at a relatively early magmatic stage. Ilmenite is observed to be exsolved from magnetite (fig. 3F) or occurs as an independent mineral. Magnetite is ten times more abundant than ilmenite (volume percent). Subhedral titanite (40–250 μm) and euhedral zircon (40–150 μm) usually occur as discrete grains in the interstices of plagioclase, K-feldspar and quartz in diorite and granodiorite, indicating that they formed at a relatively late stage of crystallization. Although primary biotite and hornblende are partially altered to chlorite and actinolite, respectively (figs. 3A and 3F), plagioclase is quite fresh and shows weak sericite alteration (fig. 3E). Thus, the pre-ore rocks are relatively fresh.

All the granodiorite porphyry samples in this study (A2-1, A2-3-2, A2-3-3, A2-6, A2-7-1, A2-7-5, A2-7-9 and A2-7-12) were collected from the center of the mineralized stockwork with disseminated mineralization outcrop area ~1.1 km^2 (fig. 2B). They are gray to light gray and massive with a porphyritic texture (figs. 3B, 3C, and 3D). The phenocryst assemblage contains plagioclase (50–60 %, 0.1–1 mm), K-feldspar (10–20 %, 0.1–0.5 mm), quartz (10–20 %, 0.1–0.5 mm), biotite (8–12 %, 0.2–0.5 mm), hornblende (3–8 %, 0.2–0.6 mm), magnetite (2–4 %, 0.1–1 mm) and apatite (~2 %, 0.1–0.3 mm) (figs. 3B, 3C, and 3D), in a matrix of plagioclase, K-feldspar, quartz, hornblende and biotite with minor accessory minerals (magnetite, pyrite, chalcopyrite, apatite, titanite and zircon) (figs. 3G, 3H, and 3I). The phenocryst content of the granodiorite porphyry is about 35 to 45 percent by volume. Acicular ilmenite with a width/length ratio of 20:500 (μm) is probably exsolved from magnetite phenocrysts (fig. 3H). Similar to the granodiorite and diorite, magnetite is far more abundant than ilmenite (estimated petrographically to be in the ratio of >15:1 by volume percent). Euhedral zircon (50–150 μm) and subhedral to anhedral titanite (50–250 μm) mainly occur in the matrix. Subhedral to euhedral apatite is observed contained within or growing with magnetite phenocryst (fig. 3H), and also occurs as independent phenocryst

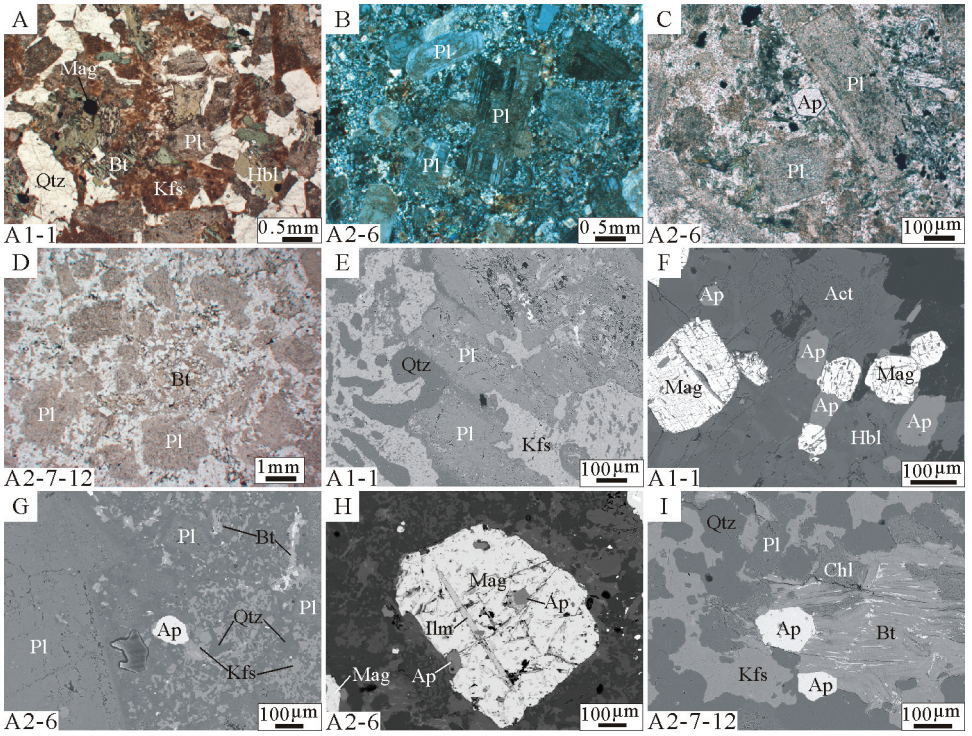

Fig. 3. Representative photomicrographs show the mineral assemblages for A1-1 granodiorite (A, plane-polarized light), A2-6 granodiorite porphyry (B, cross-polarized light; C, plane-polarized light) and A2-7-12 granodiorite porphyry (D, plane-polarized light). Representative Backscattered electron (BSE) images show primary Pl, Kfs and Qtz (E) and apatite growing with magnetite contained in or growth with partially actinolized Hbl (F) in A1-1 granodiorite; fresh Pl phenocryst in matrix of primary Pl, Kfs, Qtz, Bt and Ap (G) and apatite growing with, or contained in, magnetite phenocrysts which also contains acicular ilmenite (H) in A2-6 granodiorite porphyry; and matrix of Pl, Kfs, Qtz, Bt and Ap in A2-7-12 granodiorite porphyry (I). Abbreviations: Act, actinolite; Ap, apatite; Bt, biotite; Chl, chlorite; Hbl, hornblende; Ilm, ilmenite; Kfs, K-feldspar; Mag, magnetite; Pl, plagioclase.

(fig. 3C), indicating that apatite was an early crystallization phase. However apatite may also have crystallized during middle to late stages as indicated by the occurrence of apatite growing with assemblage of rutile and magnetite or growing independently in matrix. Phenocrysts of plagioclase, K-feldspar, biotite and hornblende are partly altered to sericite, clay minerals, chlorite, and actinolite, respectively (figs. 3B and 3I). The matrix contains a primary assemblage of plagioclase, K-feldspar, biotite and apatite (figs. 3G and 3I), suggesting that the porphyries are relatively fresh.

ANALYTICAL METHODS

In order to determine the emplacement ages of the pre-ore granodiorite and mineralized porphyries from the Aktogai deposit, four samples were chosen for secondary ion mass spectrometry (SIMS) zircon U-Pb dating. To constrain the crystallizing conditions of the pre-ore granodiorite and mineralized porphyries, the chemical compositions of apatite and plagioclase were determined. Whole rock geochemistry (major-trace elements, Sr-Nd-Pb isotopes) and zircon Hf-O isotopes were analyzed in the pre-ore granodiorite and diorite, and mineralized porphyries in order to constrain their petrogenesis. Weathered surfaces were carefully removed from all samples and zircon crystals were isolated from clean, crushed rock using heavy liquid and magnetic

separation techniques. Zircon was carefully handpicked under a binocular microscope and mounted in epoxy resin. In order to characterize the internal structures/zonation of the zircons, polished sections of zircon were carbon coated for Cathodoluminescence (CL) imaging, obtained using a CAMECA SX–50 microprobe (15kV) at the Institute of Geology and Geophysics, Chinese Academy of Sciences (IGGCAS) in Beijing. Both optical photomicrographs and CL images were taken as a guide to selection of spots for U-Pb dating and Hf-O isotopic analysis.

Measurements of U, Th and Pb were conducted using the Cameca IMS-1280 SIMS at the IGGCAS. U-Th-Pb ratios and absolute abundances were determined relative to standard zircon 91500 (Wiedenbeck and others, 1995), analyses of which were interspersed with those of unknown grains, using operating and data processing procedures similar to those described by Li and others (2009). A long-term uncertainty of 1.5 percent (1 RSD) for $^{206}Pb/^{238}U$ measurements of the standard zircons was propagated to the unknowns (Li, Q.L. and others, 2010), despite a 1 percent (1 RSD) (or less) $^{206}Pb/^{238}U$ error being measured within each analytical session. Measured compositions were corrected for common Pb using non-radiogenic ^{204}Pb. Corrections were sufficiently small to be insensitive to the choice of common Pb composition, and an average of present-day crustal composition (Stacey and Kramers, 1975) was used for common Pb, assuming that the common Pb is largely surface contamination introduced during sample preparation. Uncertainties on individual analyses in data table are reported at the 1σ level; mean ages for pooled U/Pb (and Pb/Pb) analyses are quoted with 95 percent confidence interval. Data reduction was carried out using the Isoplot/Ex v. 2.49 program (Ludwig, 2001). The results of SIMS including the standard zircon 91500 (concordia age of 1064.3 ± 3.5 Ma; n = 18) are listed in table 1.

The major element compositions of apatite and plagioclase were measured at the IGGCAS, using a JEOL-JXA8100 electron microprobe operated in wavelength dispersive spectrometer mode. The operating conditions were 15 kV accelerating voltage, 10 nA beam current and 3 μm probe beam with counting times of 20 s for Si, Ti, Al, Fe, Mn, Mg, Na, K, Ba, S and Cl, 40 s for F, and 10 s for Ca and P at their characteristic X-ray line. The following natural minerals and synthetic oxides were used for calibration: apatite (P), barite (S), benitoite (Ba), diopside (Ca and Si), rutile (Ti), jadeite (Al), garnet (Fe), bustamite (Mn), jadeite (Na), K-feldspar (K), pyrope (Mg), tugtupite (Cl), and fluorite (F). All data were corrected using the atomic number-absorption-fluorescence procedure. Analyzed compositions of apatite and plagioclase are presented in Appendix tables A1 and A2.

Major oxide abundances were obtained using X-ray fluorescence spectrometry (XRF) on fused glass disks, using a Shimadzu XRF-1500 instrument at the IGGCAS. Loss on ignition (LOI) was measured as the weight loss of the samples after 1 hour of baking at a constant temperature of 1000 °C. The FeO content of the samples was analyzed using conventional wet chemical titration methods. Sample powders (0.5 g) were fused with 5 g of lithium tetraborate ($Li_2B_4O_7$) at 1050 °C for 20 min. The accuracy and reproducibility were monitored using the Chinese national standard sample GSR1 (granite; table 2), with a relative standard deviation from recommended values of ±5 percent. Trace element concentrations, including the rare earth elements (REE), were determined by inductively coupled plasma mass spectrometry (ICP-MS) using an Agilent 7500a system at the IGGCAS. Sample powders (~50 mg) were dissolved in 1 ml of distilled 20 N HF and 0.5 ml of 7.5 N HNO_3 in Teflon screw-cap capsules, then enclosed with alloy steel sleeves and heated at 200 °C for 10 days. The solutions were dried and re-dissolved with 2 ml of 7.5 N HNO_3 in the capsules, and then were diluted in 1 percent HNO_3 to 50 ml before analysis. The standard sample GSR1 (table 2) was used to monitor the analytical accuracy and reproducibility, with a relative standard deviation of better than 5 percent for most elements.

Table 1

SIMS U-Pb zircon results for granitoids from Aktogai porphyry copper deposits, Central Kazakhstan

Spot	U (ppm)	Th (ppm)	Pb (ppm)	Th/U	f_{206} (%)	$^{207}Pb/^{206}Pb$	±1σ (%)	$^{207}Pb/^{235}U$	±1σ (%)	$^{206}Pb/^{238}U$	±1σ (%)	$t_{207/235}$ (Ma)	±1σ	$t_{206/238}$ (Ma)	±1σ
91500															
91500@1	80.5	28.7	17.0	0.356	0.00	0.07374	1.41	1.81605	2.07	0.1786	1.52	1051.3	13.6	1059.4	14.8
91500@2	81.8	29.4	17.4	0.360	0.00	0.07553	1.67	1.88203	2.26	0.1807	1.52	1074.8	15.1	1070.8	15.0
91500@3	82.2	29.4	17.6	0.357	0.00	0.07482	1.38	1.85916	2.04	0.1802	1.51	1066.7	13.6	1068.2	14.8
91500@4	85.4	30.8	18.3	0.361	0.06	0.07457	1.35	1.86533	2.02	0.1814	1.50	1068.9	13.5	1074.7	14.9
91500@5	81.3	28.7	17.2	0.353	0.02	0.07567	1.34	1.86535	2.01	0.1788	1.50	1068.9	13.4	1060.4	14.7
91500@6	79.3	28.1	16.8	0.355	0.04	0.07596	1.68	1.87820	2.26	0.1793	1.51	1073.4	15.1	1063.3	14.9
91500@7	79.2	28.0	16.9	0.354	0.00	0.07553	1.38	1.87917	2.04	0.1804	1.50	1073.8	13.6	1069.4	14.8
91500@8	79.5	28.9	16.7	0.363	0.00	0.07436	1.35	1.81602	2.02	0.1771	1.50	1051.3	13.3	1051.3	14.6
91500@9	81.6	29.6	17.5	0.363	0.00	0.07594	1.69	1.89873	2.26	0.1814	1.50	1080.6	15.1	1074.4	14.9
91500@10	81.5	29.7	17.4	0.365	0.00	0.07693	1.53	1.90715	2.14	0.1798	1.50	1083.6	14.4	1065.9	14.8
91500@11	75.8	27.6	15.8	0.364	0.05	0.07310	2.07	1.78709	2.56	0.1773	1.50	1040.8	16.8	1052.2	14.6
91500@12	78.5	28.7	16.4	0.365	0.00	0.07330	1.46	1.80042	2.13	0.1781	1.55	1045.6	14.0	1056.8	15.2
91500@13	78.2	28.9	16.6	0.369	0.05	0.07406	1.45	1.82909	2.09	0.1791	1.50	1056.0	13.8	1062.1	14.7
91500@14	75.7	27.3	15.9	0.361	0.00	0.07535	1.56	1.85261	2.17	0.1783	1.51	1064.4	14.4	1057.8	14.8
91500@15	77.9	28.7	16.6	0.369	0.05	0.07514	1.46	1.86719	2.10	0.1802	1.50	1069.5	14.0	1068.2	14.8
91500@16	77.7	28.4	16.6	0.366	0.00	0.07513	1.61	1.87384	2.20	0.1809	1.50	1071.9	14.7	1071.9	14.9
91500@17	76.4	27.6	16.1	0.362	0.08	0.07545	1.52	1.85115	2.14	0.1779	1.50	1063.8	14.2	1055.7	14.6
91500@18	79.4	28.1	16.9	0.354	0.00	0.07517	1.98	1.86331	2.50	0.1798	1.52	1068.2	16.7	1065.8	15.0
A1-1															
A1-1@3	1533	2200	126	1.435	0.00	0.05311	0.71	0.40134	1.66	0.0548	1.50	342.6	4.8	343.9	5.0
A1-1@4	318	303	23.4	0.954	0.04	0.05366	1.52	0.40526	2.13	0.0548	1.50	345.5	6.3	343.8	5.0
A1-1@5	615	625	46.0	1.016	0.00	0.05313	1.10	0.40268	1.86	0.0550	1.50	343.6	5.4	345.0	5.0
A1-1@6	1013	1749	89.0	1.726	0.33	0.05228	1.49	0.40265	2.13	0.0559	1.52	343.6	6.2	350.4	5.2
A1-1@8	560	757	43.8	1.353	0.85	0.05413	2.04	0.39859	2.54	0.0534	1.52	340.6	7.4	335.4	5.0
A1-1@9	190	175	13.5	0.920	0.00	0.05276	2.08	0.39196	2.59	0.0539	1.55	335.8	7.4	338.3	5.1
A1-1@11	253	211	18.2	0.831	0.03	0.05312	1.71	0.40181	2.28	0.0549	1.50	343.0	6.6	344.3	5.0

Table 1
(continued)

Spot	U (ppm)	Th (ppm)	Pb (ppm)	Th/U	f_{206} (%)	$^{207}Pb/^{206}Pb$	±1σ (%)	$^{207}Pb/^{235}U$	±1σ (%)	$^{206}Pb/^{238}U$	±1σ (%)	$t_{207/235}$ (Ma)	±1σ	$t_{206/238}$ (Ma)	±1σ
A1-1															
A1-1@15	156	139	11.4	0.889	0.00	0.05422	2.16	0.41275	2.66	0.0552	1.55	350.9	7.9	346.4	5.2
A1-1@16	772	1209	64.8	1.566	0.11	0.05440	1.11	0.41342	1.87	0.0551	1.50	351.3	5.6	345.8	5.1
A1-1@17	106	78.4	7.54	0.742	0.53	0.05258	3.36	0.40291	3.68	0.0556	1.51	343.8	10.8	348.7	5.1
A1-1@18	122	83.3	8.48	0.686	0.16	0.05181	2.50	0.39750	2.92	0.0556	1.51	339.8	8.5	349.1	5.1
A1-1@19	1054	767	75.1	0.728	0.58	0.05326	1.28	0.40784	1.98	0.0555	1.51	347.3	5.8	348.4	5.1
A2-1															
A2-1@1	76.6	84.4	5.48	1.102	0.16	0.05588	3.01	0.39346	3.37	0.0511	1.52	336.9	9.7	321.1	4.8
A2-1@2	55.3	42.9	3.74	0.776	0.00	0.05318	3.66	0.37946	3.97	0.0518	1.53	326.6	11.1	325.3	4.8
A2-1@4	52.2	34.5	3.39	0.661	0.00	0.05206	3.82	0.36769	4.12	0.0512	1.54	317.9	11.3	322.0	4.8
A2-1@5	56.8	40.8	3.84	0.718	0.33	0.05225	3.59	0.37374	3.90	0.0519	1.52	322.4	10.8	326.0	4.8
A2-1@9	44.7	33.7	3.02	0.754	0.00	0.05100	4.14	0.36411	4.42	0.0518	1.53	315.3	12.0	325.4	4.9
A2-1@10	97.1	66.0	6.49	0.680	0.12	0.05653	2.92	0.40773	3.29	0.0523	1.51	347.2	9.7	328.7	4.9
A2-1@11	79.7	47.8	5.19	0.600	0.00	0.05223	3.07	0.37630	3.44	0.0522	1.57	324.3	9.6	328.3	5.0
A2-1@12	225	313	17.5	1.394	0.37	0.05397	1.82	0.38796	2.37	0.0521	1.52	332.9	6.7	327.6	4.8
A2-1@13	92.3	78.3	6.24	0.849	0.14	0.05408	2.84	0.38095	3.22	0.0511	1.52	327.7	9.1	321.2	4.8
A2-1@15	166	110	10.8	0.666	0.07	0.05259	2.11	0.37875	2.59	0.0522	1.50	326.1	7.2	328.2	4.8
A2-1@16	158	174	11.8	1.103	0.32	0.05375	2.22	0.39216	2.68	0.0529	1.51	335.9	7.7	332.4	4.9
A2-1@18	82.5	47.1	5.35	0.571	0.00	0.05402	2.98	0.38968	3.34	0.0523	1.51	334.1	9.6	328.7	4.8
A2-1@19	319	284	22.6	0.890	1.17	0.05131	3.64	0.37842	3.95	0.0535	1.54	325.9	11.1	335.9	5.0
A2-1@20	87.6	79.5	6.11	0.908	0.00	0.05529	3.67	0.39596	3.97	0.0519	1.52	338.7	11.5	326.5	4.8
A2-1@21	82.1	57.9	5.65	0.705	0.00	0.05111	3.20	0.38140	3.54	0.0541	1.51	328.1	10.0	339.8	5.0
A2-3-2															
A2-3-2@0	50.3	29.6	3.21	0.587	0.00	0.05466	3.95	0.38777	4.22	0.0515	1.50	332.7	12.0	323.4	4.7
A2-3-2@2	66.3	70.5	4.80	1.063	0.20	0.05473	3.38	0.39038	3.70	0.0517	1.52	334.6	10.6	325.1	4.8
A2-3-2@4	65.2	38.9	4.26	0.597	0.00	0.05575	3.37	0.40167	3.71	0.0523	1.53	342.9	10.8	328.3	4.9

Table 1
(continued)

Spot	U (ppm)	Th (ppm)	Pb (ppm)	Th/U	f_{206} (%)	$^{207}Pb/^{206}Pb$	±1σ (%)	$^{207}Pb/^{235}U$	±1σ (%)	$^{206}Pb/^{238}U$	±1σ (%)	$t_{207/235}$ (Ma)	±1σ	$t_{206/238}$ (Ma)	±1σ
A2-3-2															
A2-3-2@5	48.4	33.0	3.17	0.681	0.00	0.05314	3.95	0.38263	4.23	0.0522	1.53	329.0	12.0	328.2	4.9
A2-3-2@6	106	90.1	7.54	0.849	0.00	0.05223	4.04	0.38889	4.33	0.0540	1.54	333.6	12.4	339.0	5.1
A2-3-2@7	143	102	9.70	0.709	0.09	0.05129	2.30	0.37488	2.75	0.0530	1.51	323.3	7.7	333.0	4.9
A2-3-2@9	59.4	37.7	3.81	0.634	0.00	0.05316	3.62	0.37684	3.93	0.0514	1.52	324.7	11.0	323.2	4.8
A2-3-2@10	98.2	64.2	6.63	0.654	0.39	0.05370	2.69	0.39684	3.09	0.0536	1.52	339.4	9.0	336.6	5.0
A2-3-2@11	135	127	9.55	0.937	0.00	0.05056	2.40	0.36847	2.83	0.0529	1.51	318.5	7.8	332.0	4.9
A2-3-2@12	145	100	9.80	0.691	0.08	0.05500	2.21	0.40270	2.69	0.0531	1.54	343.6	7.9	333.5	5.0
A2-3-2@13	71.1	78.0	5.16	1.097	0.27	0.05282	4.37	0.38148	4.65	0.0524	1.61	328.1	13.1	329.1	5.2
A2-3-2@14	56.7	38.7	3.87	0.683	0.60	0.05168	4.09	0.38448	4.37	0.0540	1.56	330.3	12.4	338.8	5.1
A2-3-2@15	86.6	63.9	5.87	0.738	0.00	0.05457	2.93	0.39739	3.31	0.0528	1.53	339.8	9.6	331.8	4.9
A2-3-2@16	168	109	11.4	0.651	0.00	0.05374	2.08	0.40054	2.57	0.0541	1.51	342.0	7.5	339.4	5.0
A2-3-2@18	101	66.7	6.73	0.662	0.00	0.05205	3.42	0.38091	3.77	0.0531	1.59	327.7	10.6	333.4	5.2
A2-7-1															
A2-7-1@0	83.8	80.7	5.85	0.964	0.17	0.05441	3.16	0.38485	3.51	0.0513	1.52	330.6	10.0	322.5	4.8
A2-7-1@1	98.1	61.3	6.40	0.625	0.00	0.05330	4.04	0.38342	4.32	0.0522	1.50	329.6	12.2	327.8	4.8
A2-7-1@2	68.8	42.4	4.45	0.616	0.50	0.05049	5.72	0.36504	5.91	0.0524	1.52	316.0	16.2	329.4	4.9
A2-7-1@3	105	64.0	6.90	0.610	0.13	0.05245	2.82	0.37806	3.20	0.0523	1.50	325.6	8.9	328.5	4.8
A2-7-1@4	72.6	54.5	4.76	0.751	0.00	0.05648	3.25	0.39907	3.58	0.0512	1.50	341.0	10.4	322.2	4.7
A2-7-1@5	265	283	19.1	1.070	0.12	0.05181	1.67	0.37751	2.25	0.0528	1.50	325.2	6.3	332.0	4.9
A2-7-1@6	57.0	42.9	3.83	0.753	0.00	0.05347	3.68	0.38666	3.98	0.0524	1.52	331.9	11.3	329.5	4.9
A2-7-1@7	327	283	22.3	0.865	0.35	0.05218	2.09	0.37199	2.57	0.0517	1.50	321.1	7.1	325.0	4.8
A2-7-1@8	296	318	21.6	1.074	0.00	0.05339	1.65	0.38762	2.23	0.0527	1.50	332.6	6.3	330.8	4.9
A2-7-1@9	110	62.0	6.94	0.566	0.27	0.05393	2.78	0.38453	3.20	0.0517	1.58	330.4	9.1	325.0	5.0
A2-7-1@11	68.4	44.2	4.34	0.646	0.32	0.05349	3.49	0.37196	3.82	0.0504	1.55	321.1	10.6	317.2	4.8
A2-7-1@12	138	94.1	9.20	0.683	0.00	0.05144	2.38	0.37687	2.81	0.0531	1.50	324.7	7.9	333.8	4.9
A2-7-1@13	56.6	33.3	3.60	0.588	0.00	0.05190	3.83	0.36943	4.14	0.0516	1.56	319.2	11.4	324.5	5.0

Table 1
(continued)

A2-7-1															
A2-7-1@14	202	124	13.4	0.618	0.04	0.05144	1.95	0.38033	2.48	0.0536	1.54	327.3	7.0	336.8	5.0
A2-7-1@15	165	157	11.6	0.957	0.00	0.05405	2.15	0.39125	2.63	0.0525	1.52	335.3	7.5	329.9	4.9
A2-7-1@16	79.8	60.1	5.35	0.754	0.16	0.05657	3.36	0.41078	3.68	0.0527	1.50	349.4	10.9	330.9	4.8
A2-7-1@17	66.4	77.3	4.83	1.164	0.10	0.05084	4.28	0.36528	4.55	0.0521	1.52	316.2	12.4	327.4	4.9
A2-7-1@19	226	196	15.7	0.870	0.05	0.05286	2.48	0.38443	2.89	0.0527	1.50	330.3	8.2	331.3	4.8
A2-7-1@21	162	178	11.8	1.101	0.00	0.05408	2.10	0.39005	2.58	0.0523	1.50	334.4	7.4	328.7	4.8
A2-7-1@22	65.6	55.6	4.57	0.847	0.00	0.05008	3.53	0.36598	3.84	0.0530	1.51	316.7	10.5	332.9	4.9
A2-7-1@23	80.0	89.2	5.84	1.114	0.00	0.05366	3.09	0.38671	3.47	0.0523	1.57	332.0	9.9	328.4	5.0

f_{206} is the proportion of common ^{206}Pb in total measured ^{206}Pb.

TABLE 2

Major-trace element abundance and Sr-Nd-Pb isotopic compositions of granitoid rocks from the Aktogai porphyry Cu deposit, Cental Kazakhstan

sample	GSR-1		A1-1	A2-3-1	A2-3-3	A2-6	A2-7-5	A2-7-9	A2-7-12
Rock type	granite		granodiorite	diorite	granodiorite porphyry				
Age (Ma)	recommended	measured	344.7		331-328	331-328	331-328	331-328	331-328
Major elements (wt.%)									
SiO_2	72.83	72.95	64.64	62.05	66.21	65.07	69.01	68.89	68.67
TiO_2	0.29	0.28	0.59	0.71	0.54	0.57	0.43	0.44	0.41
Al_2O_3	13.4	13.36	15.02	17.42	16.67	16.51	15.54	15.81	15.96
Fe_2O_3			2.41	3.13	1.60	2.27	0.57	0.57	0.54
FeO			2.56	2.59	1.97	1.77	1.16	1.00	1.07
MnO	0.06	0.06	0.11	0.06	0.03	0.02	0.02	0.02	0.02
MgO	0.42	0.41	2.20	2.73	1.63	1.58	1.50	1.21	1.25
CaO	1.55	1.58	4.09	3.78	2.19	2.91	1.42	1.64	1.40
Na_2O	3.13	3.20	3.21	3.27	4.35	4.38	4.21	3.88	3.85
K_2O	5.01	5.05	3.31	1.99	2.79	2.86	3.96	4.44	4.84
P_2O_5	0.09	0.08	0.12	0.29	0.23	0.24	0.18	0.17	0.18
LOI		0.80	1.42	2.08	1.76	1.88	1.82	2.20	1.74
TOTAL			99.67	100.11	99.97	100.05	99.83	100.26	99.91
$Fe_2O_3^T$	2.14	2.17	5.28	6.04	3.81	4.26	1.87	1.69	1.74
A/CNK			0.92	1.21	1.18	1.06	1.12	1.11	1.13
A/NK			1.69	2.31	1.64	1.60	1.38	1.41	1.38
Mg#			42.65	44.34	43.61	39.38	59.75	56.87	57.09
Trace elements (ppm)									
Li	131	134	10.29	10.61	6.08	6.46	6.73	6.74	5.50
Be	12.4	12.9	0.90	1.18	1.43	1.33	1.43	1.21	1.20
Sc	6.10	5.91	17.96	14.95	6.62	6.38	5.77	5.52	4.80
V	24.0	24.8	127.9	172.7	124.5	122.0	78.72	83.62	70.84
Co	3.40	3.31	13.69	15.68	7.24	6.95	5.17	4.68	4.50
Ni	2.30	2.22	6.86	10.34	5.85	4.27	4.35	4.94	2.78
Cu	3.20	3.23	67.10	2938	1881	1135	1582	3035	2134
Zn	28.0	26.9	74.83	52.19	33.20	33.60	34.25	29.85	24.42
Ga	19.0	18.6	16.46	21.12	21.71	21.95	17.34	16.42	16.68

TABLE 2
(continued)

sample	GSR-1		A1-1	A2-3-1	A2-3-3	A2-6	A2-7-5	A2-7-9	A2-7-12
Rock type	granite		granodiorite	diorite	granodiorite porphyry				
Age (Ma)	recommended	measured	344.7		331-328	331-328	331-328	331-328	331-328
Trace elements (ppm)									
Rb	466	460	96.84	65.59	66.25	62.28	72.01	80.17	93.31
Sr	106	108	360.7	820.5	896.6	922.9	718.5	520.7	575.6
Y	62.0	63.1	19.69	13.19	11.30	8.25	9.77	9.35	7.98
Zr	167	171	186.2	117.1	114.0	101.9	112.3	122.3	106.4
Nb	40.0	38.9	4.27	3.81	3.66	3.82	3.91	4.21	3.83
Cs	38.4	39.1	3.74	4.73	1.81	1.64	2.28	3.03	4.33
Ba	343	338	760.8	549.8	837.7	876.2	1002.8	1074.3	1075.8
La	54.0	53.8	15.31	16.08	19.52	21.16	18.74	22.51	17.14
Ce	108	104	30.69	32.11	38.01	41.32	36.13	42.69	33.67
Pr	12.7	12.3	4.04	4.54	5.13	5.47	4.45	5.07	4.23
Nd	47.0	46.1	16.14	17.47	19.05	20.12	16.55	18.56	15.78
Sm	9.7	9.61	3.52	3.70	3.65	3.62	2.91	3.33	2.75
Eu	0.85	0.89	0.88	1.08	0.95	0.87	0.78	0.84	0.68
Gd	9.30	9.23	3.39	3.04	2.80	2.51	2.40	2.37	2.10
Tb	1.65	1.59	0.54	0.44	0.39	0.31	0.33	0.32	0.27
Dy	10.2	9.9	3.41	2.48	2.09	1.55	1.75	1.75	1.45
Ho	2.05	2.18	0.71	0.48	0.40	0.29	0.34	0.33	0.29
Er	6.50	6.61	2.06	1.27	1.06	0.75	0.93	0.92	0.79
Tm	1.06	1.12	0.30	0.19	0.16	0.11	0.14	0.14	0.12
Yb	7.40	7.56	1.95	1.22	1.00	0.71	0.94	0.92	0.78
Lu	1.15	1.21	0.30	0.18	0.15	0.11	0.15	0.14	0.12
Hf	6.30	6.41	5.77	3.45	3.35	3.09	3.58	3.69	3.26
Ta	7.20	7.38	0.31	0.22	0.23	0.22	0.27	0.31	0.28
Tl	1.93	2.01	0.41	0.32	0.32	0.30	0.30	0.35	0.39
Bi	0.53	0.49	0.29	0.13	0.09	0.05	0.13	0.09	0.35
Pb	31.0	32	18.11	4.58	8.29	8.68	8.06	9.54	8.77
Th	54.0	54.8	9.66	4.07	5.23	4.99	7.25	7.31	7.02
U	18.8	18.1	2.44	1.14	2.44	3.45	1.59	1.15	2.83

Table 2
(continued)

sample	GSR-1		A1-1	A2-3-1	A2-3-3	A2-6	A2-7-5	A2-7-9	A2-7-12
Rock type	granite		granodiorite	diorite	granodiorite porphyry				
Age (Ma)	recommended	measured	344.7		331-328	331-328	331-328	331-328	331-328
Trace elements									
Sr/Y			18.32	62.23	79.35	111.9	73.52	55.70	72.13
La/Yb			7.87	13.20	19.52	29.85	19.98	24.60	21.92
YbN			7.84	4.91	4.03	2.86	3.78	3.69	3.15
(La/Yb)N			5.32	8.92	13.19	20.17	13.50	16.62	14.81
(Gd/Yb)N			1.41	2.02	2.27	2.87	2.07	2.10	2.18
Tzircon saturation (°C)			834	807	807	790	806	813	801
Tapatite saturation (°C)			866	939	955	948	959	952	954
Eu/Eu*			0.78	0.98	0.91	0.88	0.90	0.91	0.87
Sr-Nd isotopes									
Age (Ma)			345	331	331-328	331-328	331-328	331-328	331-328
Rb (ppm)			89.41	62.40	61.90	58.21	68.53	75.78	83.72
Sr (ppm)			345.6	819.5	883.0	924.3	720.6	521.4	574.0
$^{87}Rb/^{86}Sr$			0.748872	0.220322	0.202868	0.182228	0.275214	0.420651	0.422090
$^{87}Sr/^{86}Sr$			0.707368	0.704939	0.705084	0.704786	0.705255	0.705938	0.705899
2σ			0.000012	0.000012	0.000014	0.000013	0.000014	0.000011	0.00001
$(^{87}Sr/^{86}Sr)i$			0.703691	0.703901	0.704128	0.703928	0.703971	0.703974	0.703929
Sm (ppm)			3.35	3.49	2.94	2.85	2.78	3.09	2.36
Nd (ppm)			14.61	16.85	15.96	16.32	15.36	17.76	13.18
$^{147}Sm/^{144}Nd$			0.138664	0.125289	0.111547	0.105713	0.109541	0.105204	0.108554
$^{143}Nd/^{144}Nd$			0.512779	0.512742	0.512635	0.512726	0.512718	0.512700	0.512727
2σ			0.000009	0.00001	0.000012	0.000011	0.00001	0.000011	0.000013
$(^{143}Nd/^{144}Nd)i$			0.512466	0.512470	0.512394	0.512497	0.512483	0.512474	0.512494
εNd(t)			2.7	2.0	-0.1	1.7	1.6	1.2	1.7
εNd(t)			5.3	5.1	3.6	5.6	5.2	5.0	5.4
TDM(Ma)			757.5	706.7	770.5	600.6	635.3	635.5	615.5
T_2DM(Ma)			668.4	678.1	800.1	635.3	662.5	676.6	643.9

TABLE 2
(continued)

sample	GSR-1		A1-1	A2-3-1	A2-3-3	A2-6	A2-7-5	A2-7-9	A2-7-12
Rock type	granite		granodiorite	diorite	granodiorite porphyry				
Age (Ma)	recommended	measured	344.7		331-328	331-328	331-328	331-328	331-328
Pb isotopes									
$^{208}Pb/^{204}Pb$			38.410	38.810	38.658	38.565	38.758	38.727	38.742
2σ			0.014	0.015	0.025	0.019	0.013	0.016	0.024
$^{207}Pb/^{204}Pb$			15.555	15.545	15.609	15.594	15.544	15.552	15.546
2σ			0.013	0.016	0.026	0.019	0.012	0.016	0.024
$^{206}Pb/^{204}Pb$			18.492	18.976	19.416	19.368	18.647	18.456	18.631
2σ			0.014	0.015	0.026	0.019	0.010	0.016	0.024
$(^{208}Pb/^{204}Pb)i$			37.948	38.344	38.490	38.403	38.645	38.359	38.140
$(^{207}Pb/^{204}Pb)i$			15.538	15.529	15.604	15.583	15.538	15.542	15.521
$(^{206}Pb/^{204}Pb)i$			18.177	18.692	19.319	19.148	18.537	18.270	18.155

Mg# = 100*Mg/(Mg+Fe) in mole. Tzircon saturation (°C) and Tapatite saturation (°C) are calculated according to Watson and Harrison (1983) and Harrison and Watson (1984). $\varepsilon Nd)_{CHUR} \times (e^{\lambda(Sm)t} - 1)$; $\varepsilon Nd(t) = [(^{143}Nd/^{144}Nd)_i/(^{143}Nd/^{144}Nd)_{CHUR,i} - 1] \times 10000$; $f_{Sm/Nd} = [(^{147}Sm/^{144}Nd)s/(^{147}Sm/^{144}Nd)_{CHUR}] - 1$; $TDM = 1/\lambda(Sm)\ \ln\{[(^{143}Nd/^{144}Nd)_s - (^{143}Nd/^{144}Nd)_{DM}]/[(^{147}Sm/^{144}Nd)_s - (^{147}Sm/^{144}Nd)_{DM}] + 1\}$; $T_2DM = 1/\lambda(Sm)\ln\{1 + ((^{143}Nd/^{144}Nd)_S - ((^{143}Sm/^{144}Nd)_S - (^{147}Sm/^{144}Nd)_C)(e^{\lambda(Sm)t} - 1))/((^{147}Sm/^{144}Nd)_C - (^{147}Sm/^{144}Nd)_{DM})\}$; where s=sample, $(^{147}Sm/^{144}Nd)_{CHUR} = 0.1967$, $(^{143}Nd/^{144}Nd)_{CHUR} = 0.512638$, $(^{147}Sm/^{144}Nd)_{DM} = 0.2136$, and $(^{143}Nd/^{144}Nd)_{DM} = 0.51315$ (Jacobsen and Wasserburg, 1980) and $(^{147}Sm/^{144}Nd)_C = 0.118$ (Jahn and Condie, 1995). $\lambda^{87}Rb$ = 1.42E-11 y^{-1} (Steiger and Jager, 1977), and $\lambda^{147}Sm$ = 6.54E-12 y^{-1} (Lugmair and Marti, 1978), t=the emplacement age of the granite. Lead isotope data recalculated using the contents of Pb, U and Th and the constants recommended by IUGS ($\lambda^{232}Th$ = 4.9475E-11 y^{-1}, $\lambda^{235}U$ = 9.8485E-10 y^{-1}, and $\lambda^{238}U$ = 1.55125E-10 y^{-1}).

Whole rock Sr, Nd and Pb isotopic compositions were determined on a Finnigan MAT-262 mass spectrometer operated in static mode at the Isotope Laboratory of IGGCAS. The measured $^{86}Sr/^{88}Sr$ and $^{143}Nd/^{144}Nd$ ratios were normalized to $^{86}Sr/^{88}Sr = 0.1194$ and $^{146}Nd/^{144}Nd = 0.7219$, respectively. During the course of analyses, the mean $^{87}Sr/^{86}Sr$ ratio of NBS987 standard was 0.710250 ± 9 (2σ, n = 4), and the mean $^{143}Nd/^{144}Nd$ ratio of Jndi-1 standard was 0.512115 ± 11 (2σ, n = 4). The measured results for standard BCR-2 were Nd 27.5 ppm, Sm 6.25 ppm, $^{147}Sm/^{144}Nd$ 0.1377, $^{143}Nd/^{144}Nd$ 0.512637 ± 10 (2σ, n = 3), and Rb 46.2 ppm and Sr 326.6 ppm, $^{87}Rb/^{86}Sr$ 0.4095 and $^{87}Sr/^{86}Sr = 0.705056 \pm 11$ (2σ, n = 3), which are comparable with the published data (Raczek and others, 2003). Within-run Pb isotope fractionation was corrected using correction factors derived from measurements of the international standard NBS-981. Repeated analyses of NBS-981 gave $^{204}Pb/^{206}Pb = 0.05897 \pm 15$, $^{207}Pb/^{206}Pb = 0.91445 \pm 80$, $^{208}Pb/^{206}Pb = 2.16170 \pm 180$ (2σ, n = 3), which are comparable with published data (Todt and others, 1996). Details of analytical procedures were described by Chen and others (2002). Results for major and trace elements including the standard sample GSR1, and Sr-Nd-Pb isotopic compositions of granitoids from the Aktogai deposit are listed in table 2.

Zircon Lu-Hf isotopic analysis was carried out on a Neptune multi-collector ICP-MS equipped with a Geolas-193 laser-ablation system at the IGGCAS. Lu-Hf isotopic analyses were obtained on the same zircon grains that were previously analyzed for U-Pb and O isotopes, with ablation pits 63 μm in diameter, an ablation time of 26 s, repetition rate of 10 Hz, and energy density of 10 J/cm^2. The detailed analytical procedures were similar to those described by Wu and others (2006). During analyses, the $^{176}Hf/^{177}Hf$ ratio of standard zircon (GJ-1) was 0.282015 ± 15 (1σ, n = 33), similar to the recommended $^{176}Hf/^{177}Hf$ ratio of 0.282000 ± 5 (2σ) measured using solution methods (Morel and others, 2008). Zircon Hf isotopic data from four samples are listed in table 3.

Oxygen isotopes on zircon were measured using the Cameca IMS-1280 SIMS at the IGGCAS, following the procedures of Li, X. H., and others (2010a). The Cs+ primary ion beam was accelerated at 10 kV, with an intensity of *ca.* 2 nA corresponding to a beam size of 10 μm in diameter. The instrumental mass fractionation factor (IMF) was corrected using the 91500 zircon standard with a $\delta^{18}O$ value of 9.9 permil (Wiedenbeck and others, 2004). The internal accuracy achieved based on a set of analyses of matrix-matched reference material was commonly better than ± 0.5 permil (2SD). Measured values of $\delta^{18}O$ are reported in the standard delta notation (per mil, ‰) relative to VSMOW. Repeated analyses of an in-house standard (Penglai zircon) during the course of analysis yielded mean $\delta^{18}O$ value of 5.31 ± 0.05 permil (2σ; n = 42), which is in good agreement with the previously reported value (5.31 ± 0.10‰) for Penglai zircon (Li, X. H., and others, 2010b). Zircon O isotopic data from four samples are listed in table 4.

RESULTS

Geochronology

Concordia diagrams and representative CL images with analytical numbers, $\varepsilon Hf(t)$ and $\delta^{18}O$ values are shown in figure 4. The size range of zircon grains was similar for granodiorite and porphyries (50~150μm), with the length/width ratio of 1:1 to 3:1 and Th/U ratios ranging from 0.6 to 1.7. In addition, all zircon grains showed well developed oscillatory or sector zoning in CL images (fig. 4). These observations support a magmatic origin for granodiorite and porphyries. Figure 4 displays concordia ages of 344.7 ± 2.9 Ma (2σ, MSWD = 0.17, n = 12) for A1-1 granodiorite, 327.7 ± 2.5 Ma (2σ, MSWD = 1.2, n = 15) for A2-1 granodiorite porphyry, 331.4 ± 2.6 Ma (2σ, MSWD = 0.06, n = 15) for A2-3-2 granodiorite porphyry and 328.1 ± 2.1 Ma (2σ,

TABLE 3

Lu-Hf isotopic data for zircons from granitoid rocks from the Aktogai porphyry Cu deposit, Central Kazakhstan

No.	Age (Ma)	$^{176}Yb/^{177}Hf$	$^{176}Lu/^{177}Hf$	$^{176}Hf/^{177}Hf$	2σ	$^{176}Hf/^{177}Hf_i$	$\varepsilon_{Hf}(0)$	$\varepsilon_{Hf}(t)$	2σ	T_{DM} (Ma)	T_{DM}^{C} (Ma)	$f_{Lu/Hf}$
A1-1												
A1-1@0	344.7	0.06271	0.00159	0.28297	0.00002	0.28296	7.2	14.4	0.9	399	431	-0.95
A1-1@8	335.4	0.09072	0.00222	0.28297	0.00002	0.28296	7.2	14.0	0.8	407	446	-0.93
A1-1@10	344.7	0.04582	0.00116	0.28299	0.00003	0.28298	7.8	15.1	0.9	371	386	-0.97
A1-1@11	344.3	0.07316	0.00179	0.28297	0.00002	0.28296	7.1	14.2	0.8	406	441	-0.95
A1-1@16	345.8	0.04640	0.00116	0.28297	0.00003	0.28296	6.9	14.2	1.1	408	444	-0.97
A1-1@17	348.7	0.05821	0.00143	0.28300	0.00003	0.28299	8.1	15.4	0.9	361	368	-0.96
A2-1												
A2-1@0	327.7	0.01615	0.00044	0.28296	0.00003	0.28296	6.7	13.8	1.1	405	452	-0.99
A2-1@1	321.1	0.03570	0.00087	0.28296	0.00003	0.28295	6.5	13.4	1.0	419	477	-0.97
A2-1@2	325.3	0.02727	0.00069	0.28300	0.00003	0.28300	8.1	15.1	1.0	352	369	-0.98
A2-1@3	327.7	0.03032	0.00075	0.28297	0.00003	0.28297	7.1	14.1	0.9	395	435	-0.98
A2-1@4	322.0	0.01825	0.00049	0.28301	0.00003	0.28301	8.6	15.5	1.0	333	339	-0.99
A2-1@5	326.0	0.03306	0.00083	0.28301	0.00003	0.28300	8.4	15.4	1.0	342	351	-0.97
A2-1@6	327.7	0.01978	0.00051	0.28297	0.00003	0.28297	7.2	14.3	0.9	388	425	-0.98
A2-1@8	327.7	0.02890	0.00078	0.28291	0.00003	0.28290	4.7	11.8	0.9	488	585	-0.98
A2-1@9	325.4	0.02034	0.00054	0.28292	0.00003	0.28292	5.3	12.3	0.9	463	547	-0.98
A2-1@10	328.7	0.03696	0.00102	0.28299	0.00003	0.28298	7.7	14.7	1.1	371	396	-0.97
A2-1@11	328.3	0.01873	0.00053	0.28300	0.00003	0.28299	8.0	15.1	0.9	357	375	-0.98
A2-1@12	327.6	0.03416	0.00092	0.28302	0.00003	0.28301	8.6	15.6	1.1	335	339	-0.97
A2-1@13	321.2	0.02295	0.00062	0.28298	0.00003	0.28297	7.2	14.1	0.9	388	429	-0.98
A2-1@14	327.7	0.04383	0.00116	0.28302	0.00002	0.28302	8.9	15.9	0.8	324	322	-0.97
A2-1@15	328.2	0.04438	0.00114	0.28299	0.00002	0.28298	7.7	14.6	0.9	375	402	-0.97
A2-1@16	332.4	0.04302	0.00113	0.28298	0.00003	0.28298	7.5	14.6	1.0	381	410	-0.97
A2-1@18	328.7	0.04664	0.00125	0.28301	0.00003	0.28301	8.6	15.6	1.0	338	344	-0.96
A2-1@19	335.9	0.03583	0.00095	0.28298	0.00003	0.28297	7.2	14.4	1.0	391	425	-0.97
A2-1@20	326.5	0.02980	0.00076	0.28300	0.00003	0.28300	8.1	15.1	1.0	355	372	-0.98
A2-3-2												
A2-3-2@0	323.4	0.01675	0.00046	0.28297	0.00003	0.28296	6.9	13.9	0.9	398	444	-0.99
A2-3-2@1	331.4	0.01903	0.00051	0.28297	0.00003	0.28296	6.9	14.1	0.9	399	440	-0.98
A2-3-2@2	325.1	0.01629	0.00044	0.28300	0.00003	0.28300	8.2	15.3	0.9	346	358	-0.99
A2-3-2@3	331.4	0.01276	0.00034	0.28290	0.00003	0.28290	4.7	11.9	0.9	484	579	-0.99

Table 3
(*continued*)

No.	Age (Ma)	$^{176}Yb/^{177}Hf$	$^{176}Lu/^{177}Hf$	$^{176}Hf/^{177}Hf$	2σ	$^{176}Hf/^{177}Hf_i$	$\varepsilon_{Hf}(0)$	$\varepsilon_{Hf}(t)$	2σ	T_{DM} (Ma)	T_{DM}^{C} (Ma)	$f_{Lu/Hf}$
A3-2												
A2-3-2@4	328.3	0.02461	0.00069	0.28299	0.00002	0.28298	7.6	14.7	0.9	372	398	-0.98
A2-3-2@5	328.2	0.02570	0.00071	0.28299	0.00003	0.28299	7.8	14.8	1.1	366	389	-0.98
A2-3-2@6	339.0	0.01763	0.00048	0.28291	0.00002	0.28290	4.8	12.1	0.9	482	571	-0.99
A2-3-2@7	333.0	0.03788	0.00102	0.28300	0.00003	0.28299	8.0	15.1	0.9	361	378	-0.97
A2-3-2@9	323.2	0.01588	0.00042	0.28297	0.00003	0.28296	6.9	13.9	1.1	397	443	-0.99
A2-3-2@10	336.6	0.02691	0.00076	0.28296	0.00002	0.28296	6.8	14.0	0.8	405	447	-0.98
A2-3-2@13	329.1	0.03118	0.00078	0.28297	0.00003	0.28296	6.9	13.9	0.9	403	447	-0.98
A2-3-2@14	338.8	0.01846	0.00049	0.28291	0.00003	0.28290	4.8	12.1	1.0	482	570	-0.99
A2-3-2@15	331.8	0.02620	0.00072	0.28298	0.00003	0.28298	7.5	14.6	0.9	379	407	-0.98
A2-3-2@16	339.4	0.04548	0.00122	0.28300	0.00003	0.28299	8.0	15.2	1.0	363	377	-0.96
A2-3-2@18	333.4	0.01800	0.00047	0.28291	0.00002	0.28291	4.8	12.1	0.8	481	571	-0.99
A2-7-1												
A2-7-1@0	322.5	0.02218	0.00060	0.28298	0.00002	0.28298	7.3	14.3	0.9	382	419	-0.98
A2-7-1@1	327.8	0.04301	0.00113	0.28300	0.00003	0.28299	8.0	15.0	1.0	359	378	-0.97
A2-7-1@2	329.4	0.02499	0.00071	0.28299	0.00003	0.28298	7.7	14.7	1.0	371	396	-0.98
A2-7-1@3	328.5	0.01818	0.00054	0.28294	0.00002	0.28294	6.0	13.1	0.8	437	503	-0.98
A2-7-1@4	322.2	0.02504	0.00067	0.28297	0.00002	0.28297	7.0	14.0	0.8	395	439	-0.98
A2-7-1@5	332.0	0.03439	0.00100	0.28301	0.00003	0.28301	8.5	15.6	0.9	340	344	-0.97
A2-7-1@6	329.5	0.04267	0.00116	0.28301	0.00003	0.28300	8.4	15.4	1.0	346	355	-0.96
A2-7-1@8	330.8	0.07234	0.00209	0.28299	0.00003	0.28298	7.7	14.5	1.0	382	410	-0.94
A2-7-1@9	325.0	0.03008	0.00088	0.28300	0.00003	0.28300	8.1	15.1	0.9	355	373	-0.97
A2-7-1@10	328.1	0.02225	0.00065	0.28299	0.00003	0.28299	7.7	14.8	0.9	368	392	-0.98
A2-7-1@11	317.2	0.01725	0.00051	0.28299	0.00002	0.28299	7.7	14.6	0.9	366	397	-0.98
A2-7-1@12	333.8	0.05201	0.00144	0.28301	0.00003	0.28300	8.4	15.5	0.9	346	354	-0.96
A2-7-1@14	336.8	0.02440	0.00067	0.28299	0.00001	0.28299	7.8	15.1	0.5	363	378	-0.98
A2-7-1@18	328.1	0.02086	0.00057	0.28293	0.00002	0.28292	5.5	12.6	0.8	456	534	-0.98
A2-7-1@19	331.3	0.05891	0.00172	0.28292	0.00002	0.28291	5.3	12.2	0.8	479	562	-0.95
A2-7-1@20	328.1	0.04250	0.00126	0.28300	0.00002	0.28299	8.1	15.1	0.7	357	373	-0.96
A2-7-1@21	328.7	0.03304	0.00088	0.28299	0.00002	0.28299	7.8	14.9	0.7	365	386	-0.97

TABLE 3
(continued)

No.	Age (Ma)	$^{176}Yb/^{177}Hf$	$^{176}Lu/^{177}Hf$	$^{176}Hf/^{177}Hf$	2σ	$^{176}Hf/^{177}Hf_i$	$\varepsilon_{Hf}(0)$	$\varepsilon_{Hf}(t)$	2σ	T_{DM} (Ma)	T_{DM}^{C} (Ma)	$f_{Lu/Hf}$
A2-7-1												
A2-7-1@22	332.9	0.02319	0.00064	0.28296	0.00002	0.28296	6.7	13.9	0.7	408	454	-0.98
A2-7-1@23	328.4	0.04969	0.00128	0.28297	0.00002	0.28296	6.9	13.9	0.8	407	452	-0.96

The notations of εHf, $f_{Lu/Hf}$ T_{DM} and T_{DM}^{C} are defined as: $\varepsilon Hf(0)=[(^{176}Hf/^{177}Hf)_S/(^{176}Hf/^{177}Hf)_{CHUR}-1]\times10000$; $\varepsilon Hf(t)=\{[(^{176}Hf/^{177}Hf)_S-(^{176}Lu/^{177}Hf)_S\times(e^{\lambda t}-1)]/[(^{176}Hf/^{177}Hf)_{CHUR}-(^{176}Lu/^{177}Hf)_{CHUR}\times(e^{\lambda t}-1)]-1\}\times10000$; $f_{Lu/Hf}=(^{176}Lu/^{177}Hf)_S/(^{176}Lu/^{177}Hf)_{CHUR}-1$; $T_{DM}=1/\lambda\times\{1+[(^{176}Hf/^{177}Hf)_S-(^{176}Hf/^{177}Hf)_{DM})]/[(^{176}Lu/^{177}Hf)_S-(^{176}Lu/^{177}Hf)_{DM})]\}$; $T_{DM}^{C}=T_{DM}-(T_{DM}-t)[(f_{cc}-f_s)/(f_{cc}-f_{DM})]$; where, $(^{176}Lu/^{177}Hf)_S$ and $(^{176}Hf/^{177}Hf)_S$ are the measured values of samples, $(^{176}Lu/^{177}Hf)_{CHUR}=0.0332$ and $(^{176}Hf/^{177}Hf)_{CHUR}=0.282772$ (Blichert-Toft and others, 1997); $(^{176}Lu/^{177}Hf)_{DM}=0.0384$ and $(^{176}Hf/^{177}Hf)_{DM}=0.28325$ (Griffin and others, 2000), t=crystallization time of zircon. $\lambda=0.01867Ga^{-1}$ (Soderlund and others, 2004) was used in our calculations, where, f_{cc}, f_s, f_{DM} are $f_{Lu/Hf}$ values of the continental crust, the sample and the depleted mantle, respectively. In our calculation, $f_{cc}=-0.55$ and $f_{DM}=0.16$ (Griffin and others, 2000), and t=the age of $t_{206/238}$.

Table 4

Zircon oxygen isotopic compositions of granitoids from the Aktogai porphyry Cu deposit, Central kazakhstan

Sample	Age (Ma)	$\delta^{18}O$	2σ	Sample	Age (Ma)	$\delta^{18}O$	2σ	Sample	Age (Ma)	$\delta^{18}O$	2σ	Sample	Age (Ma)	$\delta^{18}O$	2σ
A1-1				A2-1				A2-3-2				A2-7-1			
A1-1@0	344.7*	5.1	0.3	A2-1@0	327.7*	5.4	0.3	A2-3-2@0	323.4	5.7	0.4	A2-7-1@0	322.5	5.2	0.4
A1-1@1	344.7*	4.9	0.2	A2-1@1	321.1	5.1	0.3	A2-3-2@1	331.4*	5.3	0.3	A2-7-1@1	327.8	4.5	0.3
A1-1@2	344.7*	4.8	0.4	A2-1@2	325.3	5.2	0.3	A2-3-2@2	325.1	5.9	0.3	A2-7-1@2	329.4	5.4	0.3
A1-1@3	343.9	5.3	0.3	A2-1@3	327.7*	5.5	0.2	A2-3-2@3	331.4*	5.0	0.3	A2-7-1@3	328.5	4.7	0.2
A1-1@4	343.8	4.9	0.3	A2-1@4	322.0	5.1	0.2	A2-3-2@4	328.3	5.5	0.4	A2-7-1@4	322.2	5.4	0.3
A1-1@5	345.0	4.4	0.3	A2-1@5	326.0	5.4	0.4	A2-3-2@5	328.2	5.2	0.3	A2-7-1@5	332.0	5.0	0.3
A1-1@6	350.4	4.7	0.3	A2-1@6	327.7*	4.6	0.2	A2-3-2@6	339.0	5.4	0.2	A2-7-1@6	329.5	5.0	0.2
A1-1@7	344.7*	4.8	0.3	A2-1@7	327.7*	5.1	0.3	A2-3-2@7	333.0	4.7	0.4	A2-7-1@7	325.0	5.3	0.3
A1-1@8	335.4	4.9	0.3	A2-1@8	327.7*	4.3	0.3	A2-3-2@8	331.4*	4.9	0.2	A2-7-1@8	330.8	5.3	0.4
A1-1@9	338.3	5.0	0.4	A2-1@9	325.4	5.3	0.3	A2-3-2@9	323.2	5.5	0.3	A2-7-1@9	325.0	4.5	0.4
A1-1@10	344.7*	4.7	0.3	A2-1@10	328.7	5.5	0.3	A2-3-2@10	336.6	5.0	0.3	A2-7-1@10	328.1*	5.3	0.3
A1-1@11	344.3	4.8	0.3	A2-1@11	328.3	5.6	0.2	A2-3-2@11	332.0	5.3	0.3	A2-7-1@11	317.2	4.9	0.3
A1-1@13	344.7*	4.8	0.4	A2-1@12	327.6	5.3	0.3	A2-3-2@12	333.5	4.7	0.4	A2-7-1@12	333.8	5.0	0.3
A1-1@14	344.7*	4.9	0.3	A2-1@13	321.2	5.3	0.2	A2-3-2@13	329.1	5.0	0.4	A2-7-1@13	324.5	5.4	0.3
A1-1@15	346.4	4.6	0.4	A2-1@14	327.7*	4.6	0.3	A2-3-2@14	338.8	5.1	0.4	A2-7-1@14	336.8	4.7	0.4
A1-1@16	345.8	4.7	0.3	A2-1@15	328.2	5.0	0.2	A2-3-2@15	331.8	4.8	0.2	A2-7-1@15	329.9	5.5	0.3
A1-1@17	348.7	4.5	0.2	A2-1@16	332.4	5.4	0.2	A2-3-2@16	339.4	4.4	0.3	A2-7-1@16	330.9	5.1	0.3
A1-1@18	349.1	5.0	0.3	A2-1@17	327.7*	5.3	0.4	A2-3-2@17	331.4*	5.0	0.4	A2-7-1@17	327.4	5.5	0.3
A1-1@19	348.4	4.3	0.3	A2-1@18	328.7	5.0	0.3	A2-3-2@18	333.4	5.0	0.3	A2-7-1@18	328.1*	5.5	0.4
A1-1@20	344.7*	3.8	0.3	A2-1@19	335.9	5.0	0.3	A2-3-2@19	331.4*	5.0	0.3	A2-7-1@19	331.3	5.2	0.3
				A2-1@20	326.5	5.1	0.4	A2-3-2@20	331.4*	4.4	0.4	A2-7-1@20	328.1*	4.9	0.3
				A2-1@21	339.8	4.9	0.3	A2-3-2@21	331.4*	4.9	0.4	A2-7-1@21	328.7	4.8	0.3
								A2-3-2@22	331.4*	4.8	0.4	A2-7-1@22	332.9	5.3	0.3
												A2-7-1@23	328.4	5.4	0.3

344.7* is the concordia age; 344.7 is the age of $t_{206/238}$.

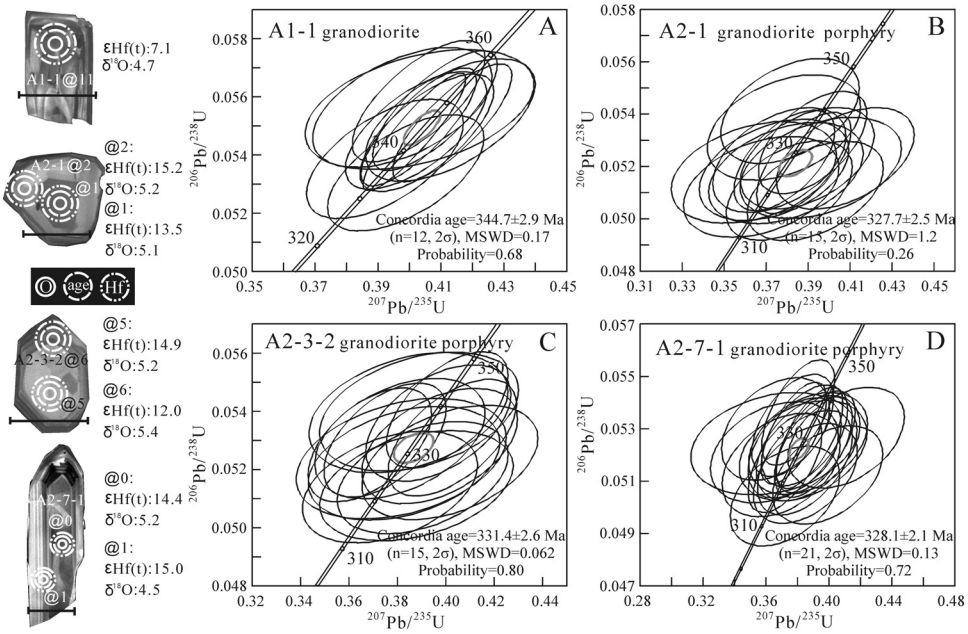

Fig. 4. SIMS U-Pb zircon concordia diagrams for (A) A1-1 granodiorite, (B) A2-1 granodiorite porphyry, (C) A2-3-2 granodiorite porphyry, (D) A2-7-1 granodiorite porphyry from the giant Aktogai porphyry Cu deposit. Representative cathodoluminescence (CL) images of zircons with analytical position for O, U-Pb and Hf isotopes analyses, εHf(t) and $\delta^{18}O$ values are shown. The scale bar is 100 μm long.

MSWD = 0.13, n = 21) for A2-7-1 granodiorite porphyry. Our results indicate that the pre-ore granodiorite formed at 344.7 Ma, while the mineralized porphyries intruded at 327.7~331.4 Ma.

Mineral Chemistry

The analyzed apatite samples in the A1-1 granodiorite contained minor amounts of FeO (0.20 – 0.56 wt.%), Cl (0.11 – 1.78 wt.%) and F (2.31 – 3.53 wt.%), and trace amounts of MnO (<0.19 wt.%) and SO_3 (<0.17 wt.%) (table A1). All the apatite samples from the granodiorite porphyry showed higher amounts of MnO (0.17 – 0.40 wt.%) (fig. 5). The apatite formed in the relatively early to middle stages of crystallization showed significantly higher contents of SO_3 than that crystallizing during the late stage (fig. 5). For example, apatite contained in magnetite phenocrysts, apatite occurring with assemblages of magnetite and rutile, and apatite crystallized in the matrix had SO_3 values of 0.34 to 0.64 weight percent, 0.21 to 0.28 weight percent and 0.02 to 0.19 weight percent, respectively (fig. 5).

The compositions of the plagioclase in A1-1 granodiorite yielded values of $An_{0.44-0.53}$ (table A2). The phenocryst of plagioclase from A2-6 granodiorite porphyry had values of $An_{0.30-0.39}$. Figure 6 shows that plagioclase from both the A1-1 granodiorite and A2-6 granodiorite porphyry do not show significant compositional variations or repeated oscillatory zoning in An, Ab, SiO_2 and FeO contents.

Geochemistry

Major and trace element compositions.—Petrographic characteristics indicate that all rocks are relatively fresh and have only suffered minor alteration. Due to significant Sr mobility in hydrothermal fluids, Farmer and DePaolo (1987) indicated that the Sr

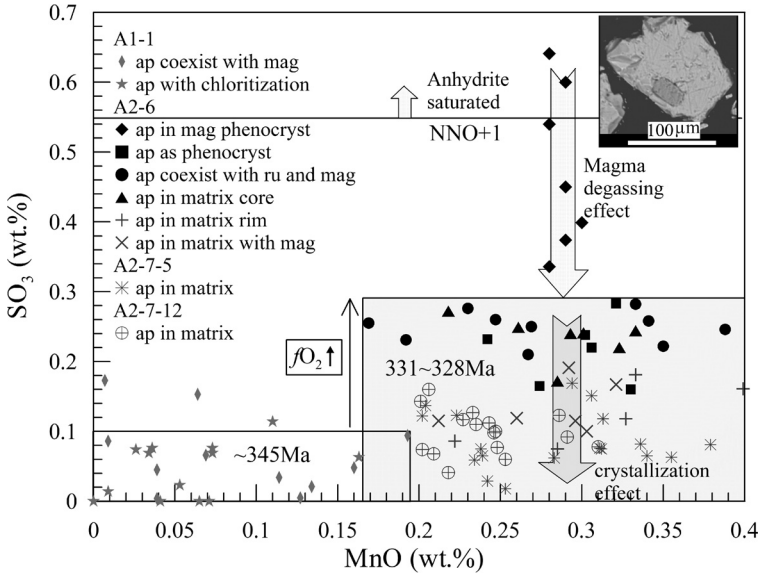

Fig. 5. Plot of MnO versus SO_3 in apatite from the Aktogai deposit. The minimum SO_3 content in apatite (indicated by the horizontal line) in the silicic melt and anhydrite saturated field are from Parat and Holtz (2005) and Peng and others (1997). Inset figure is the backscattered electron (BSE) image of apatite with anhydrite inclusions in A2-6 granodiorite porphyry. Abbreviation: ap, apatite; bt, biotite; mag, magnetite; ru, rutile. Please see the text for more details.

isotopic compositions of altered rocks, including potassic to propylitic alteration zones in porphyry Cu deposit systems, should show high radiogenic and large variation. The more radiogenic and widely varying Sr isotopic compositions [$(^{87}Sr/^{86}Sr)_i$ = 0.7062 to 0.7138] in Aktogai rocks studied by Heinhorst and others (2000) suggest obvious alteration for previously published rocks. However, all our samples show restricted and less radiogenic Sr isotopic compositions, indicating that they retain primary features without significant alteration. In addition, the relatively low loss on ignition values (LOI = 1.42 – 2.20 wt.%) and the lack of correlation of LOI with mobile element concentrations (for example, Cs, Rb, K, Ba, Sr, Na) suggest that most of the compositions reported are close to the original igneous values. Thus, the geochemical results of whole rock represent primary characteristics.

The rocks show a restricted compositional variation of SiO_2 (62.05 – 69.01 wt.%), TiO_2 (0.41 – 0.71 wt.%), Al_2O_3 (15.02 – 17.42 wt.%), MgO (1.21 – 2.73 wt.%), and Na_2O (3.21 – 4.38 wt.%). In the Nb/Y versus SiO_2 diagram (fig. 7A; Winchester and Floyd, 1977), all samples plot in a range from diorite to granodiorite fields and show sub-alkaline feature. The pre-ore granodiorite (A1-1) shows characteristics of metaluminous granitoids (A/CNK = 0.92, A/NK = 1.69), low Sr/Y (18.32) and $(La/Yb)_N$ (5.32), high Y (19.69 ppm) and Yb_N (7.84) (figs. 7B, 7C, and 7D) which exemplify normal arc magmatism. However, the ore-forming granodiorite porphyries show peraluminous features (A/CNK = 1.06 – 1.18, A/NK = 1.38 – 1.64), high Sr/Y (55.70 – 111.9) and $(La/Yb)_N$ (13.19 – 20.17), low Y (7.98 – 11.30 ppm) and Yb_N (2.86 – 4.03) (figs. 7B-7D). On the plots of Y versus Sr/Y and Yb_N versus $(La/Yb)_N$ (figs. 7C and 7D), all porphyries locate in the field of high Sr/Y rocks. The pre-ore diorite (A2-3-1) displayed similar characteristics to those of the granodiorite porphyries (figs. 7B, 7C, and 7D).

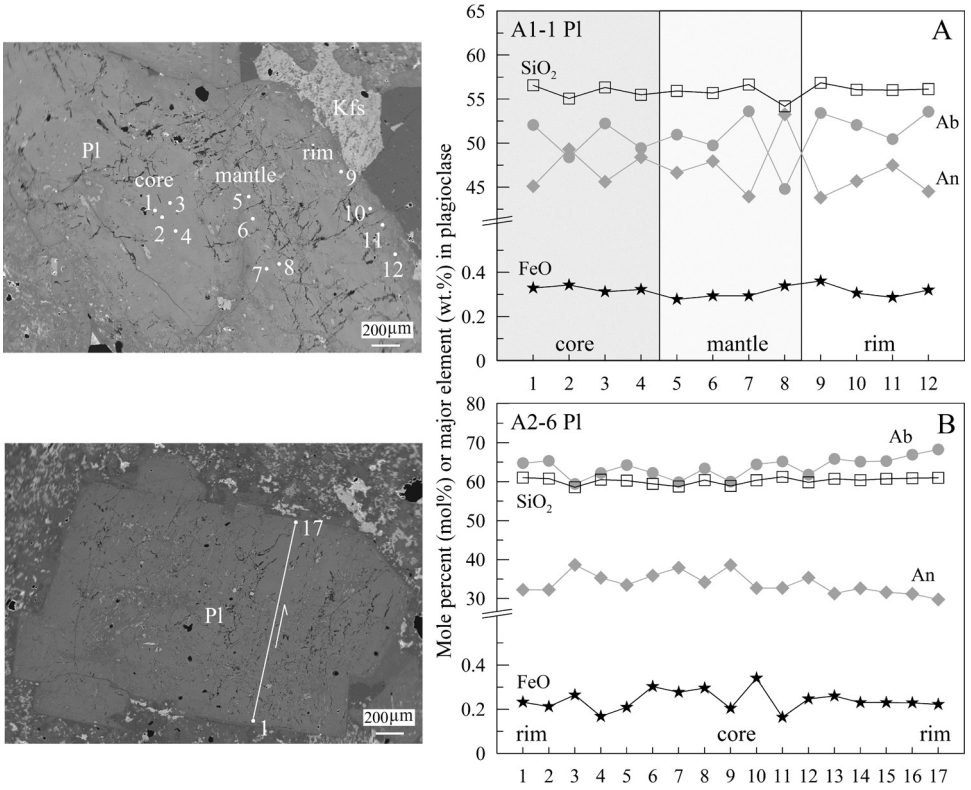

Fig. 6. BSE images and measured electron microprobe profiles including contents of SiO_2, Na_2O and CaO, mole percent of Ab, An and Or for plagioclase crystals from the Aktogai deposit. White lines with arrows on BSE images show electron microprobe transect location and direction.

On the primitive mantle-normalized incompatible trace element spidergrams, all samples show a strong depletion in high field strength element (HFSE, such as Nb, Ta and Ti), and variable enrichment in light REE and large ion lithophile elements (LILE, such as K, Rb, Sr, Ba, U) (figs. 8A and 8B). However, relative to pre-ore granodiorite (A1-1), all porphyries and diorite samples display more fractionated LREE/HREE with slightly negative Eu anomalies with Eu/Eu* [$Eu_N/(Sm_N*Gd_N)^{0.5}$] ranging from 0.87 to 0.98 (figs. 8C and 8D).

Sr-Nd-Pb isotopes.—The pre-ore rocks (A1-1 and A2-3-1) and ore-forming granodiorite porphyries (except A2-3-3 with $(^{87}Sr/^{86}Sr)_i = 0.70413$, $(^{143}Nd/^{144}Nd)_i = 0.51239$, ε_{Nd} (t) = + 3.6) show similar and restricted Sr-Nd isotopic compositions with $(^{87}Sr/^{86}Sr)_i$ values of 0.70369 to 0.70397, $(^{143}Nd/^{144}Nd)_i$ values of 0.51247 to 0.51250, ε_{Nd} (t) values of + 5.0 to + 5.6 (fig. 9A), T_2DM (Nd) values of 640 to 680 Ma. In addition, all rocks show $(^{206}Pb/^{204}Pb)_i$ values ranging from 18.16 to 19.15, $(^{207}Pb/^{204}Pb)_i$ values ranging from 15.52 to 15.58 (fig. 9B), and $(^{208}Pb/^{204}Pb)_i$ values ranging from 37.95 to 38.65 (table 2; fig. 9B).

Zircon Hf-O isotopes.—Zircon Hf isotope analyses from all samples show similar isotopic compositions with $^{176}Lu/^{177}Hf$ and $^{176}Hf/^{177}Hf$ ratios of 0.00034 to 0.00222 and 0.28291 to 0.28302, respectively (table 3). The calculated εHf (t) values range from + 11.8 to + 15.9 ($2\sigma < 1.1$; figs. 10A and 10D), T_{DM}^{C} (Hf) ages vary from 320 to 590 Ma (fig. 10E), and $f_{Lu/Hf}$ values range from -0.93 to -0.99 (table 3). The zircon Hf

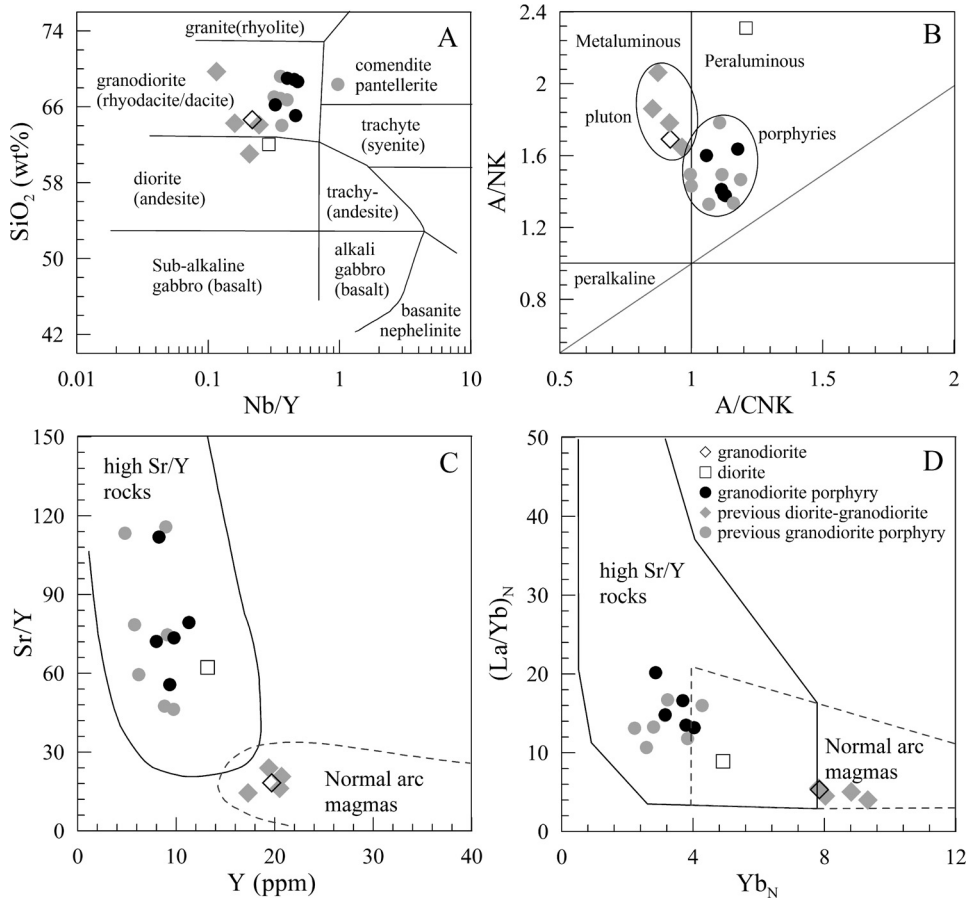

Fig. 7. Plots of (A) Nb/Y versus SiO_2 (after Winchester and Floyd, 1977), (B) A/CNK [molar ratio $Al_2O_3/(CaO+Na_2O+K_2O)$] versus A/NK [molar ratio $Al_2O_3/(Na_2O+K_2O)$], (after Maniar and Piccoli, 1989), (C) Y versus Sr/Y (after Defant and Drummond, 1990) and (D) Yb_N versus $(La/Yb)_N$ (after Martin and others, 2005) for granitoids from the Aktogai deposit. N represents chondrite-normalized value with chondrite values from Taylor and McLennan (1985). Previously published data are from Heinhorst and others (2000), Liu and others (2012) and Shen and others (2015).

isotopic data show similar but slightly lower values than depleted mantle in the Carboniferous (fig. 10).

Eighty-nine zircon $\delta^{18}O$ compositions ($2\sigma < 0.4$ ‰) show limited variations with values of + 3.8 to + 5.3 ‰ (mean + 4.8 ‰; $1\sigma = 0.32$; n = 20) for pre-ore granodiorite (A1-1), + 4.3 to + 5.7 ‰ (mean + 5.2 ‰; $1\sigma = 0.33$; n = 22), + 4.4 to + 5.9 ‰ (mean + 5.1 ‰; $1\sigma = 0.37$; n = 23) and + 4.5 to + 5.5 ‰ (mean + 5.1 ‰; $1\sigma = 0.32$; n = 24) for ore-forming granodiorite porphyry A2-1, A2-3-2 and A2-7-1, respectively (table 4; fig. 10), all of which are slightly lower than values for depleted mantle (5.3 ± 0.3 ‰).

DISCUSSION

Petrogenesis

Whole rock geochemistry shows that all the Aktogai rocks have a typical sub-alkaline arc signature: LILE and light REE enriched, right inclined REE patterns,

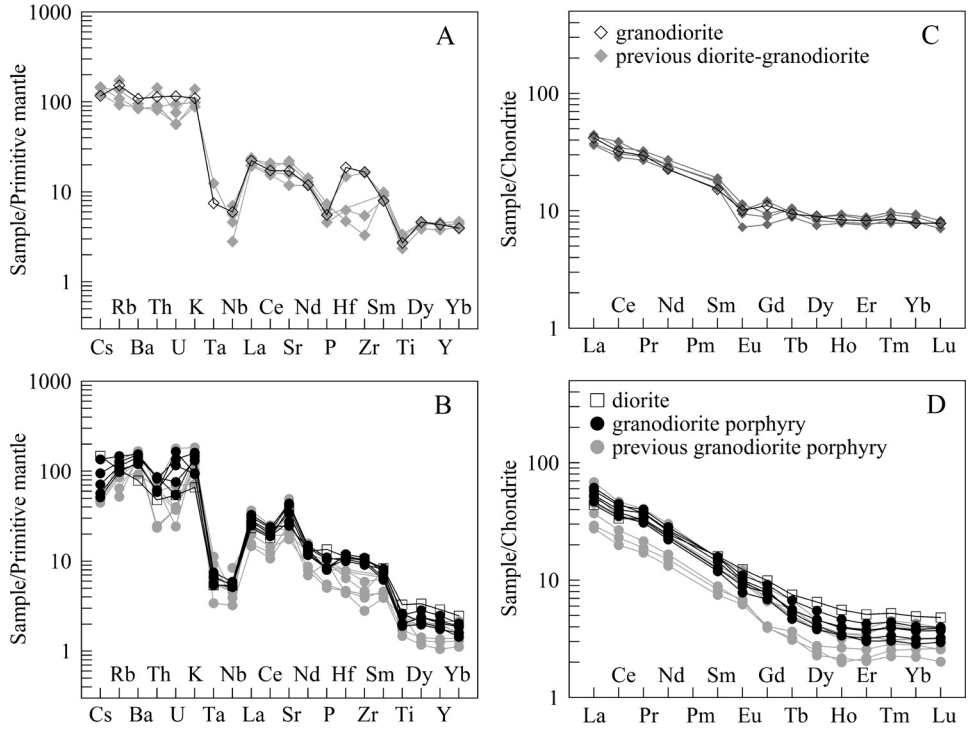

Fig. 8. Primitive mantle-normalized trace element diagrams (A, B) and Chondrite-normalized rare earth element (REE) patterns (C, D) for the Aktogai granitoids rocks. The primitive mantle values and chondrite values are from Sun and McDonough (1989), and Taylor and McLennan (1985), respectively. Data sources for previously published data of the Aktogai granitoids are the same as in figure 7.

HFSE depleted. Isotopic compositions indicate that all the Aktogai rocks share a similar magma source. Windley and others (2007) indicated that the Devonian to Carboniferous Balkhash-Yili magmatic arc, within which the giant Aktogai and Kounrad porphyry Cu deposits occur, is an Andean-type magmatic arc. The highly enriched Sr-Nd isotopic compositions ($(^{87}Sr/^{86}Sr)_i$ = 0.71050, εNd (t) = −7.8, T_2DM (Nd) = 1700 Ma) in barren granite (Kt-1) northwest of Aktogai deposit, also suggest the existence of an ancient continental crustal source (Li and others, 2016a), consistent with an Andean-type magmatic arc. Most researchers proposed that the giant Aktogai porphyry Cu deposit was formed during subduction (Heinhorst and others, 2000; Li and others, 2008; Chen and others, 2014; Shen and others, 2015; Li and others, 2016a, 2016b), similar to the giant porphyry Cu deposits in the Eastern Pacific. Thus, all the Aktogai rocks are arc-related magmatism.

Chen and others (2014) obtained a SHRIMP U-Pb age of 335.7 ± 1.3 Ma for the granodiorite [xh080919-4(1)] which also has low Sr/Y (20.7) and La/Yb (8.1) ratios (Liu and others, 2012). All mineralized porphyries have high Sr/Y ratios and ages of 327.7~331.4 Ma. In addition, the pre-ore high Sr/Y diorite (in this study), was collected near to the Aktogai ore-body (fig. 2A), while previously published diorite (AQ3; Heinhorst and others, 2000) collected probably far from the ore-body shows similar low Sr/Y features with our granodiorite. Thus, the pre-ore diorite probably intruded into the Koldar pluton between 331.4 Ma and 335.7 Ma, and likely closer to 331.4 Ma. Considering that the pre-ore diorite (in this study) is only a trace component of the Koldar pluton and younger than the major component of granodiorite with ages

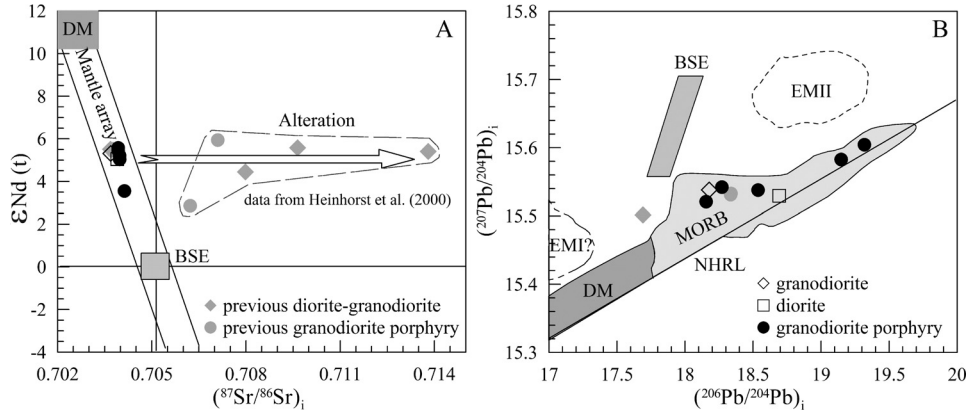

Fig. 9. Plots of (A) $(^{87}Sr/^{86}Sr)_i$ versus εNd(t) and (B) $(^{206}Pb/^{204}Pb)_i$ versus $(^{207}Pb/^{204}Pb)_i$ for rocks from the Aktogai deposit, indicating the Aktogai granitoids showing a MORB affinity. The reservoir of Mid-Oceanic Ridge Basalt (MORB) is from White and Hofmann (1982), the bulk silicate Earth (BSE) value is from Allègre and others (1988), the northern hemisphere reference line (NHRL) is from Hart (1984), the depleted mantle (DM) and enriched mantle (EMI, EMII) are from Zindler and Hart (1986). Data sources for previously published data of the Aktogai granitoids are the same as in figure 7. Figure 9A indicates that the rocks from Heinhorst and others (2000) suffered from significant hydrothermal alteration.

of 335.7~344.7 Ma (Chen and others, 2014; this study), the granodiorite (a major component) could be used to represent the general characteristics of the Koldar pluton. In addition, we also summarized all the previously published pre-ore rocks which consistently show an affinity to normal arc magmatism with high Y and Yb_N, low Sr/Y and $(La/Yb)_N$ characteristics (fig. 7). However, all the mineralized porphyries show low Y and Yb_N, high Sr/Y and $(La/Yb)_N$ (fig. 7).

Petrogenesis of the Aktogai high Sr/Y rocks.—Several genetic models have been proposed to explain the origin of arc-related high Sr/Y rocks, including: (1) magma mixing of felsic and basaltic magmas, and combined mantle or crust assimilation fractional crystallization (Guo and others, 2007); (2) high-pressure fractional crystallization (HPFC) involving garnet of basaltic magma derived from melting of the mantle wedge (Macpherson and others, 2006); (3) amphibole ± clinopyroxene fractional crystallization of parental arc basaltic magmas (Castillo and others, 1999; Davidson and others, 2007; Richards and Kerrich, 2007; Richards, 2011; Richards and others, 2012); (4) partial melting of young and hot subducted oceanic slab (Defant and Drummond, 1990); (5) partial melting of thickened basaltic lower crust (Atherton and Petford, 1993; Petford and Atherton, 1996; Chung and others, 2003; Li and others, 2011; Li and others, 2016a); (6) partial melting of delaminated lower crust (Kay and Kay, 1993; Xu and others, 2002). Each of these is considered below in relation to the origin of the Aktogai high Sr/Y rocks.

Magma mixing will form significant resorption textures and reversed mineral zoning in minerals, such as clinopyroxene phenocrysts with low Mg# cores but high Mg# mantle and rim (Guo and others, 2007), or plagioclase phenocrysts with low An core but high An mantle and rim (Tepley and othes, 2000; Cao and others, 2014c). However, the plagioclase from the Aktogai granodiorite and granodiorite porphyry do not show significant An variations, indicating a lack of significant magma mixing. In addition, magma mixing with ancient crust derived magma will usually contribute to increases in $(^{87}Sr/^{86}Sr)_i$ but decreases in εNd(t) with increasing SiO_2. The constant $(^{87}Sr/^{86}Sr)_i$ and εNd(t) values obtained in this work (figs. 11A and 11B) suggest insignificant magma mixing with high radiogenic continental crust, which is consistent

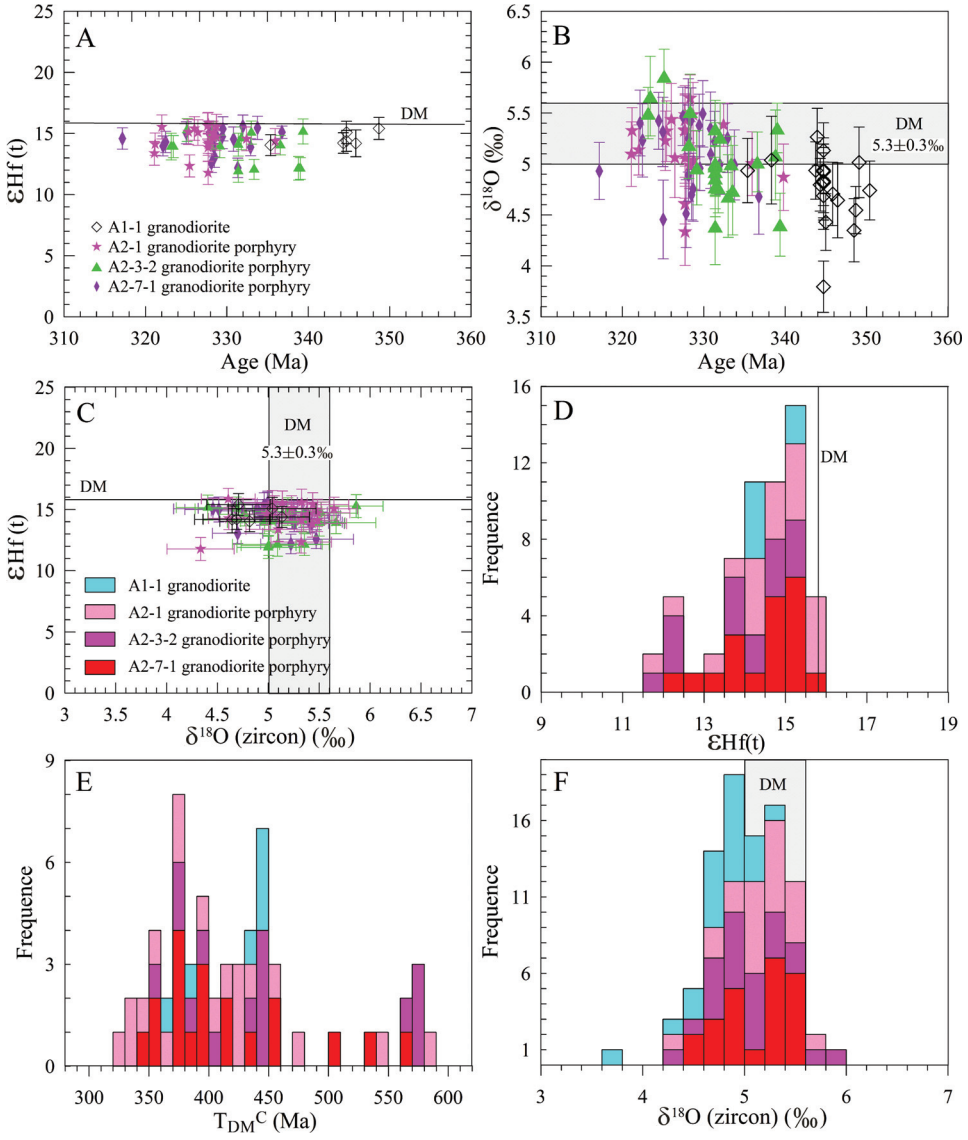

Fig. 10. Plots of age versus εHf(t) (A) and $\delta^{18}O$ (B), $\delta^{18}O$ versus εHf(t) (C), histograms of εHf(t) (D), T_{DM}^{C} (Ma) (E) and $\delta^{18}O$ (‰) (F) for zircon of granitoids from the Aktogai deposit.

with the restricted variations in zircon Hf and O isotopes [ε_{Hf} (t) = + 11.8 to + 15.9; $\delta^{18}O$ = + 3.8 to + 5.9 ‰; fig. 10].

HPFC of hydrous basaltic melts requires garnet fractionation which yields obvious geochemical trends (Macpherson and others, 2006). For example, Yb content significantly decreases with La/Yb ratios significantly increasing (fig. 11C), and La/Yb, Dy/Yb, Sr/Y ratios increase with increasing magma SiO_2 values (figs. 11D, 11E, and 11F). On the other hand, fractionation of amphibole ± clinopyroxene for parental arc basaltic magmas (Castillo and others, 1999; Davidson and others, 2007; Richards and Kerrich, 2007; Richards, 2011; Richards and others, 2012) was proposed as a preferential

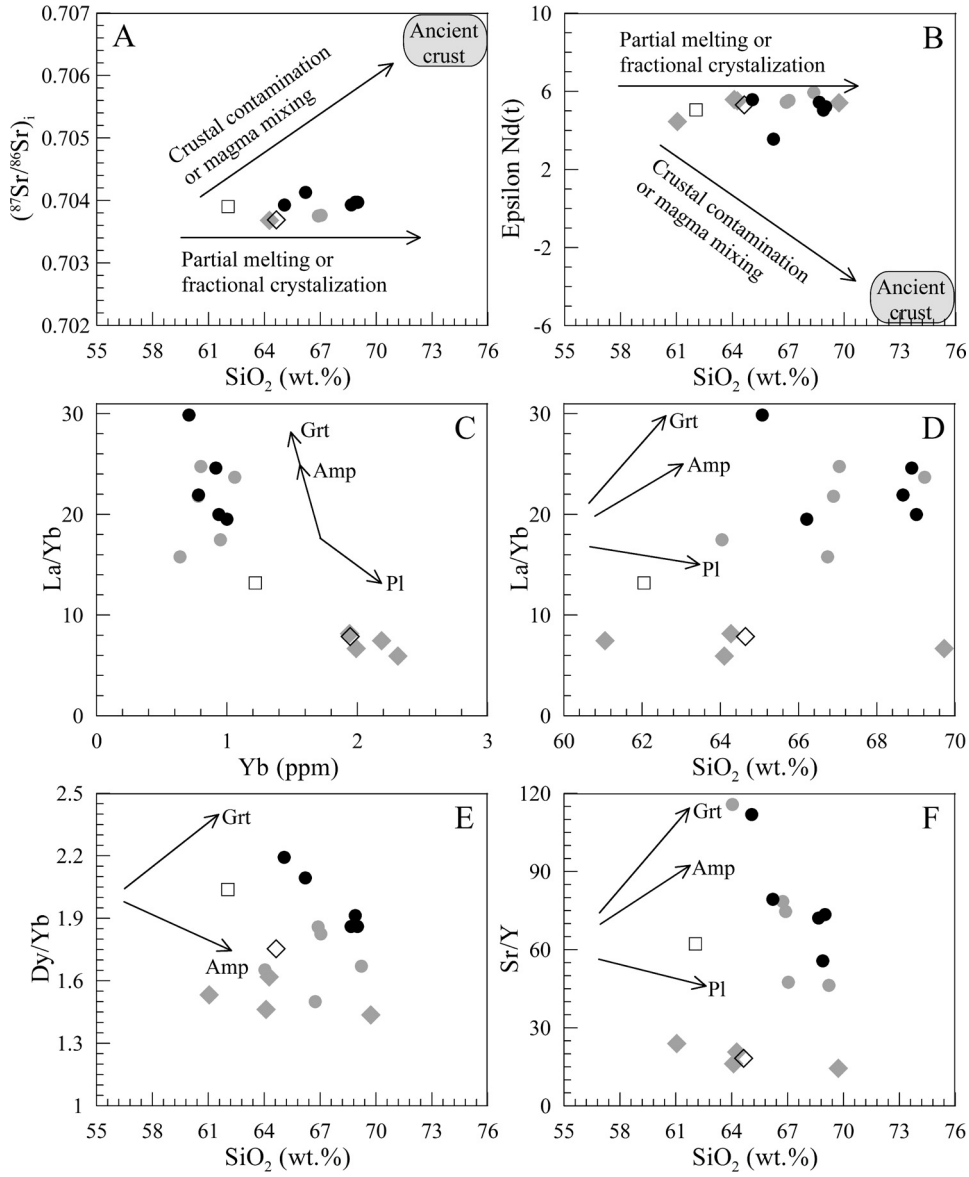

Fig. 11. Plots of SiO_2 versus $(^{87}Sr/^{86}Sr)_i$ (A), εNd (t) (B), Yb versus La/Yb (C), SiO_2 versus La/Yb (D), Dy/Yb (E) and Sr/Y (F) for granitoids from the Aktogai deposit. Crystal fractionation paths of various minerals are from Castillo and others (1999), Macpherson and others (2006); Davidson and others (2007). Due to significant alteration indicated by figure 9A, previous Sr isotopic compositions from Heinhorst and others (2000) are not shown in figure 11A. Data sources for previously published data of the Aktogai granitoids are the same as in figure 7.

mechanism for generating evolved magmas with strongly fractionated REE patterns and high Sr/Y ratios. Arc magmatic rocks usually contain high H_2O concentrations, consistent with the occurrence of hornblende and biotite in all Aktogai rocks. High H_2O contents in magma (>3%) will suppress plagioclase formation and lead to crystallization of amphibole and garnet (Moore and Carmichael, 1998; Müntener and

others, 2001; Richards and others, 2012). Due to different REE distribution coefficient (Kd) for amphibole and garnet ($Kd_{Dy/Yb}$amphibole > 1, $Kd_{Dy/Yb}$garnet < 1; Blundy and Wood, 2003), garnet fractionation will increase Dy/Yb, but amphibole fractionation will decrease Dy/Yb (Macpherson and others, 2006; Davidson and others, 2007). Figure 11E shows a decrease in Dy/Yb with differentiation for the Aktogai high Sr/Y rocks, which support the fractionation of amphibole but not garnet. However, the fractionation of amphibole and garnet will generate an evolved magma with higher contents of Sr/Y due to both $Kd_{Sr/Y}$amphibole and $Kd_{Sr/Y}$garnet $<< 1$ (Pearce and Norry, 1979; Anderson and Cullers, 1987; Martin, 1987). Figure 11F displays a decrease Sr/Y ratios with increasing SiO_2 for all rocks which does not support the fractionation of both amphibole and garnet.

In addition, the following features are not consistent with fractionation models: first, both the pre-ore and ore-forming rocks contain amphibole and biotite, indicating high H_2O contents in all rocks, while distinct geochemical characteristics occur in both rocks. Second, it is difficult to explain the obvious higher fO_2 and apatite saturation temperatures for the mineralized porphyries (figs. 5 and 14) using fractionation models. Third, fractionation models usually generate continuous evolution from low Sr/Y to high Sr/Y features (Castillo and others, 1999; Davidson and others, 2007; Richards and Kerrich, 2007; Richards, 2011), while the Aktogai pre-ore and ore-forming rocks show distinct evolution trends (fig. 11). If fractionation models are correct, the decreasing in Sr/Y with SiO_2 increasing (fig. 11) requires the fractionation of plagioclase. However, plagioclase will preferentially incorporate Eu relative to Sm and Gd (Drake and Weill, 1975) and cause the obvious negative Eu anomaly in the residual magma, which is not consistent with week Eu anomaly in high Sr/Y rocks. Thus, we propose that both the HPFC and amphibole ± clinopyroxene fractional crystallization of hydrous basaltic melts seems an unlikely mechanism for generation of the high Sr/Y rocks of the Aktogai deposit.

Both the Aktogai high Sr/Y rocks (diorite and ore-forming porphyries) and pre-ore low Sr/Y rocks show similar Sr-Nd-Pb-Hf-O isotopic compositions, indicating a common magma source for all the granitoids. All the granitoids exhibit MORB-like or depleted mantle-derived isotopes (figs. 9 and 10), suggesting an affinity with subducted oceanic crust or juvenile lower crust (defined as the model ages not much older than the formation ages and MORB-like isotopic compositions). If the high Sr/Y rocks were generated by partial melting of young and hot subducted oceanic crust (Defant and Drummond, 1990), the pre-ore rocks should also show high Sr/Y characteristics (figs. 7C and 7D). In addition, it is probable that the high Sr/Y magmas interacted with the overlying mantle wedge during ascent, and thus obtained higher contents of MgO, Ni and Co. Similarly, if the Aktogai high Sr/Y magmas were generated by partial melting of delaminated lower crust, they would also have high MgO, Ni and Co contents due to the interaction between mantle peridotite and lower crust-derived melts. However, the Aktogai high Sr/Y porphyries have relatively low MgO (1.21 – 1.63 wt.%), Ni (2.78 – 5.85 ppm) and Co (4.50 – 7.24 ppm), which is not consistent with rocks formed by melting of subducted oceanic crust or delaminated lower crust (fig. 12). Furthermore, the granitoids from the Sayak skarn Cu deposit and the Kounrad porphyry Cu deposit show coeval or slightly younger mineralization (315 Ma for Sayak and 325 – 327 Ma for Kounrad; Li and others, 2016a) than Aktogai and a petrogenetic affinity to high Sr/Y rocks (Liu and others, 2012; Shen and others, 2015). These deposits are more than 200 km and 400 km to the west of Aktogai (fig. 1). It would be very challenging to generate these types of rock with similar ages, at distinct locations, large distances apart by partial melting of young and hot subducted oceanic crust.

Although the Aktogai high Sr/Y porphyries fall in the overlap field between subducted oceanic crustal-derived high Sr/Y rocks (adakites) and thickened lower

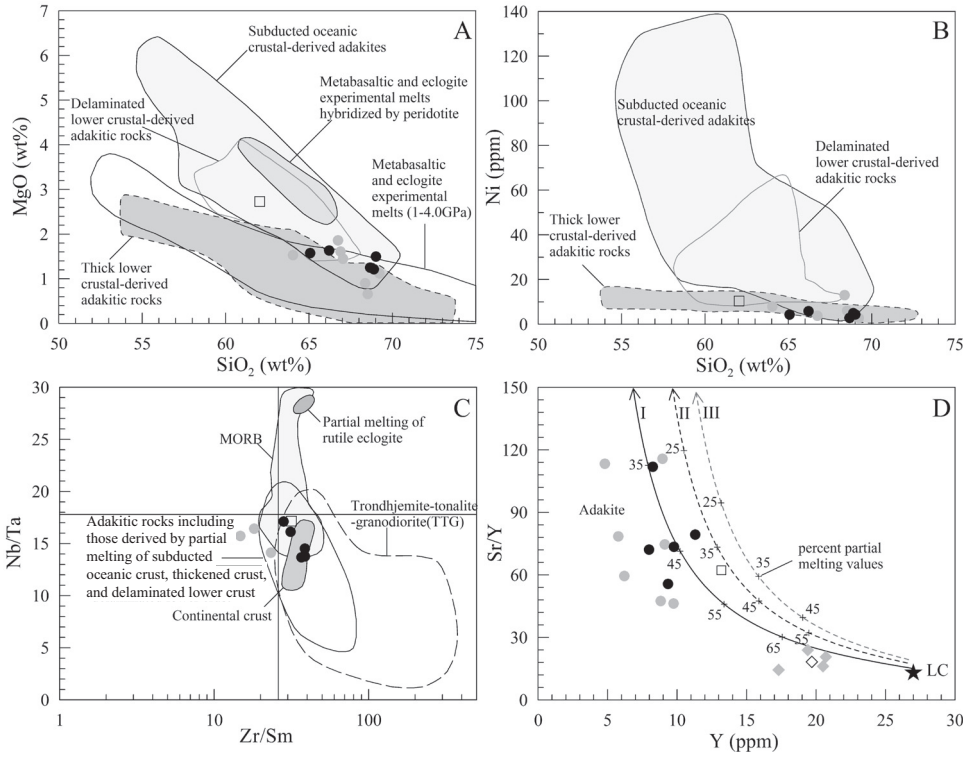

Fig. 12. Plots of SiO_2 (wt %) versus MgO wt % (A), Ni (B), Zr/Sm versus Nb/Ta (C) for the Aktogai high Sr/Y rocks, and Y versus Sr/Y (D) showing partial melting trends of (I) eclogite (50 garnet: 50 clinopyroxene), (II) eclogitic amphibolite (10 garnet:90 amphibole), (III) amphibolite (100 amphibole) with an initial lower crust composition (Wedepohl, 1995). Fields of delaminated lower crust-derived high Sr/Y rocks, subducted oceanic crust-derived high Sr/Y rocks (adakites), thick lower crust-derived high Sr/Y rocks and metabasaltic, eclogite experimental melts (1–4.0 GPa) and metabasaltic and eclogite experimental melts hybridized with peridotite in (A) and (B) are from the compilation of Wang and others (2006) and references therein. The fields in (C) are from Foley and others (2002). Percent partial melt values are listed on each of the model curves in (D). According to Shaw (1970), if the melt remains at all times in equilibrium with the residual solid, $C_{x,melt}/C_{x,initial}$ could be expressed as: $C_{x,melt}/C_{x,initial} = 1/[Dx+F(1-Dx)]$; where x is x element, $C_{x,melt}$ is concentration of x element in melt, $C_{x,initial}$ is concentration of x element in initial rock, F is the fraction of melting. Dx = bulk distribution coefficient of x element, $Dx = F_0^{\alpha}K_x^{\alpha/l}+F_0^{\beta}K_x^{\beta/l}+\ldots$, where F_0^{α} is the initial weight fraction of phase a, F_0^{β} is the initial weight fraction of phase β, $K_x^{\alpha/l}$ is the solid-liquid distribution coefficient for x element in phase α, $K_x^{\beta/l}$ is solid-liquid distribution coefficient for x element in phase β. The distribution coefficient of hornblende (0.058), garnet (0.015) and clinopyroxene (0.2) for Sr are from Pearce and Norry (1979) and hornblende (3.2), garnet (12.5) and clinopyroxene (2.0) for Y are Anderson and Cullers (1987) and Martin (1987). Data sources for previously published data of the Aktogai granitoids are the same as in figure 7.

crust-derived high Sr/Y rocks by some geochemical measures (figs. 12A and 12B), it is more likely that the Aktogai high Sr/Y rocks were derived from partial melting of thickened juvenile lower crust. On the plot of Zr/Sm versus Nb/Ta (fig. 12C; Foley and others, 2002), it is true that not all high Sr/Y rocks fall in the field of continental crust, but are more likely to locate in the field of TTG. This could be explained by the universal juvenile lower crust (Jahn and others, 2000) in the Central Asian Orogenic Belt. Young zircon T_{DM}^{C} (Hf) values (320 – 590 Ma; fig. 10E) in this study also indicate the existence of juvenile lower crust which shows more similar features with TTG than ancient continental crust. Thus, figure 12 also supports a juvelile lower crust source and does not support a source from pure subducted slab or ancient crust.

The slab melting derived rocks (adakites) always show highly oxidized characteristics (Mungall, 2002). However, juvenile, lower crust-derived rocks could also display highly oxidized conditions (Xiao and others, 2012). For example, the giant Qulong porphyry Cu deposits, Tibet (~10 Mt Cu, 0.5 Mt Mo) are genetically related to highly oxidized Miocene high Sr/Y rocks which contain widespread magmatic anhydrite as inclusions in plagioclase phenocryst, interstitial minerals between plagioclase and quartz and independent phenocrysts (Xiao and others, 2012). These highly oxidized rocks are proposed to be derived from partial melting of juvenile lower crust (Qin and others, 2014; Yang and others, 2015).

The relatively high contents of Al_2O_3 (15.54 – 17.42 wt.%) and Sr (521 – 923 ppm), and very low Y (7.09 – 13.2 ppm) and Yb (0.71 – 1.22 ppm), combined with slightly negative Eu anomalies (Eu/Eu* = 0.88 – 0.98; figs. 8C and 8D) suggest garnet and/or amphibole but little or no plagioclase in the source residue during melt extraction (Defant and Drummond, 1990; Atherton and Petford, 1993). In order to trace the assemblage in the residue and the percent of partial melting, three different residue assemblages are modeled: (I) eclogite (50 garnet: 50 clinopyroxene), (II) eclogitic amphibolite (10 garnet: 90 amphibole) and (III) amphibolite (100 amphibole). The Sr and Y contents of the lower crust are from Wedepohl (1995) based on the studies in western Europe where units are similar to those found in the Pre-Cambrian shield and Late Proterozoic to Phanerozoic fold belts of the Central Asian Orogenic belt. Figure 12D indicates that most of high Sr/Y rocks plot on the partial melting curve of (I) eclogite, with an average partial melt percentage of 45 percent, but far from the partial meting curves of (II) eclogitic amphibolite and (III) amphibolite. Thus, the high Sr/Y rocks were probably derived from partial melting of eclogitic juvenile lower crust.

Petrogenesis of the Aktogai pre-ore low Sr/Y rocks.—The pre-ore low Sr/Y rocks show similar whole rock Sr-Nd-Pb isotopes and zircon Hf-O isotopes to those of the later high Sr/Y rocks, indicating a common source. The Aktogai high Sr/Y rocks probably originated from partial melting of juvenile lower crust. Thus, the juvenile lower crust is also a likely source for the pre-ore low Sr/Y rocks. If partial melting of lower crust with similar residue assemblages (fig. 12D) is responsible for the generation of pre-ore low Sr/Y rocks, the pre-ore rocks should represent higher proportions of partial melting with lower SiO_2 than the high Sr/Y rocks, and there should be a continuous evolution trend from high Sr/Y rocks to pre-ore rocks. However, all the pre-ore low Sr/Y rocks plot below the partial melting curves (fig. 12D). In addition, these rocks show wide range of SiO_2 variations (61.0 – 69.7 wt.%) with SiO_2 contents that are not significantly lower than those of the high Sr/Y rocks. Furthermore, the pre-ore samples show distinct distribution trends compared to high Sr/Y rocks on the plots of SiO_2 versus La/Yb, Dy/Yb and Sr/Y (figs. 11D, 11E, and 11F), suggesting a different residual assemblage with absence of garnet during lower crust partial melting. The normal low Sr/Y ratios for pre-ore rocks suggest the lower crust with normal thickness (less than 30 km; Kay and Kay, 1993; Chiaradia, 2014).

Physicochemical Conditions

Temperature.—Two independent geothermometers were applied to estimate the temperature of crystallization: apatite saturation thermometry (Harrison and Watson, 1984) and zircon saturation thermometry (Watson and Harrison, 1983) (fig. 13). Restricted Sr-Nd-Hf-O isotopic compositions [$(^{87}Sr/^{86}Sr)_i$ = 0.70369 to 0.70413, $\varepsilon Nd(t)$ = + 3.6 to +5.6, $\varepsilon Hf(t)$ = + 11.8 to + 15.9, and $\delta^{18}O$ = + 3.8 to + 5.9 ‰] suggest that no samples experienced significant crustal contamination of ancient crust during magma ascent and emplacement. Constant An values in plagioclase from the Aktogai granodiorite and granodiorite porphyry indicates a lack of significant magma mixing. The petrogenesis of all samples was probably mainly controlled by partial melting

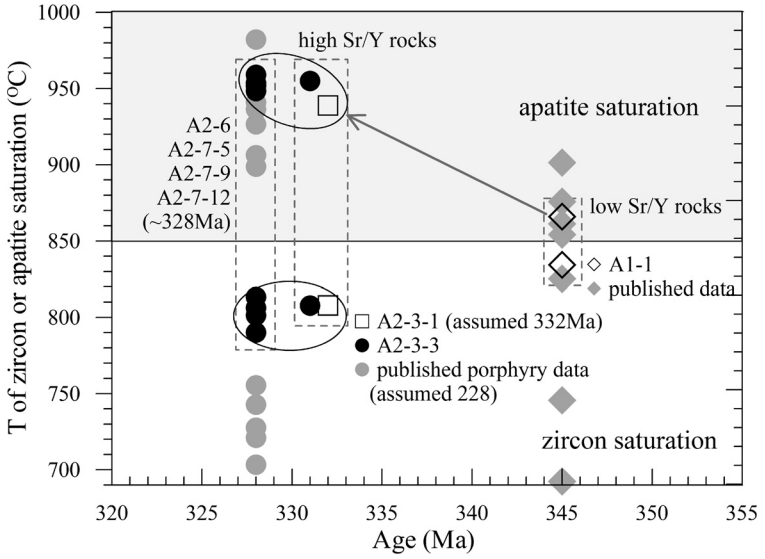

Fig. 13. Plot of age versus temperature of apatite or zircon saturation calculated after Harrison and Watson (1984) and Watson and Harrison (1983) for granitoids from the Aktogai deposit. Data sources for previously published data of the Aktogai granitoids are the same as in figure 7. Low Sr/Y granodiorite with age of 335.7 ± 1.3 (Liu and others, 2012; Chen and others, 2014) implies the high Sr/Y diorite forms between 331.4 Ma and 335.7 Ma, but closer to 331.4 Ma (332 Ma assumed in this plot).

with variable residual assemblages, but not by fractional crystallization. Thus, we use the bulk rock Zr and P_2O_5 concentrations to represent the Zr and P_2O_5 content of the melt, 47.6 weight percent of Zr according the formula of $ZrSiO_4$ and 42.0 weight percent of P_2O_5 according to the contents of apatite to represent the Zr and P_2O_5 content of zircon and apatite in the model, the temperatures of apatite-saturation ($T_{apatite\ saturation}$) and zircon-saturation ($T_{Zircon\ saturation}$) were calculated for Aktogai rocks. Results for $T_{apatite\ saturation}$ were 866 °C, 939 °C and 948 to 959 °C, and $T_{Zircon\ saturation}$ were 834 °C, 807 °C and 790 to 813 °C (fig. 13), for the granodiorite (A1-1), diorite (A2-3-1) and granodiorite porphyries, respectively (fig. 13). This indicates higher temperatures of apatite saturation relative to zircon saturation in all rocks, which is consistent with the petrographic observation of early crystallization for apatite and middle to late crystallization for zircon. Moreover, the results show higher apatite saturation for high Sr/Y rocks than for pre-ore low Sr/Y rocks (fig. 13).

Oxygen fugacity.—Although the assemblage of magnetite and ilmenite could survive under a wide range of fO_2 conditions, the obvious predominance of magnetite over ilmenite in all samples suggests a high oxidation state for these rocks. In addition, many studies have indicated that apatite would show a high SO_3 content in a highly oxidized magma (Imai and others, 1993; Parat and Holtz, 2005; Cao and others, 2012). Thus, the contents of SO_3 in apatite could be used to estimate the oxygen fugacity of the magma (Peng and others, 1997; Parat and Holtz, 2005; Smith and others, 2012; Cao and others, 2014b). The early-crystallized apatite, contained in magnetite phenocrysts, has a very high SO_3 content (0.34 – 0.64 wt.%), suggesting that the fO_2 of the porphyries was higher than NNO+1 (Peng and others, 1997; Parat and Holtz, 2005). Under this high oxygen fugacity, the magma probably contained primary anhydrite, supported by the occurrence of anhydrite inclusions in apatite (fig. 5). The widespread occurrence of veinlet anhydrite also suggests an oxidized porphyry Cu deposit system (Li and others, 2008). Although coexisting anhydrite and magnetite was not observed

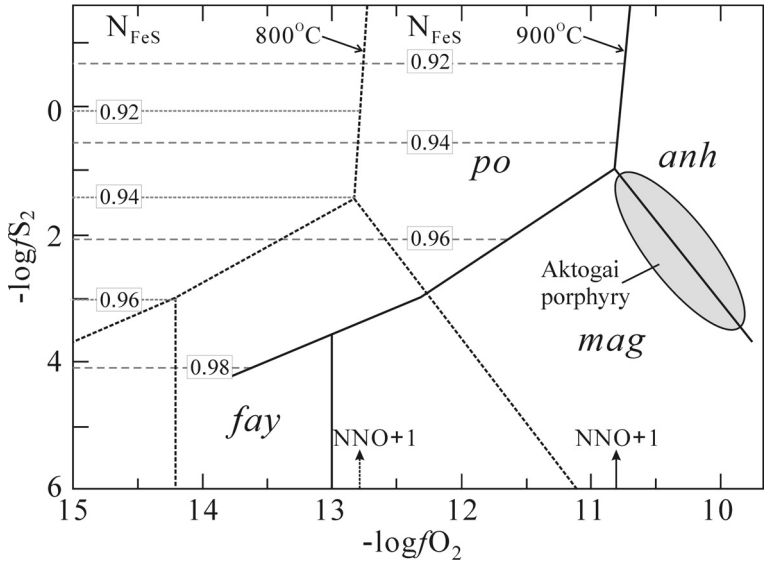

Fig. 14. Fugacity diagram of S_2 versus O_2 for Aktogai porphyritic magma. Stability fields are from Luhr (1990) and Parat and others (2002) for T = 800 and 900 °C with $P_{vapor} = P_{total} = 2$ kbar. po, pyrrhotite; anh, anhydrite; mag, magnetite; fay, fayalite. Represented N_{FeS} (= Fe/S in mole) of pyrrhotite is related to sulfur fugacity.

in the granodiorite porphyry, the occurrence of anhydrite inclusions in apatite (fig. 5) and magnetite phenocrysts (fig. 3H) implies that both the anhydrite and magnetite crystallized as early mineral phases. According to the stability field of co-existing anhydrite, pyrrhotite, and magnetite defined by experiments on El Chichón trachyandesite at 900 °C in the system O-H-S-Si-Ca-Fe-Ti (Luhr, 1990), the fS_2-fO_2 conditions for the Aktogai porphyritic magma could be constrained by the occurrence of anhydrite and magnetite, and should be $\log fS_2 > -1$ and $fO_2 >$ NNO+1 (fig. 14). This is consistent with the oxygen fugacity results determined using SO_3 contents in apatite. Due to the high volatile effect of SO_2 but not MnO, magma degassing would significantly decrease the content of SO_3 in apatite without having a significant influence on apatite MnO contents, while crystallization would decrease both the SO_3 and MnO contents in apatite. Thus, the variations of SO_3 in apatite suggest the existence of degassing at the early crystallization stage of a high Sr/Y magma. However, the average SO_3 content over a wide range of MnO contents in apatite could also be used to compare the fO_2 of different magmas. The content of maximum SO_3 (~0.3 wt.%) in porphyry apatite with widely variable MnO contents is significantly higher than maximum SO_3 (~0.1 wt.%) in apatite from the pre-ore granodiorite (A1-1) (fig. 5). This suggests higher fO_2 for the porphyry over the granodiorite.

Magma Sources

The Aktogai granitoids show very young zircon T_{DM}^{C} (Hf) values (320 – 590 Ma), suggesting the presence of juvenile mafic lower crust. In addition, the granitoids were probably derived from partial melting of juvenile mafic lower crust, without significant crustal contamination of ancient crust or mixing with ancient crust derived highly radiogenic magma during ascent and emplacement as indicated by restricted Sr-Nd-Hf-O isotopic compositions. Therefore, isotopic compositions can be used to indicate the nature of the source. All the granitoids from the Aktogai deposit show relatively enriched Sr-Nd isotopic compositions compared to depleted mantle at Carboniferous, which supports a slightly enriched mantle source, metasomatized by subducted sediment and/or fluids.

Primary zircon preserves magmatic Hf-O isotopic compositions even under strong alteration, and these signatures can be used to trace magma source (Valley and others, 2005; Kemp and others, 2007; Muñoz and others, 2012). However, O isotopes will undergo slight fractionate during magma fractional crystallization (Valley and others, 2005) and partial melting (Eiler, 2001; Muñoz and others, 2012). Melt O isotopic compositions were calculated according to the equation of δ^{18}Omelt ≈ δ^{18}OZrc + 0.0612 (wt.%SiO_2) - 2.5 (Valley and others, 2005). Assuming that the Aktogai high Sr/Y porphyries formed by partial melting of the lower crust, the SiO_2 values of porphyries were used to represent the melt SiO_2 contents (67.57 wt.%) and the δ^{18}Omelt of the Aktogai high Sr/Y porphyries was calculated to be + 6.0 to + 7.5 permil (fig. 15A). Figure 12D indicates that 35 to 55 percent partial melting of eclogitic lower crust could generate most of the high Sr/Y rocks. Assuming (1) a melting temperature of 950 °C based on $T_{apatite\ saturation}$ values; (2) a restite of 50 percent garnet and 50 percent clinopyroxene based on partial melting modeling; and (3) that the assemblage of phenocrysts (15% quartz, 55% plagioclase, 10% K-feldspar, 10% biotite, 5% amphibole, 3% magnetite, 2% apatite) represents the mineral assemblage of melt; the δ^{18}Owhole system compositions could be calculated according to the approach of Eiler (2001) and Muñoz and others (2012) as follows: (1) Calculation of mineral-pair O isotope fractionation factors based on the quartz-mineral pairs (Zheng, 1991, 1993a, 1993b, 1996). (2) Calculation of O isotope fractionation between melt and minerals comprising the residue. (3) Calculation of δ^{18}O whole system = δ^{18}Omelt - ΣIΔMelt-MxI; where I is the corresponding proportion of mineral MxI and ΣI is the proportion of residue. ΣIΔMelt-MxI values were calculated to be 0.52, 0.44, 0.36 for F(melt) = 0.35, 0.45 and 0.55, respectively (fig. 15A). When F(melt) = 0.45, the δ^{18}O (whole system) representing the δ^{18}O values of juvenile mafic lower crust show variations of + 5.5 to + 7.1 permil, slightly higher values than for depleted mantle-derived melts (5.3 ± 0.3 ‰). Juvenile lower crust forms by mantle-derived basaltic magma underplating at the base of the lower crust. Thus, the Hf-O isotopes of the lower crust could be used to trace the characteristics of mantle-derived magma.

Since Zr and Hf are conservative elements in slab fluids, and Sr and Nd are highly to moderately nonconservative elements in slab fluids (Pearce and Peate, 1995; La Flèche and others, 1998), we use a two-component Hf-O mixing model to calculate the proportion of sediment in juvenile lower crust. Considering the input of slab fluid to the mantle, the calculated sediment proportion should be the maximum value. During modeling, one end-member is characterized by depleted mantle melt Hf and O isotopic values (εHf(t) = + 15.8, δ^{18}O = +5.6 ‰; Salters and Stracke, 2004), and the other end-member by subducted oceanic sediment melt (εHf (t) = +2 from Chauvel and others, 2008; δ^{18}O = + 20 ‰ from Hoefs, 2009). The mixing calculation suggests that the source of juvenile lower crust is dominantly mantle-derived magmas (>90%) with the sediment melt proportion making up less than 10 percent (fig. 15B). In addition, average zircon Hf-O isotopes of A2-1, A2-3-2 and A2-7-1 granodiorite porphyries could be generated by less than 6 percent addition of sediment to the depleted mantle with $C_{DM}/C_{sediment}$ (Hf) = 1:2 (0.5; the ratio of Hf concentration in the depleted mantle and sediment (fig. 15B). Furthermore, a $C_{DM}/C_{sediment}$ (Hf) ratio of 0.5 not only supports the addition of sediment melt into the mantle melt, but also supports the dominance of sediment melt over fluid, since the reverse would generate C_{DM}/C_{fluid} (Hf)>>0.5 due to the conservative characteristics of Hf in slab fluids. Therefore, the juvenile lower crust was generated by less than 10 percent addition of subducted oceanic sediment melt with a small proportion of slab fluids added to the depleted mantle source.

Geodynamic Processes

Zircon U-Pb dating indicates that the pre-ore Koldar pluton and ore-forming porphyries were generated in the Carboniferous (344 – 328 Ma). These rocks can be

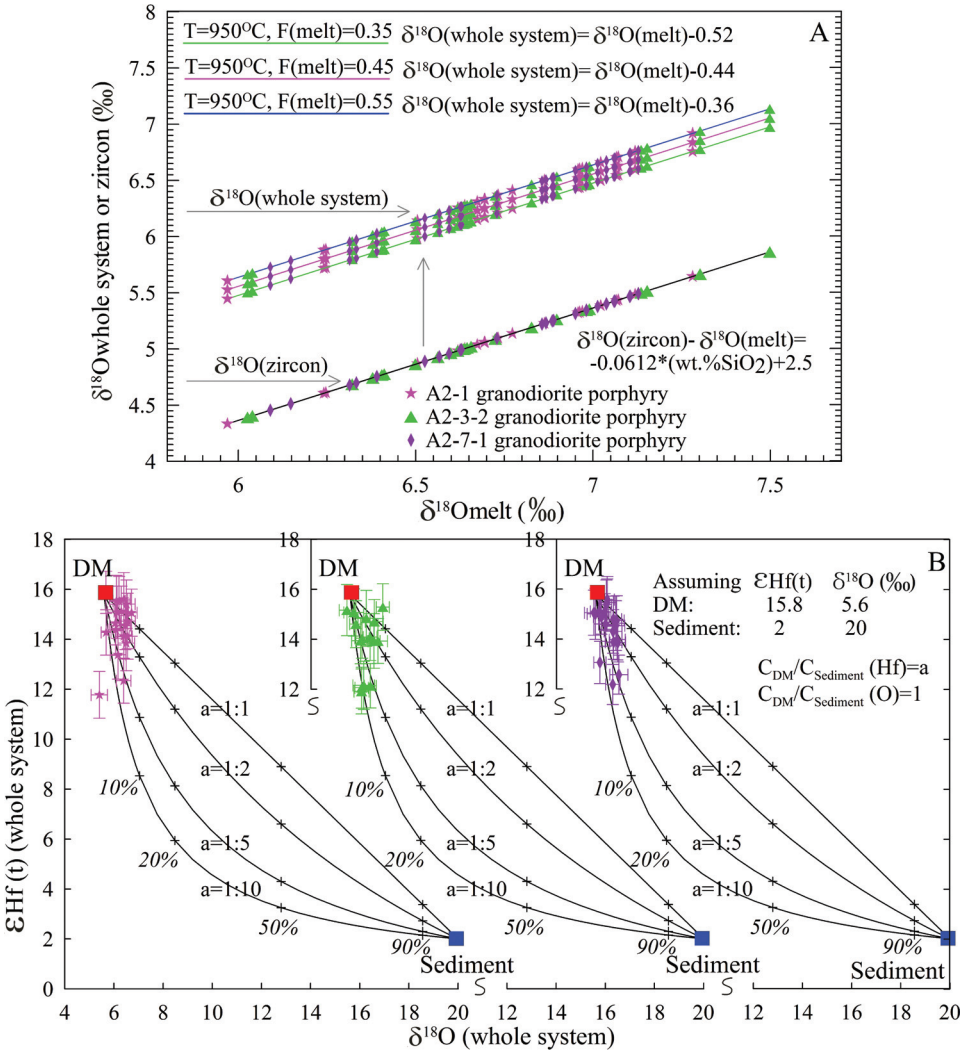

Fig. 15. Plots of (A) δ^{18}Omelt versus δ^{18}O (whole system) or zircon and (B) δ^{18}O (whole system) versus εHf(t)whole system for porphyries from the Aktogai deposit. The values of δ^{18}Omelt and δ^{18}O (whole system) calculated according to the approach of Eiler (2001) and Muñoz and others (2012). Please see the text for more details. The compositions of the end-members for mixing calculations are: (1) depleted mantle melt (DM): εHf (t) = 15.8, δ^{18}O = 5.6 ‰ (Salters and Stracke, 2004); (2) subducted oceanic sediment melt: εHf (t) = 2 (Chauvel and others, 2008), δ^{18}O = 20 ‰ (Hoefs, 2009). The mixing curves were calculated using different DM/Sediment elemental concentration ratios shown on the plots. The small cross on the curves represents the percent of mixing by sediment melt to the depleted mantle melt.

divided into two groups based on their geochemical characteristics: pre-ore Koldar pluton with characteristics of low Sr/Y ratios (normal arc magmatism), and later high Sr/Y rocks including the pre-ore diorite (trace component) and ore-forming porphyries. These samples have similar Sr-Nd-Pb-Hf-O isotopic compositions, indicating a common source for these granitoids. The very young zircon T_{DM}^{C} (Hf) values (320 – 590 Ma) indicate that these rocks were formed by partial melting of juvenile mafic lower crust. Partial melting simulations indicate that the pre-ore low Sr/Y Koldar pluton was probably produced by partial melting of normal thick juvenile lower crust,

while the Aktogai high Sr/Y rocks were probably generated by partial melting of eclogitized lower crust (fig. 12).

It is possible to combine our data with published work to deduce the mechanism responsible for melting of the lower crust. During the subduction of Junggar-Balkhash oceanic crust (Filippova and others, 2001; Windley and others, 2007), dehydrated fluid and sediment were released from the slab to metasomatize the overlying mantle wedge, causing it to melt and form an arc basaltic magma enriched in volatiles, sulfur and fluid-mobile LILE (such as Rb, K, Cs, Ba and Sr) (fig. 16A). This hot basaltic magma ascended from the mantle wedge and was emplaced at the base of the crust, forming an underplating layer, which became hot and caused partial melting of the overlying, pre-existing, non-eclogitized or normal-thickness lower crust within zone of melting, assimilation, storage and homogenization at the base of the crust (MASH; Hildreth and Moorbath, 1988; Winter, 2001; Richards, 2003), generating pre-ore calc-alkaline arc magmatism with low Sr/Y(18.32) and $(La/Yb)_N$ (5.32) (fig. 16A).

With more basaltic magma stored at the base of the crust, the lower crust was thickened significantly and transformed to eclogite or eclogitic amphibole composition. This thickening of the lower crust must have happened between the emplacement of pre-ore granodiorite (345 Ma) and the beginning of generation of the high Sr/Y rocks (diorite age >331 Ma), a duration of approximately <14 Myr. A similar timespan was postulated for the thickening of lower crust during subduction in northern Chile, where Paleocene-Early Eocene normal low Sr/Y magmatism is associated with small porphyry Cu deposits and Late Eocene-Early Oligocene high Sr/Y rocks hosting huge porphyry Cu deposits (Oyarzun and others, 2001). Although many researchers suggested that high Sr/Y rocks were derived from lower crust with thickness of >50 km (Chung and others, 2003), Qian and Hermann (2013) indicated that the most appropriate T and crustal thickness for generating lower crust-derived high Sr/Y rocks are 800 to 950 °C and 30 to 40 km. Apatite saturation temperatures indicate that the high Sr/Y rocks crystallized at 950 °C. It is reasonable to suggest that the lower crust increased in thickness from less than 30 km to 30 to 40 km during 344 to 331 Ma due to the continued addition and storage of metasomatized mantle wedge-derived basaltic magma (Winter, 2001; Richards, 2003).

High contents of MgO and Ni were recorded in delaminated lower crust-derived high Sr/Y rocks (Kay and Kay, 1993; Xu and others, 2002), while the Aktogai high Sr/Y rocks had low contents of MgO (1.21 – 1.63 wt.%) and Ni (2.78 – 5.85 ppm), suggesting foundering of lithospheric root but not thickened lower crust. The foundering of lithospheric mantle would cause upwelling of underlying hot asthenosphere, which would significantly heat the overlying eclogitized thickened lower crust and cause partial melting to generate high Sr/Y magmatism (fig. 16B). Thus, the foundering of lithospheric mantle should coincide with, or occur slightly before, high Sr/Y magmatism (331 Ma). Significant higher apatite saturation temperatures for high Sr/Y rocks than for pre-ore low Sr/Y samples indicates a higher temperature of partial melting, which is consistent with the upwelling of hot asthenosphere. The partial melting of thickened juvenile lower crust within the MASH zone formed the high Sr/Y magma, which ascended to the shallow crust to form the ore-bearing porphyries at the Aktogai deposit.

Arc magmatism, especially in large to giant porphyry copper deposits, shows high oxidation states (f_{O2} > NNO+1; Mungall, 2002; Richards, 2003). The origin of the high oxidation in porphyry Cu deposit systems is controversial, being either inherited from the oxidized sub-arc mantle (Kelley and Cottrell, 2009; Evans and others, 2012) or acquired during magmatic differentiation (Lee and others, 2010, 2012). Considering that all samples studied herein were probably derived by partial melting of the lower crust, the oxygen fugacity of the magma could reflect the oxidation state of magma source (lower crust and mantle wedge). Significantly higher SO_3 content in

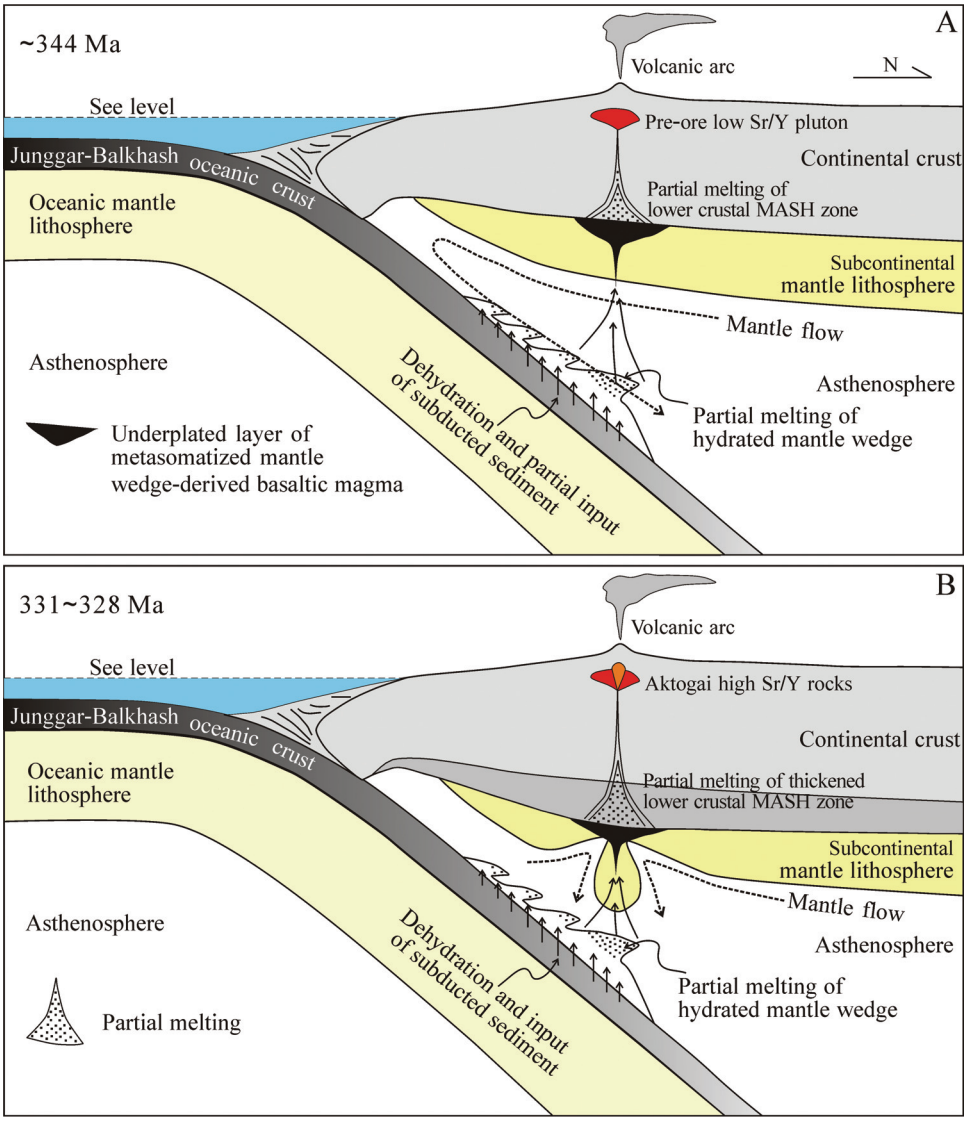

Fig. 16. Schematic illustration showing the petrogenetic models for the pre-ore metaluminous granodiorite and ore-forming high Sr/Y porphyries at the Aktogai deposit (modified after Winter, 2001; Richards, 2003; Li and others, 2016a, 2016b). (A) 344 Ma: Normal arc magmatism represented by the pre-ore major component of Koldar pluton was formed by partial melting of juvenile mafic lower crust which was generated by storage of basaltic melts derived from the metasomatized mantle wedge during the northward subduction of Junggar-Balkhash oceanic plate (Filippova and others, 2001; Windley and others, 2007); (B) 331~328 Ma: Formation of high Sr/Y rocks by partial melting of eclogitized thickened and sulfide-rich juvenile lower crust which was heated by upwelling hot asthenosphere due to the foundering of subcontinental mantle lithosphere.

porphyritic apatite relative to pre-ore granodioritic apatite suggests an increase in fO_2 from pre-ore granodiorite to porphyries. Thus, the fO_2 of lower crust has probably increased during 344.7 Ma to 331.4 Ma. The Cu contents of pre-ore low Sr-Y rocks vary from 58 to 87 ppm (Heinhorst and others, 2000; this study). This is consistent with the Cu contents of primitive arc magmas (50 – 90 ppm from Lee and others, 2012) and a not highly oxidized sub-arc mantle wedge since magmatic Cu contents are >200 ppm

under high fO_2 (Lee and others, 2012). Partial melting of normal thickness lower crust within MASH zone to produce the Koldar low Sr/Y rocks, required relatively low oxygen fugacity conditions in the mantle and juvenile lower crust and early Cu-rich sulfide fractionation and accumulation in the lower crust (Lee and others, 2012; Richards, 2013; Chiaradia, 2014). Chiaradia (2014) indicated that a large amount of Cu can be gradually accumulated within or at the base of the crust of thicker arc segments and may be incorporated into later high fO_2 magmas. Due to the continued input of dehydrated supercritical fluids and sediment melts (Mungall, 2002), the oxygen fugacity of mantle wedge and mantle-derived basaltic melt gradually increased. At the time of lithospheric mantle foundering, the fO_2 of the basaltic magma within MASH zone was high, probably keeping sulfide undersaturated and S in the form of S^{6+} which is consistent with the occurrence of primary anhydrite without pyrrhotite (fig. 5). Due to the heating of upwelling hot asthenosphere, partial melting of the thickened lower crust incorporated all the sulfide previously accumulated at the lower crust and formed the Aktogai high Sr/Y rocks with high mineralization potential. With the emplacement of the high Sr/Y porphyries, ore-forming fluids exsolved from the highly oxidized magma and caused the development of a huge alteration zone, and also precipitated ore-forming elements in the form of sulfide in different alteration zones.

CONCLUSIONS

(1) SIMS zircon U-Pb isotopic compositions show that the pre-ore granodiorite and mineralized porphyries formed at 344.7 and 327.7 to 331.4 Ma, respectively.

(2) Whole rock geochemistry indicates that the pre-ore major component of the Koldar pluton (granodiorite) and mineralized porphyries show different geochemistry (low Sr/Y and high Sr/Y rocks, respectively), but both exhibit an affinity for arc magmatism with a strong depletion in Nb, Ta and Ti and enrichment in LREE and LILE.

(3) All the granitoids show similar Sr-Nd-Pb-Hf-O isotopic compositions (($^{87}Sr/^{86}Sr)_i$ = 0.70369 to 0.70413, ε_{Nd} (t) = + 3.6 to + 5.6, ($^{206}Pb/^{204}Pb)_i$ = 18.16 to 19.32, ($^{207}Pb/^{204}Pb)_i$ = 15.52 to 15.60, ($^{207}Pb/^{204}Pb)_i$ = 37.95 to 38.65, zircon ε_{Hf} (t) = + 11.8 to + 15.9 and $\delta^{18}O$ = + 3.8 to + 5.9 ‰), and very young whole rock T_2DM (Nd) (640 to 680 Ma) and zircon $T_{DM}{}^{C}$ (Hf) (320 – 590 Ma), indicating that they were sourced from a juvenile lower crust.

(4) We proposed that the pre-ore low Sr/Y rocks were probably formed by partial melting of normal thick juvenile lower crust under relatively reducing condition during the subduction of Junggar-Balkhash oceanic crust, while the high Sr/Y rocks were generated by partial melting of thickened, eclogitized and sulfide-rich juvenile lower crust under moderately oxidizing condition.

ACKNOWLEDGMENTS

The authors are greatly indebted to Qiuli Li and Guoqiang Tang for assistance with zircon U-Pb-O isotopic analyses, Qian Mao and Yuguang Ma for assistance with mineral chemistry, He Li and Xindi Jin for assistance with whole rock major and trace elements analyses, Chaofeng Li and Xianghui Li for assistance with whole rock Sr-Nd-Pb isotopic analyses, Yueheng Yang and Yang Li for assistance with *in situ* zircon Hf isotopic analyses. The manuscript was improved by the thoughtful comments of Dr. Jeremy P. Richards, Dr. Elburg, Dr. Farmer and Dr. Richard Price. In particular, we express our gratitude to Dr. James Mungall, one anonymous reviewer and the Associate Editor Richard Walker for their constructive comments and excellent suggestions that helped to improve the manuscript. This work was supported by National Natural Sciences Foundation of China (41402081, 41390444), International Postdoctoral Exchange Fellowship Program of China (20150085), China Scholarship Council Fund (201404910182) and Special Fund for Scientific Research in the Public Interest of Ministry of Land and Resources of China (201411024-5).

TABLE A1

EPMA of chemical composition (wt. %) and calculated formula of apatite from the Aktogai porphyry Cu deposit, Central Kazakhstan

Sample		A1-1 granodiorite										
Occurrence		growing with magnetite										
No.	detection limit	1	2	3	4	5	6	7	8	9	10	11
P_2O_5	0.08	42.82	41.67	42.44	41.70	42.32	42.49	42.36	42.19	41.95	41.60	42.08
CaO	0.02	54.25	53.59	53.85	53.34	53.74	53.44	54.04	54.65	53.03	53.25	53.31
SiO_2	0.05	0.21	0.28	0.19	0.21	0.26	0.24	0.22	0.12	0.21	0.29	0.32
FeO	0.02	0.41	0.44	0.26	0.28	0.33	0.30	0.40	0.20	0.29	0.37	0.29
MnO	0.02	0.07	bdl	0.06	0.13	bdl	0.16	0.04	0.04	0.19	0.13	0.11
Na_2O	0.03	0.04	bdl	0.03	0.10	0.05	0.14	0.08	bdl	0.08	bdl	0.05
Cl	0.01	0.34	0.15	0.32	0.90	0.60	0.70	1.30	0.37	1.78	1.65	1.70
F	0.02	3.45	3.30	3.20	2.83	3.12	2.78	2.67	2.85	2.31	2.34	2.60
SO_3	0.02	0.07	0.17	0.15	0.02	0.09	0.05	0.05	bdl	0.09	bdl	0.03
F,Cl=-O		0.15	0.30	0.34	0.35	0.27	0.54	0.36	0.63	0.40	0.43	0.19
Total		101.50	99.31	100.16	99.16	100.23	99.76	100.79	99.79	99.54	99.20	100.31
Cations per formula unit on the basis of 26 O												
P^{5+}		6.045	5.993	6.047	6.027	6.043	6.059	6.029	6.020	6.045	6.023	6.044
Ca^{2+}		9.692	9.752	9.710	9.755	9.711	9.643	9.733	9.867	9.670	9.758	9.691
Si^{4+}		0.035	0.048	0.032	0.036	0.043	0.040	0.036	0.020	0.036	0.050	0.055
Fe^{3+}		0.057	0.062	0.036	0.040	0.046	0.042	0.056	0.029	0.041	0.053	0.040
Mn^{2+}		0.010	0.001	0.009	0.019	0.001	0.023	0.006	0.006	0.028	0.018	0.016
Na^{+}		0.014	0.000	0.009	0.033	0.017	0.047	0.026	0.000	0.026	0.003	0.016
Cl^{-}		0.095	0.043	0.092	0.261	0.170	0.199	0.370	0.106	0.514	0.477	0.490
F^{-}		1.818	1.775	1.705	1.527	1.666	1.481	1.418	1.517	1.243	1.263	1.397
S^{6+}		0.008	0.022	0.019	0.003	0.011	0.006	0.006	0.001	0.012	0.001	0.004
O^{2-}		25.000	25.000	25.000	25.000	25.000	25.000	25.000	25.000	25.000	25.000	25.000
X(Fap)		0.909	0.887	0.852	0.764	0.833	0.741	0.709	0.758	0.622	0.632	0.698
X(Cap)		0.047	0.021	0.046	0.131	0.085	0.099	0.185	0.053	0.257	0.238	0.245
X(Hap)		0.044	0.091	0.102	0.106	0.082	0.160	0.106	0.189	0.121	0.130	0.057
O(F)		1.818	1.775	1.705	1.527	1.666	1.481	1.418	1.517	1.243	1.263	1.397
O(Cl)		0.095	0.043	0.092	0.261	0.170	0.199	0.370	0.106	0.514	0.477	0.490

Table A1
(continued)

Sample	A1-1 granodiorite												
Occurrence	growing with biotite												
No.	1	2	3	4	5	6	7	8	9	10	11	12	13
P_2O_5	42.34	42.49	41.83	41.85	42.31	42.11	42.23	41.89	41.98	42.72	42.59	41.61	41.53
CaO	55.14	55.34	53.47	53.37	54.91	53.85	53.71	53.77	53.99	55.42	54.49	53.49	53.61
SiO_2	0.15	0.13	0.20	0.14	0.16	0.16	0.20	0.17	0.22	0.09	0.15	0.29	0.21
FeO	0.27	0.30	0.33	0.35	0.29	0.40	0.40	0.42	0.56	0.22	0.24	0.43	0.38
MnO	bdl	0.04	0.03	0.07	0.07	0.11	0.04	0.07	0.07	0.05	bdl	0.16	0.03
Na_2O	bdl	bdl	0.06	0.10	bdl	0.08	0.16	0.08	bdl	bdl	bdl	0.17	0.03
Cl	0.11	0.14	1.75	1.62	0.15	0.90	0.91	0.94	0.25	0.17	0.11	0.70	0.74
F	3.20	3.37	2.45	2.39	3.30	3.11	3.18	2.98	3.21	3.37	3.53	2.79	2.72
SO_3	bdl	bdl	0.07	0.07	bdl	0.11	0.08	0.08	bdl	0.02	bdl	0.06	0.07
F,Cl=-O	0.47	0.31	0.30	0.41	0.36	0.14	0.08	0.22	0.36	0.31	0.17	0.50	0.53
Total	100.74	101.50	99.89	99.54	100.82	100.68	100.82	100.17	99.92	101.75	100.92	99.20	98.80
Cations per formula unit on the basis of 26 O													
P^{5+}	6.001	6.001	6.027	6.035	6.005	6.019	6.032	6.014	6.003	6.013	6.045	5.995	5.999
Ca^{2+}	9.890	9.891	9.748	9.740	9.863	9.742	9.710	9.769	9.771	9.872	9.787	9.753	9.801
Si^{4+}	0.026	0.021	0.034	0.024	0.026	0.026	0.034	0.028	0.036	0.015	0.026	0.049	0.037
Fe^{3+}	0.038	0.042	0.047	0.050	0.041	0.056	0.057	0.059	0.080	0.030	0.033	0.061	0.054
Mn^{2+}	0.001	0.006	0.004	0.011	0.010	0.016	0.005	0.010	0.009	0.007	0.000	0.023	0.005
Na^{+}	0.000	0.000	0.020	0.032	0.000	0.027	0.051	0.027	0.002	0.005	0.000	0.057	0.009
Cl^{-}	0.031	0.038	0.504	0.468	0.041	0.258	0.260	0.269	0.072	0.049	0.030	0.203	0.214
F^{-}	1.693	1.777	1.318	1.288	1.748	1.658	1.695	1.599	1.715	1.770	1.869	1.499	1.469
S^{6+}	0.002	0.000	0.009	0.009	0.000	0.014	0.010	0.010	0.000	0.003	0.000	0.008	0.009
O^{2-}	25.000	25.000	25.000	25.000	25.000	25.000	25.000	25.000	25.000	25.000	25.000	25.000	25.000
X(Fap)	0.847	0.889	0.659	0.644	0.874	0.829	0.847	0.800	0.858	0.885	0.934	0.749	0.734
X(Cap)	0.015	0.019	0.252	0.234	0.021	0.129	0.130	0.134	0.036	0.024	0.015	0.101	0.107
X(Hap)	0.138	0.092	0.089	0.122	0.105	0.042	0.023	0.066	0.106	0.090	0.051	0.149	0.159
O(F)	1.693	1.777	1.318	1.288	1.748	1.658	1.695	1.599	1.715	1.770	1.869	1.499	1.469
O(Cl)	0.031	0.038	0.504	0.468	0.041	0.258	0.260	0.269	0.072	0.049	0.030	0.203	0.214

Table A1

(continued)

Sample	A2-6 granodiorite porphyry													
Occurrence	contained in magnetite phenocryst								occuring as phenocryst					
No.	1	2	3	4	5	6	7	8	1	2	3	4	5	6
P_2O_5	42.43	42.46	42.59	42.26	42.35	42.40	42.30	42.50	42.27	42.35	43.20	42.55	42.64	42.77
CaO	53.10	52.86	52.97	52.32	52.60	52.70	52.38	52.91	54.33	53.89	54.77	54.31	53.84	54.54
SiO_2	0.20	0.22	0.25	0.20	0.23	0.24	0.21	0.24	0.07	0.03	0.01	0.07	0.13	0.08
FeO	0.75	0.58	0.84	1.30	1.00	1.15	1.27	0.94	0.22	0.25	0.22	0.31	0.23	0.22
MnO	0.29	0.28	0.30	0.28	0.32	0.28	0.29	0.29	0.33	0.32	0.24	0.27	0.31	0.30
Na_2O	0.08	0.08	0.13	0.22	0.17	0.19	0.20	0.15	0.13	0.17	0.03	0.08	0.10	bdl
Cl	0.97	0.97	0.97	1.31	1.15	1.20	1.27	1.05	0.40	0.41	0.36	0.44	0.39	0.36
F	2.28	2.32	2.29	2.07	2.15	2.20	2.10	2.25	2.87	2.90	3.08	2.91	2.99	2.93
SO_3	0.37	0.34	0.40	0.64	0.52	0.54	0.60	0.45	0.16	0.28	0.23	0.17	0.22	0.24
F,Cl=-O	0.87	0.83	0.87	0.90	0.90	0.84	0.89	0.87	0.61	0.57	0.48	0.57	0.52	0.61
Total	99.60	99.27	99.86	99.71	99.59	100.06	99.73	99.91	100.17	100.02	101.67	100.55	100.31	100.83
Cations per formula unit on the basis of 26 O														
P^{5+}	6.027	6.045	6.029	5.995	6.011	6.002	6.000	6.016	6.012	6.021	6.067	6.026	6.042	6.028
Ca^{2+}	9.547	9.523	9.488	9.394	9.448	9.440	9.403	9.479	9.778	9.696	9.735	9.734	9.655	9.729
Si^{4+}	0.034	0.036	0.042	0.034	0.039	0.040	0.035	0.040	0.012	0.006	0.002	0.012	0.022	0.013
Fe^{3+}	0.105	0.082	0.118	0.182	0.140	0.161	0.178	0.131	0.031	0.035	0.031	0.044	0.032	0.030
Mn^{2+}	0.041	0.040	0.042	0.040	0.045	0.040	0.041	0.041	0.047	0.046	0.034	0.039	0.043	0.043
Na^{+}	0.026	0.024	0.041	0.073	0.055	0.062	0.065	0.049	0.041	0.054	0.010	0.027	0.031	0.000
Cl^{-}	0.277	0.276	0.274	0.373	0.327	0.340	0.361	0.298	0.115	0.117	0.102	0.124	0.110	0.103
F^{-}	1.209	1.233	1.210	1.095	1.140	1.163	1.113	1.190	1.522	1.542	1.618	1.540	1.583	1.541
S^{6+}	0.047	0.042	0.050	0.081	0.065	0.068	0.075	0.056	0.020	0.036	0.004	0.021	0.028	0.030
O^{2-}	25.000	25.000	25.000	25.000	25.000	25.000	25.000	25.000	25.000	25.000	25.000	25.000	25.000	25.000
X(Fap)	0.604	0.617	0.605	0.548	0.570	0.582	0.556	0.595	0.761	0.771	0.809	0.770	0.792	0.770
X(Cap)	0.138	0.138	0.137	0.186	0.163	0.170	0.180	0.149	0.058	0.058	0.051	0.062	0.055	0.051
X(Hap)	0.257	0.245	0.258	0.266	0.267	0.248	0.263	0.256	0.181	0.171	0.140	0.168	0.154	0.178
O(F)	1.209	1.233	1.210	1.095	1.140	1.163	1.113	1.190	1.522	1.542	1.618	1.540	1.583	1.541
O(Cl)	0.277	0.276	0.274	0.373	0.327	0.340	0.361	0.298	0.115	0.117	0.102	0.124	0.110	0.103

Table A1

(continued)

Sample	A2-6 granodiorite porphyry														
Occurrence	growing with rutile and magnetite										occuring in matrix core				
No.	1	2	3	4	5	6	7	8	9	10	1	2	3	4	5
P_2O_5	42.69	42.97	43.29	43.24	42.79	42.34	42.75	42.41	42.82	43.14	42.51	42.55	42.05	42.09	42.00
CaO	54.53	54.31	54.96	54.51	54.45	53.52	54.04	54.40	54.49	53.96	53.90	54.47	53.83	54.34	54.12
SiO_2	0.10	bdl	bdl	bdl	bdl	0.18	0.19	0.12	0.08	bdl	0.13	0.11	0.18	0.19	0.10
FeO	0.28	0.22	0.28	0.40	0.47	0.33	0.32	0.33	0.32	0.35	0.24	0.28	0.29	0.23	0.19
MnO	0.34	0.35	0.19	0.17	0.23	0.25	0.39	0.27	0.27	0.33	0.33	0.26	0.29	0.30	0.29
Na_2O	0.10	0.06	0.03	0.05	bdl	0.10	0.08	0.11	0.15	bdl	bdl	0.06	0.06	0.15	0.13
Cl	0.41	0.39	0.27	0.29	0.38	0.42	0.41	0.37	0.36	0.38	0.50	0.54	0.55	0.45	0.44
F	2.89	3.12	3.05	3.08	2.99	2.85	2.92	3.01	2.89	3.15	3.03	3.02	3.02	2.90	2.81
SO_3	0.26	0.22	0.23	0.26	0.28	0.26	0.25	0.25	0.21	0.28	0.24	0.25	0.17	0.24	0.24
F,Cl=-O	0.62	0.42	0.56	0.51	0.54	0.61	0.59	0.51	0.65	0.40	0.42	0.43	0.39	0.56	0.63
Total	100.98	101.22	101.75	101.48	101.04	99.65	100.75	100.76	100.94	101.19	100.45	101.11	100.04	100.32	99.70
Cations per formula unit on the basis of 26 O															
P^{5+}	6.008	6.050	6.061	6.071	6.043	6.022	6.028	6.001	6.024	6.087	6.031	6.009	6.012	5.983	5.995
Ca^{2+}	9.713	9.678	9.737	9.686	9.731	9.632	9.643	9.742	9.702	9.637	9.678	9.735	9.741	9.774	9.778
Si^{4+}	0.017	0.000	0.000	0.000	0.000	0.031	0.031	0.020	0.014	0.000	0.021	0.019	0.030	0.031	0.018
Fe^{3+}	0.039	0.030	0.039	0.056	0.066	0.047	0.045	0.046	0.044	0.048	0.033	0.039	0.041	0.033	0.027
Mn^{2+}	0.048	0.049	0.027	0.024	0.032	0.035	0.055	0.038	0.038	0.047	0.047	0.037	0.041	0.043	0.042
Na^{+}	0.032	0.019	0.009	0.017	0.000	0.031	0.027	0.036	0.048	0.000	0.007	0.021	0.020	0.048	0.043
Cl^{-}	0.116	0.111	0.076	0.082	0.106	0.120	0.115	0.104	0.101	0.106	0.141	0.152	0.157	0.127	0.126
F^{-}	1.521	1.642	1.597	1.617	1.577	1.516	1.536	1.592	1.519	1.660	1.608	1.592	1.612	1.541	1.499
S^{6+}	0.032	0.028	0.004	0.007	0.010	0.033	0.031	0.031	0.026	0.010	0.031	0.031	0.022	0.030	0.030
O^{2-}	25.000	25.000	25.000	25.000	25.000	25.000	25.000	25.000	25.000	25.000	25.000	25.000	25.000	25.000	25.000
X(Fap)	0.761	0.821	0.799	0.809	0.789	0.758	0.768	0.796	0.759	0.830	0.804	0.796	0.806	0.770	0.750
X(Cap)	0.058	0.056	0.038	0.041	0.053	0.060	0.057	0.052	0.050	0.053	0.070	0.076	0.078	0.063	0.063
X(Hap)	0.182	0.123	0.164	0.151	0.158	0.182	0.175	0.152	0.190	0.117	0.126	0.128	0.115	0.166	0.187
O(F)	1.521	1.642	1.597	1.617	1.577	1.516	1.536	1.592	1.519	1.660	1.608	1.592	1.612	1.541	1.499
O(Cl)	0.116	0.111	0.076	0.082	0.106	0.120	0.115	0.104	0.101	0.106	0.141	0.152	0.157	0.127	0.126

Table A1

(continued)

Sample	A2-6 granodiorite porphyry												
Occurrence	occuring in matrix core		occuring in matrix rim					occuring in matrix with magnetite					
No.	6	7	1	2	3	4	5	1	2	3	4	5	6
P_2O_5	42.17	42.29	42.39	42.90	42.31	42.29	42.46	42.35	42.34	42.47	42.17	42.85	43.00
CaO	54.18	54.04	54.11	54.14	54.18	54.10	54.46	54.06	53.81	54.32	54.04	53.14	53.35
SiO_2	0.12	0.12	0.16	0.10	0.16	0.16	0.04	0.19	0.07	0.06	0.11	0.12	0.06
FeO	0.26	0.24	0.27	0.30	0.28	0.31	0.26	0.37	0.31	0.50	0.44	0.72	0.90
MnO	0.32	0.22	0.33	0.22	0.29	0.40	0.33	0.30	0.26	0.30	0.32	0.21	0.29
Na_2O	0.08	0.06	0.07	0.03	0.03	0.05	0.06	0.10	0.07	0.06	0.09	bdl	0.04
Cl	0.42	0.39	0.54	0.57	0.46	0.43	0.42	0.42	0.37	0.42	0.39	0.31	0.43
F	3.06	2.95	2.93	3.01	3.16	3.02	3.00	3.02	3.22	3.06	3.23	3.62	3.23
SO_3	0.22	0.27	0.12	0.09	0.08	0.16	0.18	0.12	0.12	0.10	0.17	0.12	0.19
F,Cl=-O	0.43	0.54	0.50	0.43	0.32	0.46	0.50	0.47	0.30	0.43	0.29	0.01	0.30
Total	100.39	100.02	100.42	100.92	100.61	100.45	100.70	100.46	100.26	100.87	100.67	101.07	101.19
Cations per formula unit on the basis of 26 O													
P^{5+}	6.003	6.015	6.019	6.062	6.025	6.013	6.015	6.015	6.040	6.022	6.001	6.043	6.069
Ca^{2+}	9.762	9.728	9.723	9.683	9.764	9.734	9.764	9.718	9.713	9.747	9.731	9.484	9.529
Si^{4+}	0.021	0.020	0.028	0.016	0.026	0.027	0.007	0.032	0.011	0.011	0.018	0.084	0.011
Fe^{3+}	0.036	0.033	0.037	0.042	0.039	0.044	0.036	0.051	0.044	0.070	0.062	0.100	0.125
Mn^{2+}	0.046	0.031	0.046	0.031	0.041	0.057	0.047	0.042	0.037	0.043	0.046	0.030	0.041
Na^{+}	0.025	0.018	0.024	0.009	0.010	0.017	0.020	0.034	0.023	0.019	0.029	0.006	0.013
Cl^{-}	0.119	0.110	0.154	0.161	0.131	0.122	0.118	0.120	0.104	0.120	0.111	0.087	0.123
F^{-}	1.627	1.566	1.553	1.587	1.678	1.603	1.587	1.601	1.717	1.623	1.718	1.906	1.701
S^{6+}	0.028	0.034	0.015	0.011	0.009	0.020	0.023	0.014	0.015	0.013	0.021	0.014	0.024
O^{2-}	25.000	25.000	25.000	25.000	25.000	25.000	25.000	25.000	25.000	25.000	25.000	25.000	25.000
X(Fap)	0.813	0.783	0.776	0.793	0.839	0.801	0.793	0.801	0.858	0.811	0.859	0.953	0.850
X(Cap)	0.060	0.055	0.077	0.080	0.066	0.061	0.059	0.060	0.052	0.060	0.055	0.043	0.061
X(Hap)	0.127	0.162	0.147	0.126	0.095	0.138	0.148	0.139	0.090	0.128	0.086	0.003	0.088
O(F)	1.627	1.566	1.553	1.587	1.678	1.603	1.587	1.601	1.717	1.623	1.718	1.906	1.701
O(Cl)	0.119	0.110	0.154	0.161	0.131	0.122	0.118	0.120	0.104	0.120	0.111	0.087	0.123

Table A1
(continued)

Sample	A2-7-5 granodiorite porphyry												
Occurrence	occuring in matrix												
No.	1	2	3	4	5	6	7	8	9	10	11	12	13
P_2O_5	42.85	42.35	42.53	42.67	42.68	42.91	42.91	43.24	42.89	42.93	43.06	42.82	42.73
CaO	53.67	53.24	53.36	53.61	54.47	54.09	53.95	54.06	54.44	54.45	54.42	53.07	52.70
SiO_2	bdl	0.11	0.07	0.03	bdl	0.06	bdl	0.01	0.04	0.02	bdl	0.02	bdl
FeO	0.32	0.30	0.24	0.30	0.27	0.11	0.20	0.20	0.28	0.16	0.26	0.18	0.25
MnO	0.31	0.29	0.20	0.24	0.25	0.23	0.22	0.20	0.28	0.24	0.24	0.36	0.34
Na_2O	0.06	bdl	0.06	0.09	bdl	bdl	0.04	bdl	0.05	0.06	bdl	0.06	0.05
Cl	0.36	0.47	0.47	0.44	0.22	0.28	0.19	0.21	0.38	0.25	0.26	0.28	0.37
F	2.99	2.89	3.09	3.02	3.76	3.57	3.49	3.55	3.27	3.55	3.66	3.01	3.00
SO_3	0.15	0.17	0.14	0.07	0.02	0.06	0.12	0.12	0.06	0.08	0.03	0.06	0.07
F,Cl=-O	0.53	0.54	0.36	0.45	-0.09	0.05	0.17	0.12	0.29	0.10	-0.01	0.53	0.48
Total	100.18	99.27	99.80	100.00	101.75	101.26	100.96	101.48	101.38	101.62	101.94	99.33	99.02
Cations per formula unit on the basis of 26 O													
P^{5+}	6.074	6.058	6.077	6.077	6.051	6.079	6.080	6.092	6.045	6.060	6.075	6.105	6.118
Ca^{2+}	9.626	9.638	9.647	9.662	9.773	9.700	9.673	9.638	9.709	9.727	9.716	9.576	9.548
Si^{4+}	0.000	0.018	0.012	0.005	0.000	0.011	0.000	0.001	0.007	0.004	0.000	0.003	0.000
Fe^{3+}	0.045	0.043	0.034	0.042	0.037	0.015	0.028	0.028	0.039	0.022	0.036	0.026	0.035
Mn^{2+}	0.043	0.042	0.029	0.034	0.036	0.033	0.032	0.028	0.040	0.034	0.034	0.051	0.049
Na^{+}	0.019	0.007	0.018	0.030	0.000	0.000	0.013	0.000	0.015	0.019	0.000	0.019	0.016
Cl^{-}	0.102	0.134	0.134	0.126	0.063	0.078	0.053	0.060	0.106	0.070	0.073	0.081	0.105
F^{-}	1.585	1.542	1.650	1.604	1.989	1.891	1.849	1.868	1.721	1.869	1.931	1.603	1.606
S^{6+}	0.019	0.021	0.017	0.008	0.002	0.007	0.015	0.015	0.008	0.009	0.004	0.008	0.008
O^{2-}	25.000	25.000	25.000	25.000	25.000	25.000	25.000	25.000	25.000	25.000	25.000	25.000	25.000
X(Fap)	0.792	0.771	0.825	0.802	0.995	0.946	0.925	0.934	0.860	0.935	0.965	0.801	0.803
X(Cap)	0.051	0.067	0.067	0.063	0.032	0.039	0.026	0.030	0.053	0.035	0.036	0.041	0.053
X(Hap)	0.157	0.162	0.108	0.135	-0.026	0.015	0.049	0.036	0.087	0.030	-0.002	0.158	0.144
O(F)	1.585	1.542	1.650	1.604	1.989	1.891	1.849	1.868	1.721	1.869	1.931	1.603	1.606
O(Cl)	0.102	0.134	0.134	0.126	0.063	0.078	0.053	0.060	0.106	0.070	0.073	0.081	0.105

Table A1
(continued)

Sample	A2-7-5 granodiorite porphyry					A2-7-12 granodiorite porphyry						
Occurrence	occuring in matrix					occuring in matrix						
No.	14	15	16	17	18	1	2	3	4	5	6	7
P_2O_5	42.52	43.16	43.55	43.17	43.20	42.59	42.58	42.40	42.64	42.80	43.23	43.49
CaO	53.08	53.37	53.43	54.01	53.40	53.70	53.78	53.97	53.81	53.64	54.22	54.54
SiO_2	0.03	bdl	0.01	bdl	0.04	0.10	0.12	0.11	0.10	0.08	0.12	0.11
FeO	0.30	0.22	0.28	0.25	0.32	0.32	0.27	0.26	0.26	0.24	0.27	0.28
MnO	0.31	0.34	0.38	0.31	0.31	0.29	0.24	0.31	0.20	0.21	0.25	0.22
Na_2O	0.04	0.08	0.04	0.04	0.04	bdl	0.05	bdl	0.03	0.07	0.10	0.04
Cl	0.39	0.38	0.36	0.38	0.43	0.28	0.25	0.35	0.28	0.43	0.44	0.44
F	2.97	3.32	3.27	3.12	3.17	3.48	3.49	3.25	3.18	3.52	3.45	3.46
SO_3	0.12	0.08	0.08	0.08	0.08	0.12	0.11	0.08	0.14	0.16	0.08	0.04
F,Cl=-O	0.50	0.23	0.31	0.42	0.35	0.12	0.13	0.29	0.40	0.02	0.12	0.12
Total	99.26	100.73	101.08	100.95	100.63	100.76	100.75	100.45	100.24	101.13	102.05	102.49
Cations per formula unit on the basis of 26 O												
P^{5+}	6.082	6.112	6.128	6.088	6.108	6.059	6.052	6.038	6.052	6.073	6.073	6.079
Ca^{2+}	9.608	9.565	9.516	9.640	9.555	9.669	9.673	9.726	9.666	9.631	9.639	9.648
Si^{4+}	0.005	0.000	0.002	0.000	0.006	0.016	0.019	0.018	0.017	0.014	0.021	0.019
Fe^{3+}	0.042	0.031	0.039	0.035	0.045	0.045	0.038	0.036	0.037	0.034	0.038	0.039
Mn^{2+}	0.045	0.048	0.053	0.044	0.044	0.041	0.035	0.044	0.029	0.029	0.035	0.030
Na^{+}	0.013	0.025	0.013	0.014	0.014	0.005	0.015	0.005	0.008	0.021	0.031	0.012
Cl^{-}	0.111	0.109	0.101	0.108	0.123	0.079	0.072	0.101	0.080	0.122	0.123	0.123
F^{-}	1.588	1.758	1.718	1.644	1.672	1.850	1.851	1.730	1.683	1.866	1.809	1.807
S^{6+}	0.015	0.010	0.010	0.009	0.010	0.016	0.014	0.010	0.018	0.020	0.010	0.005
O^{2-}	25.000	25.000	25.000	25.000	25.000	25.000	25.000	25.000	25.000	25.000	25.000	25.000
X(Fap)	0.794	0.879	0.859	0.822	0.836	0.925	0.925	0.865	0.842	0.933	0.905	0.903
X(Cap)	0.056	0.054	0.050	0.054	0.061	0.040	0.036	0.050	0.040	0.061	0.061	0.061
X(Hap)	0.151	0.067	0.091	0.124	0.103	0.035	0.039	0.085	0.118	0.006	0.034	0.035
O(F)	1.588	1.758	1.718	1.644	1.672	1.850	1.851	1.730	1.683	1.866	1.809	1.807
O(Cl)	0.111	0.109	0.101	0.108	0.123	0.079	0.072	0.101	0.080	0.122	0.123	0.123

Table A1

(continued)

Sample	A2-7-12 granodiorite porphyry								
Occurrence	occuring in matrix								
No.	8	9	10	11	12	13	14	15	16
P_2O_5	43.24	42.59	43.05	42.67	43.08	43.21	42.55	42.85	42.85
CaO	53.51	53.35	53.31	53.68	53.91	54.69	54.14	54.23	53.74
SiO_2	0.11	0.13	0.19	0.04	0.03	0.10	0.11	0.15	0.11
FeO	0.26	0.28	0.25	0.28	0.23	0.21	0.28	0.26	0.29
MnO	0.25	0.23	0.24	0.21	0.20	0.29	0.25	0.23	0.25
Na_2O	bdl	0.07	0.05	0.10	bdl	0.05	0.14	0.03	bdl
Cl	0.45	0.41	0.40	0.38	0.40	0.35	0.35	0.36	0.40
F	3.42	3.43	3.60	3.52	3.50	3.34	3.40	3.42	3.38
SO_3	0.10	0.13	0.11	0.07	0.07	0.09	0.10	0.12	0.06
F,Cl=-O	0.12	0.10	-0.03	0.04	0.07	0.27	0.17	0.16	0.16
Total	101.21	100.51	101.22	100.91	101.35	102.05	101.14	101.48	100.93
Cations per formula unit on the basis of 26 O									
P^{5+}	6.106	6.068	6.099	6.073	6.089	6.054	6.033	6.049	6.077
Ca^{2+}	9.563	9.619	9.558	9.668	9.644	9.697	9.715	9.689	9.647
Si^{4+}	0.019	0.021	0.032	0.007	0.005	0.016	0.019	0.025	0.019
Fe^{3+}	0.036	0.039	0.036	0.040	0.031	0.029	0.040	0.036	0.040
Mn^{2+}	0.035	0.033	0.033	0.030	0.029	0.041	0.035	0.032	0.036
Na^{+}	0.000	0.022	0.016	0.032	0.000	0.016	0.047	0.010	0.000
Cl^{-}	0.126	0.116	0.113	0.108	0.113	0.097	0.098	0.103	0.114
F^{-}	1.803	1.828	1.903	1.869	1.846	1.746	1.799	1.802	1.791
S^{6+}	0.013	0.016	0.014	0.009	0.009	0.011	0.012	0.015	0.008
O^{2-}	25.000	25.000	25.000	25.000	25.000	25.000	25.000	25.000	25.000
X(Fap)	0.902	0.914	0.951	0.935	0.923	0.873	0.900	0.901	0.895
X(Cap)	0.063	0.058	0.056	0.054	0.057	0.049	0.049	0.051	0.057
X(Hap)	0.035	0.028	-0.008	0.011	0.020	0.078	0.051	0.048	0.047
O(F)	1.803	1.828	1.903	1.869	1.846	1.746	1.799	1.802	1.791
O(Cl)	0.126	0.116	0.113	0.108	0.113	0.097	0.098	0.103	0.114

bdl: below the limit of detection.

Table A2

EPMA of chemical composition (wt.%) and calculated formula of plagioclase from the Aktogai porphyry Cu deposit, Central Kazakhstan

Sample		A1-1 granodiorite												A2-6 granodiorite porphyry	
position		core to rim												rim to rim	
No	detection limit	1	2	3	4	5	6	7	8	9	10	11	12	1	2
SiO_2	0.05	56.57	55.07	56.33	55.49	55.93	55.70	56.66	54.18	56.85	56.08	56.02	56.14	61.02	60.78
TiO_2	0.04	bdl	bdl	0.04	bdl	0.07	bdl	bdl	bdl	0.07	0.04	0.07	0.05	bdl	bdl
Al_2O_3	0.03	27.12	27.56	27.00	27.58	27.25	27.51	26.94	28.74	26.99	27.14	27.65	27.03	24.33	24.35
FeO	0.02	0.33	0.34	0.31	0.32	0.28	0.29	0.29	0.34	0.36	0.31	0.29	0.32	0.23	0.21
CaO	0.02	9.45	10.31	9.42	10.10	9.61	9.87	9.21	11.05	8.97	9.55	9.86	9.22	6.67	6.78
Na_2O	0.03	6.03	5.59	5.96	5.70	5.80	5.66	6.21	5.14	6.04	6.02	5.79	6.13	7.41	7.59
K_2O	0.02	0.50	0.41	0.37	0.38	0.41	0.40	0.43	0.34	0.47	0.39	0.36	0.33	0.52	0.42
Total		99.99	99.28	99.43	99.57	99.34	99.42	99.74	99.78	99.76	99.53	100.02	99.22	100.17	100.13
Structural formula calculated based on 8 oxygens															
Si^{4+}		2.547	2.503	2.548	2.513	2.533	2.522	2.555	2.456	2.560	2.537	2.521	2.544	2.712	2.704
Ti^{4+}		0.000	0.000	0.001	0.000	0.002	0.001	0.000	0.000	0.002	0.001	0.002	0.002	0.000	0.001
Al^{3+}		1.439	1.477	1.440	1.472	1.455	1.468	1.432	1.535	1.432	1.447	1.467	1.444	1.275	1.277
Fe^{2+}		0.012	0.013	0.012	0.012	0.011	0.011	0.011	0.013	0.014	0.012	0.011	0.012	0.009	0.008
Ca^{2+}		0.456	0.502	0.456	0.490	0.466	0.479	0.445	0.537	0.433	0.463	0.475	0.448	0.318	0.323
Na^{+}		0.526	0.493	0.522	0.501	0.510	0.497	0.543	0.451	0.528	0.528	0.505	0.539	0.638	0.654
K^{+}		0.029	0.023	0.021	0.022	0.024	0.023	0.025	0.019	0.027	0.023	0.020	0.019	0.029	0.024
Total		5.011	5.017	5.003	5.012	5.004	5.002	5.013	5.012	4.999	5.013	5.006	5.011	4.984	4.996
An		0.451	0.493	0.456	0.484	0.467	0.479	0.439	0.533	0.438	0.457	0.475	0.445	0.322	0.323
Ab		0.521	0.484	0.522	0.494	0.510	0.498	0.536	0.448	0.534	0.521	0.505	0.536	0.648	0.653
Or		0.028	0.023	0.021	0.022	0.024	0.023	0.024	0.019	0.028	0.022	0.020	0.019	0.030	0.024

Table A2
(continued)

Sample	A2-6 granodiorite porphyry														
position	rim to rim														
No	3	4	5	6	7	8	9	10	11	12	13	14	15	16	17
SiO_2	58.58	60.51	60.29	59.45	58.76	60.39	58.89	60.38	61.22	59.82	60.73	60.39	60.72	60.89	60.99
TiO_2	bdl	0.05	bdl	0.07	0.06	0.04	bdl	bdl	0.06	bdl	0.06	0.04	0.05	bdl	bdl
Al_2O_3	25.74	24.75	24.13	25.27	25.12	24.60	25.57	24.37	24.32	24.95	23.92	24.56	24.22	24.34	23.77
FeO	0.27	0.17	0.21	0.30	0.28	0.30	0.20	0.34	0.16	0.25	0.26	0.23	0.23	0.23	0.22
CaO	8.12	7.21	6.84	7.48	7.65	7.11	8.15	6.87	6.67	7.25	6.30	6.72	6.48	6.49	6.35
Na_2O	6.90	7.02	7.25	7.17	6.68	7.29	7.00	7.48	7.35	7.00	7.33	7.41	7.40	7.69	8.05
K_2O	0.34	0.42	0.39	0.33	0.37	0.43	0.25	0.51	0.36	0.49	0.49	0.39	0.54	0.33	0.35
Total	99.94	100.12	99.10	100.07	98.92	100.14	100.07	99.94	100.15	99.75	99.09	99.73	99.63	99.97	99.73
Structural formula calculated based on 8 oxygens															
Si^{4+}	2.624	2.691	2.709	2.655	2.653	2.689	2.634	2.697	2.718	2.675	2.725	2.697	2.713	2.710	2.725
Ti^{4+}	0.000	0.002	0.000	0.002	0.002	0.001	0.000	0.000	0.002	0.001	0.002	0.001	0.002	0.001	0.000
Al^{3+}	1.359	1.298	1.278	1.330	1.337	1.291	1.348	1.283	1.273	1.315	1.265	1.293	1.276	1.276	1.252
Fe^{2+}	0.010	0.006	0.008	0.011	0.010	0.011	0.008	0.013	0.006	0.009	0.010	0.009	0.009	0.009	0.008
Ca^{2+}	0.390	0.343	0.329	0.358	0.370	0.339	0.390	0.329	0.318	0.347	0.303	0.321	0.310	0.309	0.304
Na^{+}	0.599	0.605	0.631	0.621	0.584	0.629	0.607	0.648	0.633	0.607	0.638	0.641	0.641	0.664	0.697
K^{+}	0.020	0.024	0.022	0.019	0.021	0.024	0.014	0.029	0.021	0.028	0.028	0.022	0.031	0.019	0.020
Total	5.006	4.973	4.979	4.997	4.980	4.991	5.003	5.000	4.970	4.984	4.973	4.987	4.984	4.992	5.008
An	0.386	0.353	0.335	0.359	0.379	0.342	0.386	0.327	0.327	0.353	0.313	0.326	0.316	0.312	0.298
Ab	0.594	0.622	0.643	0.622	0.599	0.634	0.600	0.644	0.652	0.618	0.659	0.651	0.653	0.669	0.683
Or	0.019	0.025	0.023	0.019	0.022	0.024	0.014	0.029	0.021	0.029	0.029	0.022	0.031	0.019	0.020

bdl: below the limit of detection.

REFERENCES

Abdulin, A. A., Bespaev, H. A., Votsalevsky, E. S., Daukeev, S. Z. H., and Miroshnichenko, L. A., 1996, Map of mineral resources of Kazakhstan: Non-ferrous metals: Almaty, Kazakhstan, Kazakhstan Map Publishing House, Scale 1:2000000.

Allègre, C. J., Lewin, E., and Dupré, B., 1988, A coherent crust-mantle model for the uranium-thorium-lead isotopic system: Chemical Geology, v. 70, n. 3, p. 211–234, http://dx.doi.org/10.1016/0009-2541(88)90094-0

Anderson, J. L., and Cullers, R. L., 1987, Crust-enriched, mantle-derived tonalites in the early Proterozoic Penokean orogen of Wisconsin: The Journal of Geology, v. 95, n. 2, p. 139–154, http://dx.doi.org/10.1086/629116

Atherton, M. P., and Petford, N., 1993, Generation of sodium-rich magmas from newly underplated basaltic crust: Nature, v. 362, p. 144–146, http://dx.doi.org/10.1038/362144a0

Audétat, A., Pettke, T., and Dolejš, D., 2004, Magmatic anhydrite and calcite in the ore-forming quartz-monzodiorite magma at Santa Rita, New Mexico (USA): Genetic constraints on porphyry-Cu mineralization: Lithos, v. 72, n. 3–4, p. 147–161, http://dx.doi.org/10.1016/j.lithos.2003.10.003

Baldwin, J. A., and Pearce, J. A., 1982, Discrimination of productive and nonproductive porphyritic intrusions in the Chilean Andes: Economic Geology, v. 77, n. 3, p. 664–674, http://dx.doi.org/10.2113/gsecongeo.77.3.664

Bespaev, K. A., and Miroshnichenko, L. A., 2004, Atlas of Mineral Deposit Models: Almaty, Kazakhstan, K. I. Satpaev Institute of Geological Sciences, p. 1–141.

Blichert-Toft, J., Albarède, F., and Kornprobst, J., 1999, Lu-Hf isotope systematics of garnet pyroxenites from Beni Bousera, Morocco: Implications for basalt origin: Science, v. 283, n. 5406, p. 1303–1306, http://dx.doi.org/10.1126/science.283.5406.1303

Blundy, J., and Wood, B., 2003, Partitioning of trace elements between crystals and melts: Earth and Planetary Science Letters, v. 210, n. 3–4, p. 383–397, http://dx.doi.org/10.1016/S0012-821X(03)00129-8

Cao, M. J., Li, G. M., Qin, K. Z., Seitmuratova, E. Y., and Liu, Y. S., 2012, Major and Trace Element Characteristics of Apatites in Granitoids from Central Kazakhstan: Implications for Petrogenesis and Mineralization: Resource Geology, v. 62, n. 1, p. 63–83, http://dx.doi.org/10.1111/j.1751-3928.2011.00180.x

Cao, M. J., Zhou, Q. F., Qin, K. Z., Tang, D. M., and Evans, N. J., 2013, The tetrad effect and geochemistry of apatite from the Altay Koktokay No. 3 pegmatite, Xinjiang, China: Implications for pegmatite petrogenesis: Mineralogy and Petrology, v. 107, n. 6, p. 985–1005, http://dx.doi.org/10.1007/s00710-013-0270-x

Cao, M. J., Qin, K. Z., Li, G. M., Evans, N. J., and Jin, L. Y., 2014a, Abiogenic Fischer–Tropsch synthesis of methane at the Baogutu reduced porphyry copper deposit, western Junggar, NW-China: Geochimica et Cosmochimica Acta, v. 141, p. 179–198, http://dx.doi.org/10.1016/j.gca.2014.06.018

Cao, M. J., Qin, K. Z., Li, G. M., Jin, L. Y., Evans, N. J., and Yang, X. R., 2014b, Baogutu: An example of reduced porphyry Cu deposit in western Junggar: Ore Geology Reviews, v. 56, p. 159–180, http://dx.doi.org/10.1016/j.oregeorev.2013.08.014

Cao, M. J., Qin, K. Z., Li, G. M., Yang, Y. H., Evans, N. J., Zhang, R., and Jin, L. Y., 2014c, Magmatic process recorded in plagioclase at the Baogutu reduced porphyry Cu deposit, western Junggar, NW-China: Journal of Asian Earth Sciences, v. 82, p. 136–150, http://dx.doi.org/10.1016/j.jseaes.2013.12.019

Cao, M. J., Qin, K. Z., Li, G. M., Evans, N. J., and Jin, L. Y., 2015, *In situ* LA-(MC)-ICP-MS trace element and Nd isotopic compositions and genesis of polygenetic titanite from the Baogutu reduced porphyry Cu deposit, Western Junggar, NW China: Ore Geology Reviews, v. 65, Part 4, p. 940–954, http://dx.doi.org/10.1016/j.oregeorev.2014.07.014

Cao, M. J., Qin, K. Z., Li, G. M., Evans, N. J., Hollings, P., and Jin, L. Y., 2016, Genesis of ilmenite-series I-type granitoids at the Baogutu reduced porphyry Cu deposit, western Junggar, NW-China: Lithos, v. 246–247, p. 13–30, http://dx.doi.org/10.1016/j.lithos.2015.12.019

Castillo, P. R., Janney, P. E., and Solidum, R. U., 1999, Petrology and geochemistry of Camiguin Island, southern Philippines: Insights to the source of adakites and other lavas in a complex arc setting: Contributions to Mineralogy and Petrology, v. 134, n. 1, p. 33–51, http://dx.doi.org/10.1007/s004100050467

Chauvel, C., Lewin, E., Carpentier, M., Arndt, N. T., and Marini, J. C., 2008, Role of recycled oceanic basalt and sediment in generating the Hf-Nd mantle array: Nature Geoscience, v. 1, p. 64–67, http://dx.doi.org/10.1038/ngeo.2007.51

Chen, F., Satir, M., Ji, J., and Zhong, D., 2002, Nd-Sr-Pb isotopes of Tengchong Cenozoic volcanic rocks from western Yunnan, China: Evidence for an enriched-mantle source: Journal of Asian Earth Sciences, v. 21, n. 1, p. 39–45, http://dx.doi.org/10.1016/S1367-9120(02)00007-X

Chen, X., Seitmuratova, E., Wang, Z., Chen, Z., Han, S., Li, Y., Yang, Y., Ye, B., and Shi, W., 2014, SHRIMP U–Pb and Ar–Ar geochronology of major porphyry and skarn Cu deposits in the Balkhash Metallogenic Belt, Central Asia, and geological implications: Journal of Asian Earth Sciences, v. 79, Part B, p. 723–740, http://dx.doi.org/10.1016/j.jseaes.2013.06.011

Chiaradia, M., 2014, Copper enrichment in arc magmas controlled by overriding plate thickness: Nature Geoscience, v. 7, p. 43–46, http://dx.doi.org/10.1038/ngeo2028

Chung, S. L., Liu, D., Ji, J., Chu, M., Lee, H., Wen, D., Lo, C., Lee, T., Qian, Q., and Zhang, Q., 2003, Adakites from continental collision zones: Melting of thickened lower crust beneath southern Tibet: Geology, v. 31, n. 11, p. 1021–1024, http://dx.doi.org/10.1130/G19796.1

Defant, M. J., and Drummond, M. S., 1990, Derivation of some modern arc magmas by melting of young subducted lithosphere: Nature, v. 347, p. 662–665, http://dx.doi.org/10.1038/347662a0

Davidson, J., Turner, S., Handley, H., Macpherson, C., and Dosseto, A., 2007, Amphibole "sponge" in arc crust?: Geology, v. 35, n. 9, p. 787–790, http://dx.doi.org/10.1130/G23637A.1

Drake, M. J., and Weill, D. F., 1975, Partition of Sr, Ba, Ca, Y, Eu^{2+}, Eu^{3+}, and other REE between plagioclase feldspar and magmatic liquid: An experimental study: Geochimica et Cosmochimica Acta, v. 39, n. 5, p. 689–712, http://dx.doi.org/10.1016/0016-7037(75)90011-3

Eiler, J. M., 2001, Oxygen isotope variations of basaltic lavas and upper mantle rocks: Reviews in Mineralogy and Geochemistry, v. 43, n. 1, p. 319–364, http://dx.doi.org/10.2138/gsrmg.43.1.319

Evans, K. A., Elburg, M. A., and Kamenetsky, V. S., 2012, Oxidation state of subarc mantle: Geology, v. 40, n. 9, p. 783–786, http://dx.doi.org/10.1130/G33037.1

Farmer, G. L., and DePaolo, D. J., 1987, Nd and Sr isotope study of hydrothermally altered granite at San Manuel, Arizona; implications for element migration paths during the formation of porphyry copper ore deposits: Economic Geology, v. 82, n. 5, p. 1142–1151, http://dx.doi.org/10.2113/gsecongeo.82.5.1142

Filippova, I. B., Bush, V. A., and Didenko, A. N., 2001, Middle Paleozoic subduction belts: The leading factor in the formation of the Central Asian fold-and-thrust belt: Russian Journal of Earth Sciences, v. 3, n. 6, p. 405–426, http://dx.doi.org/10.2205/2001ES000073

Foley, S., Tiepolo, M., and Vannucci, R., 2002, Growth of early continental crust controlled by melting of amphibolite in subduction zones: Nature, v. 417, p. 837–840, http://dx.doi.org/10.1038/nature00799

Guo, F., Nakamuru, E., Fan, W., Kobayoshi, K., and Li, C., 2007, Generation of Palaeocene Adakitic Andesites by Magma Mixing; Yanji Area, NE China: Journal of Petrology, v. 48, n. 4, p. 661–692, http://dx.doi.org/10.1093/petrology/egl077

Griffin, W. L., Pearson, N. J., Belousova, E., Jackson, S. E., van Achterbergh, E., O'Reilly, S. Y., and Shee, S. R., 2000, The Hf isotope composition of cratonic mantle: LAM-MC-ICPMS analysis of zircon megacrysts in kimberlites: Geochimica et Cosmochimica Acta, v. 64, n. 1, p. 133–147, http://dx.doi.org/10.1016/S0016-7037(99)00343-9

Harrison, T. M., and Watson, E. B., 1984, The behavior of apatite during crustal anatexis: Equilibrium and kinetic considerations: Geochimica et Cosmochimica Acta, v. 48, n. 7, p. 1467–1477, http://dx.doi.org/10.1016/0016-7037(84)90403-4

Hart, S. R., 1984, A large-scale isotope anomaly in the Southern Hemisphere mantle: Nature, v. 309, p. 753–757, http://dx.doi.org/10.1038/309753a0

Hedenquist, J. W., and Lowenstern, J. B., 1994, The role of magmas in the formation of hydrothermal ore deposits: Nature, v. 370, p. 519–527, http://dx.doi.org/10.1038/370519a0

Heinhorst, J., Lehmann, B., Ermolov, P., Serykh, V., and Zhurutin, S., 2000, Paleozoic crustal growth and metallogeny of Central Asia: Evidence from magmatic-hydrothermal ore systems of Central Kazakhstan: Tectonophysics, v. 328, n. 1–2, p. 69–87, http://dx.doi.org/10.1016/S0040-1951(00)00178-5

Hildreth, W., and Moorbath, S., 1988, Crustal contributions to arc magmatism in the Andes of Central Chile: Contributions to Mineralogy and Petrology, v. 98, n. 4, p. 455–489, http://dx.doi.org/10.1007/BF00372365

Hoefs, J., 2009, Stable Isotope Geochemistry, Sixth Edition: Berlin Heidelberg, Springer Verlag, 284 p.

Imai, A., Listanco, E. L., and Fujii, T., 1993, Petrologic and sulfur isotopic significance of highly oxidized and sulfur-rich magma of Mt. Pinatubo, Philippines: Geology, v. 21, n. 8, p. 699–702, http://dx.doi.org/10.1130/0091-7613(1993)021<0699:PASISO>2.3.CO;2

Jacobsen, S. B., and Wasserburg, G. J., 1980, Sm-Nd isotopic evolution of chondrites: Earth and Planetary Science Letters, v. 50, n. 1, p. 139–155, http://dx.doi.org/10.1016/0012-821X(80)90125-9

Jahn, B. M., and Condie, K. C., 1995, Evolution of the Kaapvaal Craton as viewed from geochemical and Sm-Nd isotopic analyses of intracratonic pelites: Geochimica et Cosmochimica Acta, v. 59, n. 11, p. 2239–2258, http://dx.doi.org/10.1016/0016-7037(95)00103-7

Jahn, B., Wu, F., and Chen, B., 2000, Massive granitoid generation in Central Asia: Nd isotope evidence and implication for continental growth in the Phanerozoic: Episodes, v. 23, n. 2, p. 82–92.

Kay, R. W., and Kay, S. M., 1993, Delamination and delamination magmatism: Tectonophysics, v. 219, n. 1–3, p. 177–189, http://dx.doi.org/10.1016/0040-1951(93)90295-U

Kelley, K. A., and Cottrell, E., 2009, Water and the oxidation state of subduction zone magmas: Science, v. 325, n. 5940, p. 605–607, http://dx.doi.org/10.1126/science.1174156

Kemp, A. I. S., Hawkesworth, C. J., Foster, G. L., Paterson, B. A., Woodhead, J. D., Hergt, J. M., Gray, C. M., and Whitehouse, M. J., 2007, Magmatic and Crustal Differentiation History of Granitic Rocks from Hf-O Isotopes in Zircon: Science, v. 315, m. 5814, p. 980–983, http://dx.doi.org/10.1126/science.1136154

La Flèche, M. R., Camire, G., and Jenner, G. A., 1998, Geochemistry of post-Acadian, Carboniferous continental intraplate basalts from the Maritimes Basin, Magdalen Islands, Quebec, Canada: Chemical Geology, v. 148, n. 3–4, p. 115–136, http://dx.doi.org/10.1016/S0009-2541(98)00002-3

Lee, C. T. A., Luffi, P., Le Roux, V., Dasgupta, R., Albaréde, F., and Leeman, W. P., 2010, The redox state of arc mantle using Zn/Fe systematics: Nature, v. 468, p. 681–685, http://dx.doi.org/10.1038/nature09617

Lee, C. T. A., Luffi, P., Chin, E. J., Bouchet, R., Dasgupta, R., Morton, D. M., Le Roux, V., Yin, Q. Z., and Jin, D., 2012, Copper Systematics in Arc Magmas and Implications for Crust-Mantle Differentiation: Science, v. 336, n. 6077, p. 64–68, http://dx.doi.org/10.1126/science.1217313

Levashova, N. M., Degtyarev, K. E., Bazhenov, M. L., Collins, A. Q., and Van der Voo, R., 2003, Middle Paleozoic paleomagnetism of east Kazakhstan: Post-Middle Devonian rotations in a large-scale orocline in the central Ural–Mongol belt: Tectonophysics, v. 377, n. 3–4, p. 249–268, http://dx.doi.org/10.1016/j.tecto.2003.09.013

Li, G. M., Li, J. X., Qin, K. Z., Zhang, T. P., and Xiao, B., 2007, High temperature, salinity and strong oxidation ore-forming fluids at Duobuza gold-rich porphyry copper deposit in the Banggonghu tectonic belt, Tibet: Acta Petrologica Sinica, v. 23, p. 935–952 (in Chinese with English abstract).

Li, G. M., Qin, K. Z., and Li, J. X., 2008, Geological features and tectonic setting of porphyry copper deposits

rounding the Balkhash region, Central Kazakhstan, Central Asia: Acta Petrologica Sinica, v. 24, p. 2679–2700 (in Chinese with English abstract).
Li, G. M., Cao, M. J., Qin, K. Z., Hollings, P., Evans, N. J., and Seitmuratova, E. Y., 2016a, Petrogenesis of ore-forming and pre/post-ore granitoids from the Kounrad, Borly and Sayak porphyry/skarn Cu deposits, Central Kazakhstan: Gondwana Research, http://dx.doi.org/10.1016/j.gr.2015.10.005
Li, G. M., Cao, M. J., Qin, K. Z., Evans, N. J., Hollings, P., and Seitmuratova, E. Y., 2016b, Geochronology, petrogenesis and tectonic settings of pre- and syn-ore granites from the W-Mo deposits (East Kounrad, Zhanet and Akshatau), Central Kazakhstan: Lithos, v. 252–253, p. 16–31, http://dx.doi.org/10.1016/j.lithos.2016.01.023
Li, J. X., Qin, K. Z., Li, G. M., Xiao, B., Chen, L., and Zhao, J. X., 2011, Post-collisional ore-bearing adakitic porphyries from Gangdese porphyry copper belt, southern Tibet: Melting of thickened juvenile arc lower crust: Lithos, v. 126, n. 3–4, p. 265–277, http://dx.doi.org/10.1016/j.lithos.2011.07.018
Li, Q. L., Li, X. H., Liu, Y., Tang, G. Q., Yang, J. H., and Zhu, W. G., 2010, Precise U–Pb and Pb–Pb dating of Phanerozoic baddeleyite by SIMS with oxygen flooding technique: Journal of Analytical Atomic Spectrometry, v. 25, p. 1107–1113, http://dx.doi.org/10.1039/b923444f
Li, X. H., Liu, Y., Li, Q. L., Guo, C. H., and Chamberlain, K. R., 2009, Precise determination of Phanerozoic zircon Pb/Pb age by multicollector SIMS without external standardization: Geochemistry, Geophysics, Geosystems, v. 10, n. 4, http://dx.doi.org/10.1029/2009GC002400
Li, X. H., Li, W. X., Li, Q. L., Wang, X. C., Liu, Y., and Yang, Y. H., 2010a, Petrogenesis and tectonic significance of the ~850 Ma Gangbian alkaline complex in South China: Evidence from *in situ* zircon U–Pb dating, Hf–O isotopes and whole-rock geochemistry: Lithos, v. 114, n. 1–2, p. 1–15, http://dx.doi.org/10.1016/j.lithos.2009.07.011
Li, X. H., Long, W. G., Li, Q. L., Liu, Y., Zheng, Y. F., Yang, Y. H., Chamberlain, K. R., Wan, D. F., Guo, C. H., Wang, X. C., and Tao, H., 2010b, Penglai zircon megacrysts: A potential new working reference material for microbeam determination of Hf–O isotopes and U–Pb age: Geostandards and Geoanalytical Research, v. 34, n. 2, p. 117–134, http://dx.doi.org/10.1111/j.1751-908X.2010.00036.x
Liu, G., Chen, X. H., Dong, S. W., Chen, Z. L., Han, S. Q., Yang, Y., Ye, B. Y., and Shi, W., 2012, Late Paleozoic crustal growth and tectonic evolution in Balkhash metallogenic belt (Kazakhstan), Central Asia: Acta Petrologica Sinica, v. 28, p. 1995–2008 (in Chinese with English abstract).
Ludwig, R. K., 2001, User Manual for Isoplot/Ex rev. 2.49: Berkeley, California, Berkeley Geochronology Center Special Publication 1a, 56 p.
Luhr, J. F., 1990, Experimental phase relations of water-and sulfur-saturated arc magmas and the 1982 eruptions of El Chichón volcano: Journal of Petrology, v. 31, n. 5, p. 1071–1114, http://dx.doi.org/10.1093/petrology/31.5.1071
Lugmair, G. W., and Marti, K., 1978, Lunar initial $^{143}Nd/^{144}Nd$: Differential evolution of the lunar crust and mantle: Earth and Planetary Science Letters, v. 39, n. 3, p. 349–357, http://dx.doi.org/10.1016/0012-821X(78)90021-3
Macpherson, C. G., Dreher, S. T., and Thirlwall, M. F., 2006, Adakites without slab melting: High pressure differentiation of island arc magma, Mindanao, the Philippines: Earth and Planetary Science Letters, v. 243, n. 3–4, p. 581–593, http://dx.doi.org/10.1016/j.epsl.2005.12.034
Maniar, P. D., and Piccoli, P. M., 1989, Tectonic discrimination of granitoids: Geological Society of America Bulletin, v. 101, n. 5, p. 635–643, http://dx.doi.org/10.1130/0016-7606(1989)101<0635:TDOG>2.3.CO;2
Martin, H., 1987, Petrogenesis of Archaean trondhjemites, tonalites, and granodiorites from eastern Finland: major and trace element geochemistry: Journal of Petrology, v. 28, n. 5, p. 921–953, http://dx.doi.org/10.1093/petrology/28.5.921
Martin, H., Smithies, R. H., Rapp, R., Moyen, J. F., and Champion, D. C., 2005, An overview of adakite, tonalite-trondhjemite-granodiorite (TTG), and sanukitoid: Relationships and some implications for crustal evolution: Lithos, v. 79, n. 1–2, p. 1–24, http://dx.doi.org/10.1016/j.lithos.2004.04.048
Moore, G., and Carmichael, I. S. E., 1998, The hydrous phase equilibria (to 3 kbar) of an andesite and basaltic andesite from western Mexico: Constraints on water content and conditions of phenocryst growth: Contributions to Mineralogy and Petrology, v. 130, n. 3, p. 304–319, http://dx.doi.org/10.1007/s004100050367
Morel, M. L. A., Nebel, O., Nebel-Jacobsen, Y. J., Miller, J. S., and Vroon, P. Z., 2008, Hafnium isotope characterization of the GJ-1 zircon reference material by solution and laser-ablation MC-ICPMS: Chemical Geology, v. 255, n. 1–2, p. 231–235, http://dx.doi.org/10.1016/j.chemgeo.2008.06.040
Mungall, J. E., 2002, Roasting the mantle: Slab melting and the genesis of major Au and Au-rich Cu deposits: Geology, v. 30, n. 10, p. 915–918, http://dx.doi.org/10.1130/0091-7613(2002)030<0915:RTMSMA>2.0.CO;2
Muñoz, M., Charrier, R., Fanning, C. M., Maksaev, V., and Deckart, K., 2012, Zircon Trace Element and O–Hf Isotope Analyses of Mineralized Intrusions from El Teniente Ore Deposit, Chilean Andes: Constraints on the Source and Magmatic Evolution of Porphyry Cu–Mo Related Magmas: Journal of Petrology, v. 53, n. 6, p. 1091–1122, http://dx.doi.org/10.1093/petrology/egs010
Müntener, O., Kelemen, P. B., and Grove, T. L., 2001, The role of H_2O during crystallization of primitive arc magmas under uppermost mantle conditions and genesis of igneous pyroxenites: An experimental study: Contributions to Mineralogy and Petrology, v. 141, n. 6, p. 643–658, http://dx.doi.org/10.1007/s004100100266
Oyarzun, R., Márquez, A., Lillo, J., López, I., and Rivera, S., 2001, Giant versus small porphyry copper deposits of Cenozoic age in northern Chile: Adakitic versus normal calc-alkaline magmatism: Mineralium Deposita, v. 36, n. 8, p. 794–798, http://dx.doi.org/10.1007/s001260100205
Parat, F., and Holtz, F., 2005, Sulfur partition coefficient between apatite and rhyolite: The role of bulk S

content: Contributions to Mineralogy and Petrology, v. 150, n. 6, p. 643–651, http://dx.doi.org/10.1007/s00410-005-0041-8
Parat, F., Dungan, M. A., and Streck, M. J., 2002, Anhydrite, pyrrhotite, and sulfur-rich apatite: Tracing the sulfur evolution of an Oligocene andesite (Eagle Mountain, CO, USA): Lithos, v. 64, n. 3–4, p. 63–75, http://dx.doi.org/10.1016/S0024-4937(02)00155-X
Pearce, J. A., and Norry, M. J., 1979, Petrogenetic implications of Ti, Zr, Y, and Nb variations in volcanic rocks: Contributions to Mineralogy and Petrology, v. 69, n. 1, p. 33–47, http://dx.doi.org/10.1007/BF00375192
Pearce, J. A., and Peate, D. W., 1995, Tectonic implications of the composition of volcanic ARC magmas: Annual Review of Earth and Planetary Sciences, v. 23, p. 251–285, http://dx.doi.org/10.1146/annurev.ea.23.050195.001343
Peng, G., Luhr, J. F., and McGee, J. J., 1997, Factors controlling sulfur concentrations in volcanic apatite: American Mineralogist, v. 82, n. 11–12, p. 1210–1224, http://dx.doi.org/10.2138/am-1997-11-1217
Petford, N., and Atherton, M., 1996, Na-rich partial melts from newly underplated basaltic crust: The Cordillera Blanca Batholith, Peru: Journal of Petrology, v. 37, n. 6, p. 1491–1521, http://dx.doi.org/10.1093/petrology/37.6.1491
Qian, Q., and Hermann, J., 2013, Partial melting of lower crust at 10–15 kbar: Constraints on adakite and TTG formation: Contributions to Mineralogy and Petrology, v. 165, n. 6, p. 1195–1224, http://dx.doi.org/10.1007/s00410-013-0854-9
Qin, K. Z., and Ishihara, S., 1998, On the possibility of porphyry copper mineralization in Japan: International Geology Review, v. 40, n. 6, p. 539–551, http://dx.doi.org/10.1080/00206819809465223
Qin, K. Z., Xia, D., Li, G. M., Xiao, B., Duo, J., Jiang, G. W., and Zhao, J. X., 2014, Qulong porphyry-skarn type Cu-Mo Deposit, Tibet: Beijing, Science Press, p. 1–316 (in Chinese).
Raczek, I., Jochum, K. P., and Hofmann, A. W., 2003, Neodymium and Strontium Isotope Data for USGS Reference Materials BCR-1, BCR-2, BHVO-1, BHVO-2, AGV-1, AGV-2, GSP-1, GSP-2 and Eight MPI-DING Reference Glasses: Geostandards Newsletter, v. 27, p. 173–179.
Reich, M., Parada, M., Palacios, C., Dietrich, A., Schultz, F., and Lehmann, B., 2003, Adakite-like signature of Late Miocene intrusions at the Los Pelambres giant porphyry copper deposit in the Andes of central Chile: metallogenic implications: Mineralium Deposita, v. 38, p. 876–885.
Richards, J. P., 2003, Tectono-magmatic precursors for porphyry Cu-(Mo-Au) deposit formation: Economic Geology, v. 98, n. 8, p. 1515–1533, http://dx.doi.org/10.2113/gsecongeo.98.8.1515
——— 2011, High Sr/Y arc magmas and porphyry Cu ± Mo ± Au deposits: Just add water: Economic Geology, v. 106, n. 7, p. 1075–1081, http://dx.doi.org/10.2113/econgeo.106.7.1075
——— 2013, Giant ore deposits formed by optimal alignments and combinations of geological processes: Nature Geoscience, v. 6, p. 911–916, http://dx.doi.org/10.1038/ngeo1920
Richards, J. P., and Kerrich, R., 2007, Adakite-like rocks: Their diverse origins and questionable role in metallogenesis: Economic Geology, v. 102, n. 4, p. 537–576, http://dx.doi.org/10.2113/gsecongeo.102.4.537
Richards, J. P., Spell, T., Rameh, E., Razique, A., and Fletcher, T., 2012, High Sr/Y Magmas Reflect Arc Maturity, High Magmatic Water Content, and Porphyry Cu ± Mo ± Au Potential: Examples from the Tethyan Arcs of Central and Eastern Iran and Western Pakistan: Economic Geology, v. 107, n. 2, p. 295–332, http://dx.doi.org/10.2113/econgeo.107.2.295
Rowins, S. M., 2000, Reduced porphyry copper-gold deposits: A new variation on an old theme: Geology, v. 28, n. 6, p. 491–494, http://dx.doi.org/10.1130/0091-7613(2000)28<491:RPCDAN>2.0.CO;2
Ruprecht, P., and Wörner, G., 2007, Variable regimes in magma systems documented in plagioclase zoning patterns: El Misti stratovolcano and Andahua monogenetic cones: Journal of Volcanology and Geothermal Research, v. 165, n. 3–4, p. 142–162, http://dx.doi.org/10.1016/j.jvolgeores.2007.06.002
Sajona, F. G., and Maury, R. C., 1998, Association of adakites with gold and copper mineralization in the Philippines: Comptes Rendus de l'Académie des Sciences-Series IIA-Earth and Planetary Science, v. 326, n. 1, p. 27–34, http://dx.doi.org/10.1016/s1251-8050(97)83200-4
Salters, V. J. M., and Stracke, A., 2004, Composition of the depleted mantle: Geochemistry, Geophysics, Geosystems, v. 5, n. 5, Q05B07, http://dx.doi.org/10.1029/2003GC000597
Sengör, A. M. C., Natal'in, B. A., and Burtman, V. S., 1993, Evolution of the Altaid tectonic collage and Palaeozoic crustal growth in Eurasia: Nature, v. 364, p. 299–307, http://dx.doi.org/10.1038/364299a0
Shaw, D. M., 1970, Trace element fractionation during anatexis: Geochimica et Cosmochimica Acta, v. 34, n. 2, p. 237–243, http://dx.doi.org/10.1016/0016-7037(70)90009-8
Shen, P., Pan, H. D., and Seitmuratova, E., 2015, Characteristics of the porphyry Cu deposits in the Central Asia Metallogenic Domain: Acta Petrologica Sinica, v. 31, p. 315–332 (in Chinese with English abstract).
Sillitoe, R. H., 2010, Porphyry Copper Systems: Economic Geology, v. 105, n. 1, p. 3–41, http://dx.doi.org/10.2113/gsecongeo.105.1.3
Singer, D. A., 1995, World class base and precious metal deposits; a quantitative analysis: Economic Geology, v. 90, p. 88–104.
Singer, D., Berger, V., Menzie, W., and Berger, B., 2005, Porphyry copper deposit density: Economic Geology, v. 100, p. 491–514.
Smith, C. M., Canil, D., Rowins, S. M., and Friedman, R., 2012, Reduced granitic magmas in an arc setting: The Catface porphyry Cu–Mo deposit of the Paleogene Cascade Arc: Lithos, v. 154, p. 361–373.
Söderlund, U., Patchett, P. J., Vervoort, J. D., and Isachsen, C. E., 2004, The ^{176}Lu decay constant determined by Lu–Hf and U–Pb isotope systematics of Precambrian mafic intrusions: Earth and Planetary Science Letters, v. 219, n. 1–4, p. 311–324, http://dx.doi.org/10.1016/S0012-821X(04)00012-3
Sokolov, A. L., 1998, The regional and local controls on gold and copper mineralization in Central Asia and Kazakhstan, *in* Porter, T. M., editor, Porphyry and hydrothermal copper and gold deposits. A global

perspective, Perth, 1998, Conference Proceedings: Glenside, South Australia, Australian Mineral Foundation, p. 181–189.
Stacey, J. T., and Kramers, J., 1975, Approximation of terrestrial lead isotope evolution by a two-stage model: Earth and Planetary Science Letters, v. 26, n. 2, p. 207–221, http://dx.doi.org/10.1016/0012-821X(75)90088-6
Steiger, R. H., and Jäger, E., 1977, Subcommission on geochronology: Convention on the use of decay constants in geo- and cosmochronology: Earth and Planetary Science Letters, v. 36, n. 3, p. 359–362, http://dx.doi.org/10.1016/0012-821X(77)90060-7
Sun, S. S., and McDonough, W. F., 1989, Chemical and isotopic systematics of oceanic basalts: Implications for mantle composition and processes, *in* Saunders, A. D., and Norry, M. J., editors, Magmatism in the Ocean Basins: Geological Society, London, Special Publications, v. 42, p. 313–345, http://dx.doi.org/10.1144/gsl.sp.1989.042.01.19
Syromyatnikova, N. G., Kolesnikov, V. V., Ilyin, V. A., Bekmagambetov, D. B., Kovalskiy, V. S., Ostapova, N. V., Lupareva, N. P., Filimonova, L. E., and Plotnikova, V. P., 1990, Isotope dating of copper-porphyry mineralization and ore-controling intrusions of the Aktogay ore field (northeast Balkhash area): Isotope dating of endogenic ore formation, Conference abstract volume: Kiev, p. 76–79 (in Russian).
Taylor, S. R., and McLennan, S. M., 1985, The Continental Crust: Its Composition and Evolution: Oxford, Blackwell Scientific Publications, 312 p.
Tepley, F. J., III, Davidson, J. P., Tilling, R. I., and Arth, J. G., 2000, Magma Mixing, Recharge and Eruption Histories Recorded in Plagioclase Phenocrysts from El Chichón Volcano, Mexico: Journal of Petrology, v. 41, n. 9, p. 1397–1411, http://dx.doi.org/10.1093/petrology/41.9.1397
Thieblemont, D., Stein, G., and Lescuyer, J. L., 1997, Epithermal and porphyry deposits: The adakite connection: Comptes Rendus De L Academie Des Sciences Serie Ii Fascicule a-Sciences De La Terre Et Des Planetes, v. 325, p. 103–109.
Todt, W., Cliff, R. A., Hanser, A., and Hofmann, A. W., 1996, Evaluation of a ^{202}Pb-^{205}Pb Double Spike for High-Precision Lead Isotope Analysis, *in* Hart, S., and Basu, A., editors, Earth processes: Reading the Isotopic Code: American Geophysical Union, Geophysical Monograph Series, v. 95, p. 429–437, http://dx.doi.org/10.1029/GM095p0429
Valley, J. W., Lackey, J. S., Cavosie, A. J., Clechenko, C. C., Spicuzza, M. J., Basei, M. A. S., Bindeman, I. N., Ferreira, V. P., Sial, A. N., King, E. M., Peck, W. H., Sinha, A. K., and Wei, C. S., 2005, 4.4 billion years of crustal maturation: Oxygen isotope ratios of magmatic zircon: Contributions to Mineralogy and Petrology, v. 150, n. 6, p. 561–580, http://dx.doi.org/10.1007/s00410-005-0025-8
Wang, Q., Xu, J. F., Jian, P., Bao, Z. W., Zhao, Z. H., Li, C. F., Xiong, X. L., and Ma, J. L., 2006, Petrogenesis of adakitic porphyries in an extensional tectonic setting, dexing, South China: Implications for the genesis of porphyry copper mineralization: Journal of Petrology, v. 47, n. 1, p. 119–144, http://dx.doi.org/10.1093/petrology/egi070
Watson, E. B., and Harrison, T. M., 1983, Zircon Saturation Revisited-Temperature and Composition Effects in a Variety of Crustal Magma Types: Earth and Planetary Science Letters, v. 64, n. 2, p. 295–304, http://dx.doi.org/10.1016/0012-821X(83)90211-X
Wedepohl, K. H., 1995, The composition of the continental crust: Geochimica et Cosmochimica Acta, v. 59, n. 7, p. 1217–1232, http://dx.doi.org/10.1016/0016-7037(95)00038-2
White, W. M., and Hofmann, A. W., 1982, Sr and Nd isotope geochemistry of oceanic basalts and mantle evolution: Nature, v. 296, p. 821–825, http://dx.doi.org/10.1038/296821a0
Wiedenbeck, M., Allé, P., Corfu, F., Griffin, W. L., Meier, M., Oberli, F., von Quadt, A., Roddick, J. C., and Spiegel, W., 1995, Three natural zircon standards for U-Th-Pb, Lu-Hf, trace element and REE analyses: Geostandards Newsletter, v. 19, n. 1, p. 1–23, http://dx.doi.org/10.1111/j.1751-908X.1995.tb00147.x
Wiedenbeck, M., Hanchar, J. M., Peck, W. H., Sylvester, P., Valley, J., Whitehouse, M., Kronz, A., Morishita, Y., Nasdala, L., Fiebig, J., Franchi, I., Girard, J.-P., Greenwood, R. C., Hinton, R., Kita, N., Mason, P. R. D., Norman, M., Ogasawara, M., Piccoli, P. M., Rhede, D., Satoh, H., Schulz-Dobrick, B., Skar, O., Spicuzza, M. J., Terada, K., Tindle, A., Togashi, S., Vennemann, T., Xie, Q., and Zheng, Y.-F., 2004, Further characterisation of the 91500 zircon crystal: Geostandards and Geoanalytical Research, v. 28, n. 1, p. 9–39, http://dx.doi.org/10.1111/j.1751-908X.2004.tb01041.x
Winchester, J. A., and Floyd, P. A., 1977, Geochemical discrimination of different magma series and their differentiation products using immobile elements: Chemical Geology, v. 20, p. 325–343, http://dx.doi.org/10.1016/0009-2541(77)90057-2
Windley, B. F., Alexeiev, D., Xiao, W. J., Kroner, A., and Badarch, G., 2007, Tectonic models for accretion of the Central Asian Orogenic Belt: Journal of the Geological Society, v. 164, n. 1, p. 31–47, http://dx.doi.org/10.1144/0016-76492006-022
Winter, J. D., 2001, An introduction to igneous and metamorphic petrology: Upper Saddle River, New Jersey, Prentice-Hall, 697 p.
Wu, F. Y., Yang, Y. H., Xie, L. W., Yang, J. H., and Xu, P., 2006, Hf isotopic compositions of the standard zircons and baddeleyites used in U–Pb geochronology: Chemical Geology, v. 234, n. 1–2, p. 105–126, http://dx.doi.org/10.1016/j.chemgeo.2006.05.003
Xiao, B., Qin, K., Li, G., Li, J., Xia, D., Chen, L., and Zhao, J., 2012, Highly Oxidized Magma and Fluid Evolution of Miocene Qulong Giant Porphyry Cu-Mo Deposit, Southern Tibet, China: Resource Geology, v. 62, n. 1, p. 4–18, http://dx.doi.org/10.1111/j.1751-3928.2011.00177.x
Xu, J. F., Shinjo, R., Defant, M. J., Wang, Q. A., and Rapp, R. P., 2002, Origin of Mesozoic adakitic intrusive rocks in the Ningzhen area of east China: Partial melting of delaminated lower continental crust?: Geology, v. 30, n. 12, p. 1111–1114, http://dx.doi.org/10.1130/0091-7613(2002)030<1111:OOMAIR>2.0.CO;2
Yang, Z. M., Lu, Y. J., Hou, Z. Q., and Chang, Z. S., 2015, High-Mg diorite from Qulong in southern Tibet:

Implications for the genesis of adakite-like intrusions and associated porphyry Cu deposits in collisional orogens: Journal of Petrology, v. 56, n. 2, p. 227–254, http://dx.doi.org/10.1093/petrology/egu076

Zhang, Q., Qin, K. Z., Wang, Y. L., Zhang, F. Q., Liu, H. T., and Wang, Y., 2004, Study on adakite broadened to challenge the Cu and Au exploration in China: Acta Petrologica Sinica, v. 20, p. 195–204 (in Chinese with English abstract).

Zheng, Y. F., 1991, Calculation of oxygen isotope fractionation in metal oxides: Geochimica et Cosmochimica Acta, v. 55, n. 8, p. 2299–2307, http://dx.doi.org/10.1016/0016-7037(91)90105-E

——— 1993a, Calculation of oxygen isotope fractionation in anhydrous silicate minerals: Geochimica et Cosmochimica Acta, v. 57, n. 3, p. 1079–1091, http://dx.doi.org/10.1016/0016-7037(93)90042-U

——— 1993b, Calculation of oxygen isotope fractionation in hydroxyl-bearing silicates: Earth and Planetary Science Letters, v. 120, n. 3–4, p. 247–263, http://dx.doi.org/10.1016/0012-821X(93)90243-3

——— 1996, Oxygen isotope fractionations involving apatites: Application to paleotemperature determination: Chemical Geology, v. 127, n. 1–3, p. 177–187, http://dx.doi.org/10.1016/0009-2541(95)00088-7

Zhukov, N. M., Kolesnikov, V. V., Miroshnichenko, L. M., Egembayev, K. M., Pavlova, Z. N., and Bakarasov, E. V., 1997, Copper deposits of Kazakhstan, Reference Book: Alma Ata, VAC Publishing House, 149 p. (in Russian).

Zindler, A., and Hart, S., 1986, Chemical geodynamics: Annual Review of Earth and Planetary Sciences, v. 14, p. 493–571, http://dx.doi.org/10.1146/annurev.ea.14.050186.002425